FABRICATION AND FUNTIONALIZATION OF RGO CONTAINING POLYMERIC MATERIALS

by

Merve Aslan

B.S., Chemistry, Boğaziçi University, 2019

Submitted to the Institute for Graduate Studies in
Science and Engineering in partial fulfillment of
the requirements for the degree of
Master of Science

Graduate Program in Chemistry

Boğaziçi University

2021

ACKNOWLEDGEMENTS

To start with, I would like to thank my thesis supervisor Prof. Amitav Sanyal for accepting me as his master student and giving me the chance to improve myself each day throughout my undergraduate years until the end of my master studies under his guidance working in many research opportunities as well as his support. I feel very lucky since I had the opportunity to work on these research projects under his mentorship.

I would also like to express my gratitude to Prof. Rana Sanyal for accepting me to her lab as an undergrad at first place and opening the doors of this area for me. Her mentorship and support helped me in every part of my life.

I also want to thank to my jury member Assoc. Prof. Gökhan Çaylı for his valuable revisions and help to improve my thesis.

In addition, I would like to thank to my family and İbrahim Uğur Gürdal for their endless support and patience as well as believing in me all the time.

I would like to extend my sincere thanks to Tuba Ayça Tunca for her company, kindness, and support in every aspect of my life. I also would like to thank to Yavuz Öz and İsmail Altınbaşak for their help and patience during my research, as well as the rest of my labmates for their support and friendship.

I would like to extend my thanks to Rabah Boukherroub and Sabine Szunerits for their support and guidance during my visit in their lab at Universite de Lille. It was a plessure to do research under their mentorship. I also would like to thank to Alexandre Barras for his help and patience during my research at that time.

Financial support from the the Marie Sklodowska-Curie action (H2020-MSCA-RISE-2015, PANG-690836) is acknowledged. Also, RS-Research is acknowledged for providing the opportunity to be involved as part of the PANG690836 project.

I finally would like to thank The Scientific and Technological Research Council of Turkey (TÜBİTAK) for funding the research (Project No: 118Z890).

ABSTRACT

FABRICATION AND FUNTIONALIZATION OF RGO CONTAINING POLYMERIC MATERIALS

In recent years, rGO-containing polymeric materials have been utilized in various biomedical applications such as targeted drug delivery, protein release and photothermal therapy due to the characteristic properties of rGO such as high mechanical stability, large surface area, thermal and optical conductivity. Incorporation of rGO can be done by their encapsulation within polymeric materials, as well as through their functionalization with polymers.

In the first part of this thesis, rGO-containing hydrogels for "on-demand" protein release were developed. Hydrogels were synthesized using the fast thiol-maleimide "click" reaction, while the Diels-Alder (DA) cycloadduct of furan-maleimide was introduced into the hydrogel network to impart thermo-responsiveness. Incorporation of rGO into the hydrogel matrix made it possible to release a cargo such as protein or dye-conjugated macromolecule under Near-Infrared Light (NIR) activation, since rGO is a photothermal agent that converts light-to-heat. This rapid light-to-heat conversion results in heating of the hydrogel, leading to the retro-DA reaction of endo-linkages, resulting in hydrogel network degradation. Successful synthesis of polymeric precursors, fabrication of photothermally responsive hydrogels, and their degradation and release of dye-conjugated macromolecules is reported. In the second part of this thesis, rGO surface was modified with small molecule and PEG-based ligands containing a pyridyldisulfide (PDS) group, to enable surface functionalization through the thiol-disulfide exchange reaction. To this end, rGO surface was modified with pyrene- and PDS-containing molecules. The π-π interactions between rGO and pyrene was used to functionalize rGO through a non-covalent interaction. Thereafter, using the PDS groups on the rGO, conjugation of thiol-containing ligands such as ferrocene-thiol was achieved.

ÖZET

RGO İÇEREN POLİMERİK MADDELERİN YAPIMI VE İŞLEVSELLESTİRİLMESİ

Son yıllarda rGO içeren polimerik malzemeler, rGO'nun yüksek mekanik stabilite, geniş yüzey alanı, termal ve optik iletkenlik gibi karakteristik özelliklerinden dolayı hedeflenen ilaç dağıtımı, protein salınımı ve fototermal terapi gibi çeşitli biyomedikal uygulamalarda kullanılmaktadır. rGO'nun dahil edilmesi, polimerik malzemeler içinde kapsüllenmeleri ve ayrıca polimerlerle işlevselleştirilmeleri yoluyla yapılabilir.

Bu tezin ilk bölümünde, "istek üzerine" protein salımı için rGO içeren hidrojeller geliştirildi. Hidrojeller, hızlı tiyol-maleimid "klik" reaksiyonu kullanılarak sentezlenirken, termo-yanıtlık kazandırmak için furan-maleimidin Diels-Alder (DA) siklo katkı maddesi hidrojel ağına dahil edildi. rGO'nun hidrojel matrisine dahil edilmesi, rGO, ışığı ısıya dönüştüren bir fototermal ajan olduğundan, Yakın Kızılötesi Işık (NIR) aktivasyonu altında protein veya boya konjuge makromolekül gibi bir yükün serbest bırakılmasını mümkün kılmıştır. Bu hızlı ışıktan ısıya dönüşüm, hidrojelin ısınmasıyla sonuçlanır ve endo-bağların retro-DA reaksiyonuna yol açarak hidrojel ağının bozulmasına neden olur. Polimerik öncülerin başarılı sentezi, fototermal olarak duyarlı hidrojellerin üretimi ve bunların bozunması ve boya konjuge makromoleküllerin salınması rapor edilmiştir. Bu tezin ikinci bölümünde, rGO yüzeyi, tiyol-disülfid değişim reaksiyonu yoluyla yüzey işlevselleştirmesini sağlamak için küçük molekül ve bir piridildisülfid (PDS) grubu içeren PEG bazlı ligandlar ile modifiye edildi. Bu amaçla, rGO yüzeyi piren ve PDS içeren moleküller ile modifiye edildi. rGO ve piren arasındaki π-π etkileşimleri, kovalent olmayan bir etkileşim yoluyla rGO'yu işlevselleştirmek için kullanıldı. Daha sonra, rGO üzerindeki PDS grupları kullanılarak, ferrosen-tiol gibi tiyol içeren ligandların konjugasyonu sağlandı.

TABLE OF CONTENTS

ACKNOWLEDGEMENTS iii
ABSTRACT v
ÖZET vi
TABLE OF CONTENTS vii
LIST OF FIGURES xi
LIST OF TABLES xviii
LIST OF ACRONYMS/ABBREVIATIONS xix
1. INTRODUCTION 1
1.1. Reduced Graphene Oxide (rGO): Its Applications and Functionalization 1
1.2. Hydrogels 4
1.3. Stimuli Responsive Hydrogels in Drug Delivery Systems 6
1.4. Hydrogels Synthesized via Diels-Alder Chemistry 8
1.5. Hydrogels Synthesized via Thiol-Maleimide “Click” Chemistry 10
1.6. Photothermally-Responsive Hydrogels 12
2. PROTEIN RELEASE FROM PHOTOTHERMALLY RESPONSIVE HYDROGELS 15
2.1. Aim of the study 15
2.2. Experimental 16
2.2.1. Materials 16
2.2.2. Instrumentation 16
2.2.3. Synthesis of Bismaleimide Crosslinker 17
2.2.4. Synthesis of Linear PEG-based Allyl (PEG-Bis-A) 17
2.2.5. Synthesis of 4-PEG-Allyl (PEG-Tetra-A) 17
2.2.6. Synthesis of furan containing linear polymer (PEG-Bis-F) 18
2.2.7. Synthesis of furan containing four-armed PEG (PEG-Tetra-F) 18
2.2.8. Synthesis of maleimide containing linear polymer (PEG-Bis-M) 19
2.2.9. Synthesis of maleimide containing four-armed polymer (PEG-Tetra-M) 19
2.2.10. Synthesis of tetra thiol (4-TSH) 19

2.2.11. Synthesis of rGO 20
2.2.12. Synthesis of Bis-PEG Hydrogels (w/o rGO) 20
2.2.13. Synthesis of PEG-Tetra Hydrogels (w/o rGO) 20
2.2.14. Synthesis of Bis-PEG rGO-Hydrogels 21
2.2.15. Synthesis of PEG-Tetra rGO-Hydrogels 21
2.2.16. Characterization of Hydrogels 21
2.2.17. Determination of Remaining Thiol Groups in Hydrogels 22
2.2.18. Rheological Studies 22
2.2.19. Loading FITC-Dextran to Hydrogels 23
2.2.20. Passive Release from rGO-Hydrogel 23
2.2.21. Active Release from rGO-Hydrogels 23
2.2.22. NIR Heating Experiment of rGO-Hydrogel 24
2.3. Results and Discussion 24
2.3.1. Synthesis and characterization of BMI 24
2.3.2. Synthesis and characterization of PEG-Bis-A 27
2.3.3. Synthesis and characterization of PEG-Tetra-A 28
2.3.4. Synthesis and characterization of furan containing polymer (PEG-Bis-F) 29
2.3.5. Synthesis and characterization of furan containing four-armed polymer (PEG-Tetra-F) 30
2.3.6. Synthesis and characterization of maleimide containing polymers (PEG-Bis-M) 32
2.3.7. Synthesis and characterization of maleimide containing polymers (PEG-Tetra-M) 33
2.3.8. Synthesis of 4-TSH 35
2.3.9. Synthesis and characterization of rGO 36
2.3.10. Synthesis and characterization of Bis-PEG Hydrogels (w/o rGO) 38
2.3.11. Synthesis and characterization of rGO-containing Bis-PEG Hydrogels 41
2.3.12. Synthesis and characterization of PEG-Tetra-M hydrogels (w/o rGO) 43
2.3.13. Synthesis and characterization of rGO containing PEG-Tetra-M hydrogels 49

2.3.14. Passive Release of FITC-Dextran from rGO containing PEG-Tetra-M-HG-rGO 51
2.3.15. Active Release of FITC-Dectran from rGO-containing Hydrogels 52
2.3.16. NIR Heating Experiment of rGO-Hydrogel 53
2.4. Conclusion 54
3. FUNCTIONALIZATION OF RGO VIA DISULFIDE CHEMISTRY 55
3.1. Aim of Study 55
3.2. Experimental 56
3.2.1. Materials 56
3.2.2. Instrumentation 56
3.2.3. Synthesis of Pyrene Pyridyl Disulfide Ester (PPD) 57
3.2.4. Synthesis of PDS-PEG-Amine 57
3.2.5. Synthesis of Pyrene-PEG-PDS (PDS-PEG-Py) 58
3.2.6. Preparation of rGO/PPD 58
3.2.7. Functionalization of rGO/PPD with small compounds via Thiol-disulfide Exchange Reaction 58
3.2.8. Fuctionalization of rGO/PPD with thiolated-PEG 59
3.2.9. Functionalization of rGO/PPD with PEG via Thiol-disulfide Exchange Reaction 59
3.2.10. DTT Treatment of rGO/PPD 59
3.2.11. DTT and GSH Treatment of Functionalized rGO/PPD 60
3.3. Results and Discussion 60
3.3.1. Synthesis and Characterization of PPD 60
3.3.2. Synthesis and Characterization of PDS-PEG-Amine 62
3.3.3. Synthesis and Characterization of PDS-PEG-Py 64
3.3.4. Characterization of rGO/PPD 65
3.3.5. Functionalization of rGO/PPD with small compounds via Thiol-disulfide Exchange Reaction 68
3.3.6. Functionalization and Characterization of rGO/PPD with PEG-SH via Thiol-disulfide Exchange Reaction 71
3.3.7. Functionalization and Characterization of rGO with PDS-PEG-Py via Thiol-disulfide Exchange Reaction 73

3.3.8. DTT Treatment and Characterization of rGO/PPD 73
3.3.9. DTT and GSH Treatment and Characterization of Functionalize rGO/PPD 74
3.4. Conclusion 78
4. CONCLUSION 79
REFERENCES 80
APPENDIX A: ADDITIONAL DATA 91
APPENDIX B: COPYRIGHT NOTICES 94

LIST OF FIGURES

Figure 1.1. The forms of graphene and its derivatives that have been used for the construction of bioactive architectures: (a) single-layer graphene, (b) multilayer graphene, (c) GO, (d) RGO, (e) GOQD, (f) GQD [9]. 2

Figure 1.2. Schematic Illustration of the Synthesis of Thiol–Ene “Clickable” Maleimide-rGO and its Subsequent Functionalization [8]. 3

Figure 1.3. Hydrogels formation via (a) physical gelation and (b) chemical gelation [51]. 5

Figure 1.4. Drug release through a hydrogel membrane in a reservoir system [28]. 6

Figure 1.5. Drug release from matrix systems[28]. 6

Figure 1.6. Hydrogels fabricated via Michael type click reaction of thiol-maleimide [34]. 8

Figure 1.7. The DA reaction between a diene and a dienophile [35]. 9

Figure 1.8. Schematic representation of synthesis and degradation of the redox-responsive DA hydrogel [42]. 10

Figure 1.9. Thiol-maleimide "click" reaction mechanism [44]. 11

Figure 1.10. Schematic illustration of stimuli-responsive hydrogel system via thiol-maleimide "click" reaction [51]. 12

Figure 1.11. Cargo release from photothermally reactive hydrogel 13

Figure 1.12. Illustration of on-demand insulin release from photothermally responsive rGO hydrogel [72]. 14

Figure 2.1. Illustration of aim of the project. 16

Figure 2.2. Synthesis of BMI. 25

Figure 2.3. ^{1}H-NMR spectrum of protected maleic anhydride. 25

Figure 2.4. ^{1}H-NMR spectrum of protected BMI. 26

Figure 2.5. ^{1}H-NMR spectrum of BMI. 26

Figure 2.6. Synthesis of PEG-Bis-A. 27

Figure 2.7. ^{1}H-NMR of PEG-Bis-A. 27

Figure 2.8. Synthesis of PEG-Tetra-A. 28

Figure 2.9. ^{1}H-NNMR of PEG-Tetra-A. 28

Figure 2.10. Synthesis of PEG-Bis-F. 29

Figure 2.11. ^{1}H-NMR spectrum of PEG-Bis-F. 30

Figure 2.12. Synthesis of PEG-Tetra-F. 31

Figure 2.13. ^{1}H-NMR spectrum of PEG-Tetra-F. 31

Figure 2.14. Synthesis of PEG-Bis-M. 32

Figure 2.15. 1H-NMR of PEG-Bis-M. 33

Figure 2.16. Synthesis of PEG-Tetra-M. 34

Figure 2.17. ^{1}H-NMR of PEG-Tetra-M. 35

Figure 2.18. Synthesis of 4-TSH. 35

Figure 2.19. H-NMR spectrum of 4-TSH. 36

Figure 2.20. ATR-FTIR spectra of rGO and GO. 37

Figure 2.21. UV spectra of rGO and GO. 37

Figure 2.22. Raman spectrum of rGO. 38

Figure 2.23. PEG-Bis-M-HG$_5$ after synthesis (left) and after swelling (left). 38

Figure 2.24. PEG-Bis-M-HG$_{10}$ after synthesis (left) and after swelling (right). 39

Figure 2.25. SEM images of a) PEG-Bis-M-HG$_5$ and b) PEG-Bis-M-HG$_{10}$ in the scale bar 200 μm. 39

Figure 2.26. Swelling data of PEG-Bis-M-HG$_{10}$. 40

Figure 2.27. Frequency sweep test of PEG-Bis-HG$_{10}$. 41

Figure 2.28. PEG-Bis-M-HG-rGO$_{10}$ after fabrication (left) and after swelling (right). 41

Figure 2.29. PEG-Bis-M-HG-rGO$_{30}$ after fabrication (left) and after swelling (right). 42

Figure 2.30. SEM images of a) PEG-Bis-M-HG-rGO$_{10}$ and b) PEG-Bis-M-HG-rGO$_{30}$ in sacle of 200 μm. 42

Figure 2.31. Swelling profile of PEG-Bis-M-HG-rGO$_{30}$. 43

Figure 2.32. SEM images of a) PEG-Tetra-M-HG10 b) PEG-Tetra-M-HG20 and c) PEG-Tetra-M-HG30 in scale bar of 200 μm. 44

Figure 2.33. Comparison of Swelling Capacities of PEG-Tetra-M-HGs. 44

Figure 2.34. Amplitude Sweep Test of PEG-Tetra-M-HG$_{10}$. 45

Figure 2.35. Frequency Sweep Test of PEG-Tetra-M-HG$_{10}$. 46

Figure 2.36. Amplitude Sweep Test of PEG-Tetra-M-HG$_{20}$. 46

Figure 2.37. Frequency Sweep Test of PEG-Tetra-M-HG$_{20}$. 47

Figure 2.38. Amplitude Sweep Test of PEG-Tetra-M-HG$_{30}$. 47

Figure 2.39. Frequency Sweep Test of PEG-Tetra-M-HG$_{30}$. 48

Figure 2.40. Comparison of the G' values of PEG-Tetra-M-HGs. 48

Figure 2.41. SEM images of (a) PEG-Tetra-M-HG-rGO$_{10}$, (b) PEG-Tetra-M-HG-rGO$_{20}$ and (c) PEG-Tetra-M-HG-rGO$_{30}$. 49

Figure 2.42. Swelling Profiles of PEG-Tetra-M-HG-rGOs. 50

Figure 2.43. Frequency Sweep Tests of PEG-Tetra-M-HG-rGOs. 51

Figure 2.44. Release Profiles of PEG-Tetra-M-HG-rGOs. 52

Figure 2.45. Active release of FITC-Dextran from PEG-Tetra-M-HG-rGO$_{30}$ under NIR light. 53

Figure 2.46. Rheology data of NIR heating experiment of PEG-Tetra-M-HG-rGO_{30}. 53

Figure 3.1. Schematic representation of the project. 56

Figure 3.2. Synthesis of PPD. 61

Figure 3.3. ^{1}H-NMR spectrum of PPD. 61

Figure 3.4. ^{13}C-NMR of PPD. 62

Figure 3.5. Synthesis of PDS-PEG-Amine. 63

Figure 3.6. ^{1}H-NMR Spectrum of PDS-PEG-Amine. 63

Figure 3.7. Synthesis of PDS-PEG-Py. 64

Figure 3.8. ^{1}H-NMR of PDS-PEG-Py. 64

Figure 3.9. Illustration of rGO/PPD stacking. 65

Figure 3.10. ATR-FT-IR of rGO, PPD and rGO/PPD. 66

Figure 3.11. XPS of rGO. 66

Figure 3.12. XPS of rGO/PPD 67

Figure 3.13. S_{2p} Scan of rGO/PPD. 67

Figure 3.14. CV data of PPD Stacking. 68

Figure 3.15. Schematic illustration of modification of rGO/PPD with 6-(Ferrocenyl)hexanethiol. 69

Figure 3.16. XPS data of rGO/PPD-FSH. 69

Figure 3.17. XPS of Fe 2p electron. 70

Figure 3.18. Schematic illustration of exchange reaction between rGO/PPD and 1H,1H,2H,2H-Perfluorodecanthiol. 70

Figure 3.19. XPS data of rGO/PPD-FSH. 71

Figure 3.20. Schematic Illustration of modification of rGO/PPD with PEG-SH. 72

Figure 3.21. Water Solubility Experiment of rGO/PPD-PEG. 72

Figure 3.22. ATR-FT-IR Data of rGO/PPD-PEG Stacking and DTT Treatment. 72

Figure 3.23. Dispersion data of (a) rGO, (b) rGO-PEG-PDS for (1) 0h and (b) 12h in water. 73

Figure 3.24. Illustration of DTT Treatment of rGO/PPD. 74

Figure 3.25. Pyridinethione Release from rGO/PPD after DTT treatment. 74

Figure 3.26. Schematic Illustration of DTT Cleavage of rGO/ ppd-FeSH. 75

Figure 3.27. XPS data of rGO/PPD-FeSH After DTT Treatment. 75

Figure 3.28. Schematic Representation of GSH nad DTT Treatment of rGO/PPD-FSH. 76

Figure 3.29. XPS Data of rGO/PPD-FSH After GSH Treatment. 77

Figure 3.30. XPS data of rGO/PPD-FSH After DTT Treatment. 77

Figure A. 1. ATR-FT-IR data of (a) PEG-Bis-A, (b) PEG-Bis-F and (c) PEG-Bis-M. ...92

Figure A. 2. ATR-FT-IR data of (a) PEG-Tetra-A, (b) PEG-Tetra-F and (c) PEG-Tetra-M. ...93

Figure B. 1. Copyright notice for Figure 1.1. ...95

Figure B. 2. Copyright notice for Figure 1.2. ...96

Figure B. 3. Copyright notice for Figure 1.3. ...97

Figure B. 4. Copyright notice for Figure 1.4 and Figure 1.5. ...98

Figure B. 5. Copyright notice for Figure 1.6. ...99

Figure B. 6. Copyright notice for Figure 1.7. ...100

Figure B. 7. Copyright notice for Figure 1.8. ...101

Figure B. 8. Copyright for Figure 1.9. ...102

Figure B. 9. Copyright for Figure 1.10. ...103

Figure B. 10. Copyright notice for Figure 1.12. ...104

LIST OF TABLES

Table 2.1. Optimization of thiol-ene "click" reaction. 29

LIST OF ACRONYMS/ABBREVIATIONS

2D	2 dimensional
3D	3 dimensional
ATR-FTIR	The Attenuated Total Reflection-Fourier Transform Infrared
$CDCl_3$	Chloroform
DA	Diels-Alder
DMAP	4-(Dimethylamino)pyridine
DMPA	2,2-Dimethoxy-2-phenylacetophenone
DTT	Dithiothreitol
EDCI	1-Ethyl-3-(3-dimethylaminopropyl)carbodiimide
EtOAc	Ethyl acetate
FITC-BSA	Fluorescein isothiocyanate labelled bovine serum albumin
FITC-Dextran	Fluorescein isothiocyanate dextran
G’	Storage Modulus
G’’	Loss Modulus
GO	Graphene oxide
GSH	Glutathione
HG	Hydrogel
kDa	Kilo Dalton
LVE	Linear Viscoelastic
MeOH	Methanol
M_n	Number Average Molecular Weight
NaH	Sodium Hydride
NHS	N-Hydroxysuccinimide
NMR	Nuclear Magnetic Resonance
NIR	Near-Infrared
PBS	Phosphate Buffer Saline
PDS	Pyridyldisulfide
PEG-Bis-A	Linear PEG Allyl
PEG-Bis-F	Furan Containing Linear PEG

PEG-Bis-M	Maleimide Containing Linear PEG
PEG-Tetra-A	Four-Armed PEG Allyl
PEG-Tetra-F	Four-Armed Furan Containing PEG
PEG-Tetra-M	Four-Armed Maleimide Containing PEG
PPD	Pyrene-Pyridine Disulfide Ester
Py	Pyrene
rGO	Reduced Graphene Oxide
rpm	Revolutions per Minute
rt	Room Temperature
SEM	Scanning Electron Microscopy
S_N2	Nucleophilic Substitution, Second Order
THF	Tetrahydrofuran
UV	Ultraviolet
Vis	Visible
w/v	Weight per Volume
w/o	Without
XPS	X-Ray Photoelectron Spectroscopy

1. INTRODUCTION

1.1. Reduced Graphene Oxide (rGO): Its Applications and Functionalization

Graphene is a single layered allotrope of carbon atoms that has a two-dimensional (2D) honeycomb-like structure with sp^2 and sp^3 hybridization. Graphene oxide (GO) and reduced graphene oxide (rGO) are derivatives of graphene with somewhat similar properties (Figure 1.1). GO is the water dispersible derivate of graphene that contains different functional groups such as epoxy rings, carboxylic acids, carboxy, alkoxy and hydroxyl groups on its surface and edges, whereas rGO is the derivative of graphene that has obtained via reduction of GO [1]. Through this reduction process, GO loses most of its functional groups as well as its facile dispersibility in water and as a result gives rGO, the derivative with less functional groups and dispersibility in water and as a result the derivative less functional groups. However, there is a reason for interest in the reduction of GO to rGO; GO has far less conductivity that of graphene like rGO. Furthermore, due to extended conjugation present in rGO, their optical and mechanical properties are quite different [1,2].

Recently, rGO has gained a lot of attention of researches in various application areas such as sensors [3,4], biomedical applications [5], supercapacitors [6] and absorbers [7]. In biomedical applications, appropriate functionalization of graphene is quite important. In a recent example, Oz *et al.* developed a targeted drug delivery system via functionalization of rGO [8]. In the study, they used a dopamine ligand (dopa-MAL) to functionalize rGO via π –π stacking between rGO sheets and dopamine aromatic groups. Later, they have further modified rGO by using click chemistry between maleimide and thiol bearing targeting peptide c(RGDfC). Lastly, they loaded doxorubicin (DOX) an anticancer drug non-covalently and demonstrated its suitability as a suitable drug delivery system to kill cancer cells (Figure 1.2).

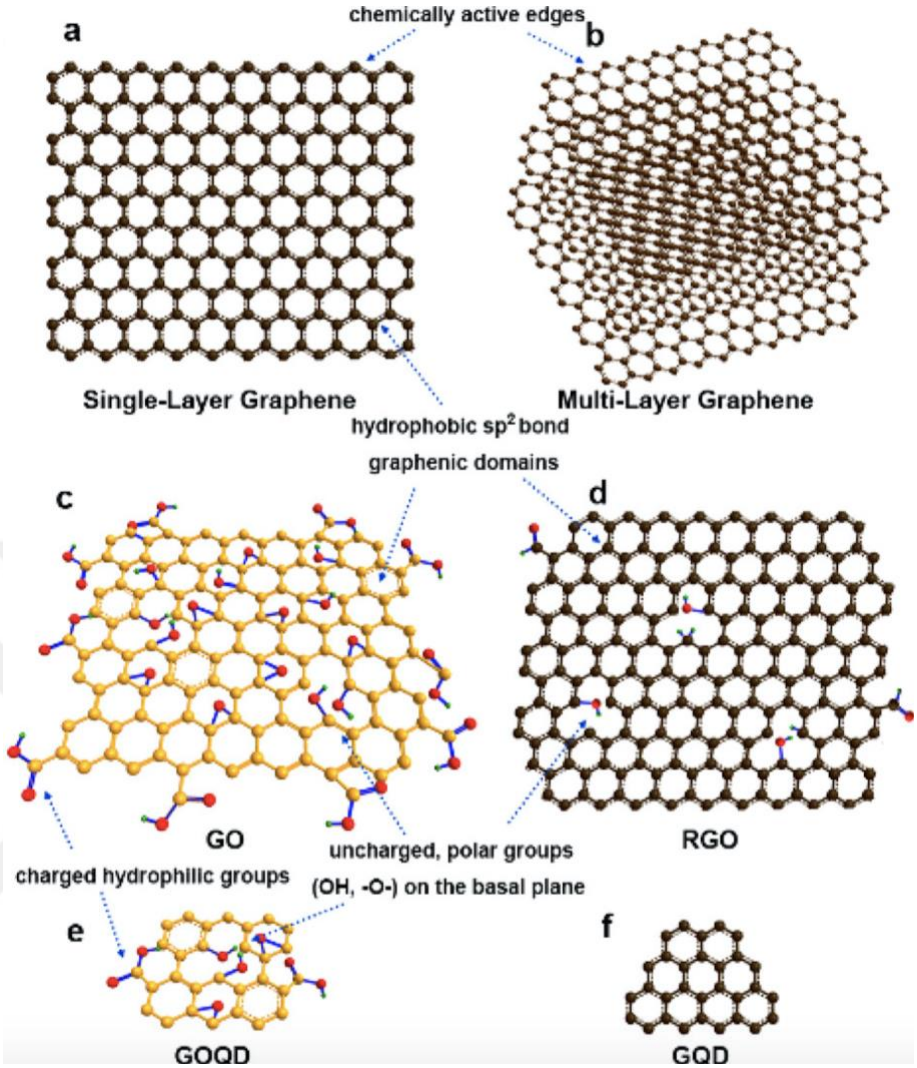

Figure 1.1. The forms of graphene and its derivatives that have been used for the construction of bioactive architectures: (a) single-layer graphene, (b) multilayer graphene, (c) GO, (d) RGO, (e) GOQD, (f) GQD [9].

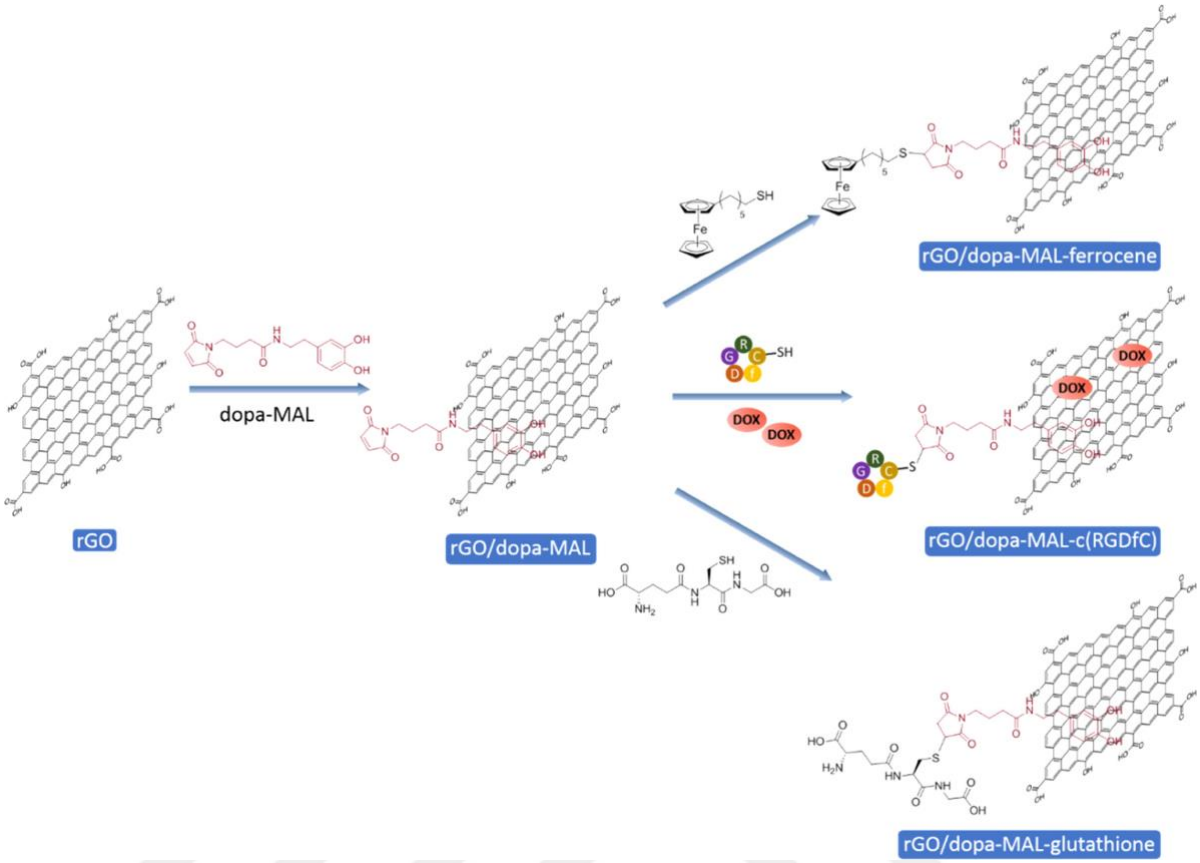

Figure 1.2. Schematic Illustration of the Synthesis of Thiol–Ene "Clickable" Maleimide-rGO and its Subsequent Functionalization [8].

Even though graphene/rGO/GO have numerous intrinsic properties, further functionalization is often required to introduce new characteristics. Non-covalent methods such as π –π , H-bonding, ionic and electrostatic interactions can be used to functionalized rGO rather than covalent methods used to functionalize GO such as carbon skeleton, hydroxy and carboxyl functionalization [10]. The reason for that is after reduction of GO to rGO number of available functional groups for covalent functionalization decreases. Thus, non-covalent functionalization is often a preferred way to functionalize rGO rather than the covalent functionalization. When it comes to chemical functionalization of graphene, GO is the mostly used derivative due to the functional groups on its edges and surface. In a recent example, Pinerio-Garcia et al. functionalized graphene oxide chemically via thiol-ene Michael addition reaction [11]. Even though direct chemical functionalization of rGO is possible, the amount of functionalization may nnot be enough for further applications since these reactive functional groups on rGO edges and surface are not in high enough quantities. Thereafore, alternative methods are needed to enable chemical functionalization of rGO.

1.2. Hydrogels

Hydrogels are three-dimensional (3D) polymeric networks that consist of hydrophilic macromonomers that can absorb large amount of water [12]. Recently, due to their various application areas such as tissue engineering, sensors and drug delivery systems, hydrogels have drawn interest of researchers [13,14]. Nowadays, new platforms to deliver therapeutics are required each passing day and hydrogel platforms are one of those encouraging delivery vehicles with their high loading efficiency as well as their ability to retain cargo bioactivity [15,16].

There are several parameters effecting the properties of hydrogels such as cross-linking, synthesis method, configuration, charge and the chemical composition of the polymer. In cross-linking based classification, hydrogels could be categorized as physical hydrogels when the polymer chains in hydrogel matrix interacts through physical interactions such as hydrogen bonding, molecular entanglements, ionic or hydrophobic forces between functional groups that are present in the polymer chains [17,18]. On the other hand, when the polymer chains were combined through covalent bonds they are called chemically cross-linked hydrogels. In chemical synthesis process, hydrogels can be prepared via two different methods: using radical polymerization of monomers, or crosslinking polymer chains through reactions such as Michael addition, esterification, amidation, and other click type reactions (Figure 1.3) [19].

For the development of hydrogel-based delivery systems, ‘click’ chemistry is a promising method to synthesize as well as to functionalize hydrogels in a good yields under mild conditions [20]. Metal-free conjugation based strategies of click chemistry such as Diels-Alder [21], radical thiol-ene [22] and nucleophilic thiol-ene [23] cycloaddition reactions are widely used for the fabrication of hydrogels. The thiol-Micheal addition reaction is an excellent method for hydrogel formation. It requires a nucleophile that is the base or nucleophile-catalyzed thiolate addition into an alkene which is electron-deficient. As nucleophile-catalyzed click reaction, Micheal type thiol-maleimide click reaction is one of the widely used methods to obtain hydrogels with fast gelation kinetics [24,25].

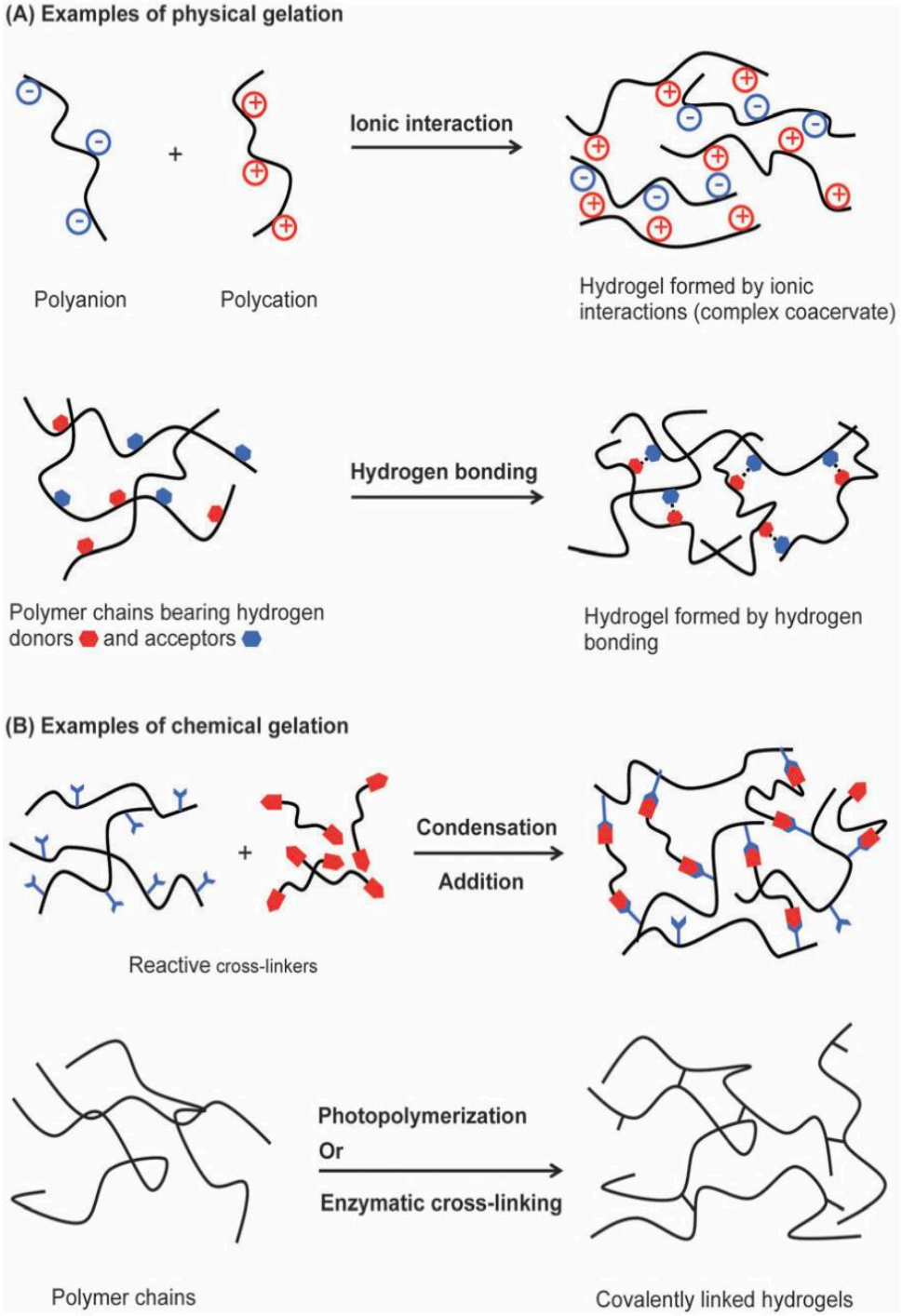

Figure 1.3. Hydrogels formation via (a) physical gelation and (b) chemical gelation [51].

1.3. Stimuli Responsive Hydrogels in Drug Delivery Systems

Due to their unique physical properties such as porosity and compatibility with aqueous environment, hydrogels have attracted a certain interest in drug delivery applications. Their porosity can be tuned by adjusting cross-link density and by doing so they permit loading of drugs into the gel matrix [26]. The drug release from hydrogel may be achieved by diffusion, swelling, chemical or stimuli responsivity. In the diffusion controlled mechanism, the reservoir core containing drug or protein is coated with a hydrogel membrane (Figure 1.4). And the release of the drug or protein is achieved through the macromolecular hydrogel mesh or pores filled with water in a time-dependent manner and constant drug release rate. In the swelling-controlled release, the drug or the protein is homogeneously dispersed in the hydrogel and the release starts when the hydrogel starts to swell in a bio-fluid as the expansion during swelling facilitates the drug diffusion beside the chain relaxation (Figure 1.5) [27,28].

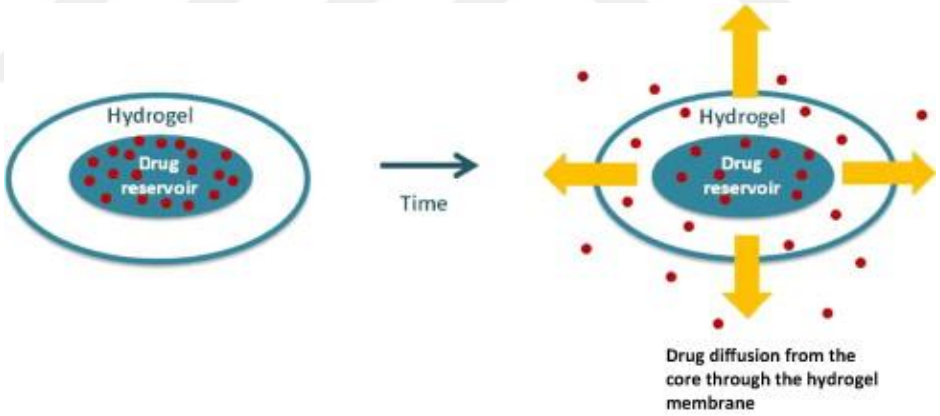

Figure 1.4. Drug release through a hydrogel membrane in a reservoir system [28].

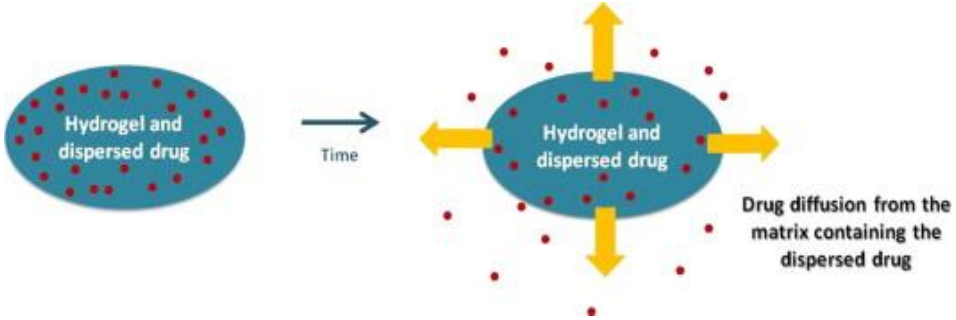

Figure 1.5. Drug release from matrix systems[28].

Even though hydrogels are important in delivery of macromolecules, passive and active release is a major challenge in using hydrogel based delivery platforms. Scaffolds that exhibit minimum level of passive release, can be tuned for effective release by incorporating stimuli responsiveness. Until now, for degradation of hydrogels to achieve release of molecules, different stimuli-responsive triggers as UV-irradiation, NIR irradiation, pH, temperature, redox potential and enzymes have been introduced into various polymeric matrices at physiological conditions [24-28]. Stimuli responsiveness can result in changes in volume transitions, or crosslinking density. The latter can be achieved by either temperature dependent changes in polymer chain configurations or bond cleavages. While several examples of therapeutic release through swelling-deswelling induced volume transitions are known for triggering delivery, reports of change in crosslink density through bond rapture are rare. To achieve bond rapture release mechanism, specific stimuli-responsive functional groups or junction points are needed to be introduced into the hydrogel network.

Recently, Kloxin and coworkers utilized the advantages of Micheal type click reaction to fabricate hydrogels from multi-armed polyethylene glycol (PEG) polymers [34]. In this study, thiol and maleimide-containing four-armed poly(ethylene glycol) macromers are reacted via thiol-maleimide click reaction to obtain injectable hydrogels. This click chemistry resulted in the fast gelation of these two functional groups, therefore, yielding applicable injectable hydrogels as well as triple stimuli-responsive hydrogels since the system has a photodegradable backbone, hydrolytically degradable back bone and reducing-environment sensitive linkage (Figure 1.6).

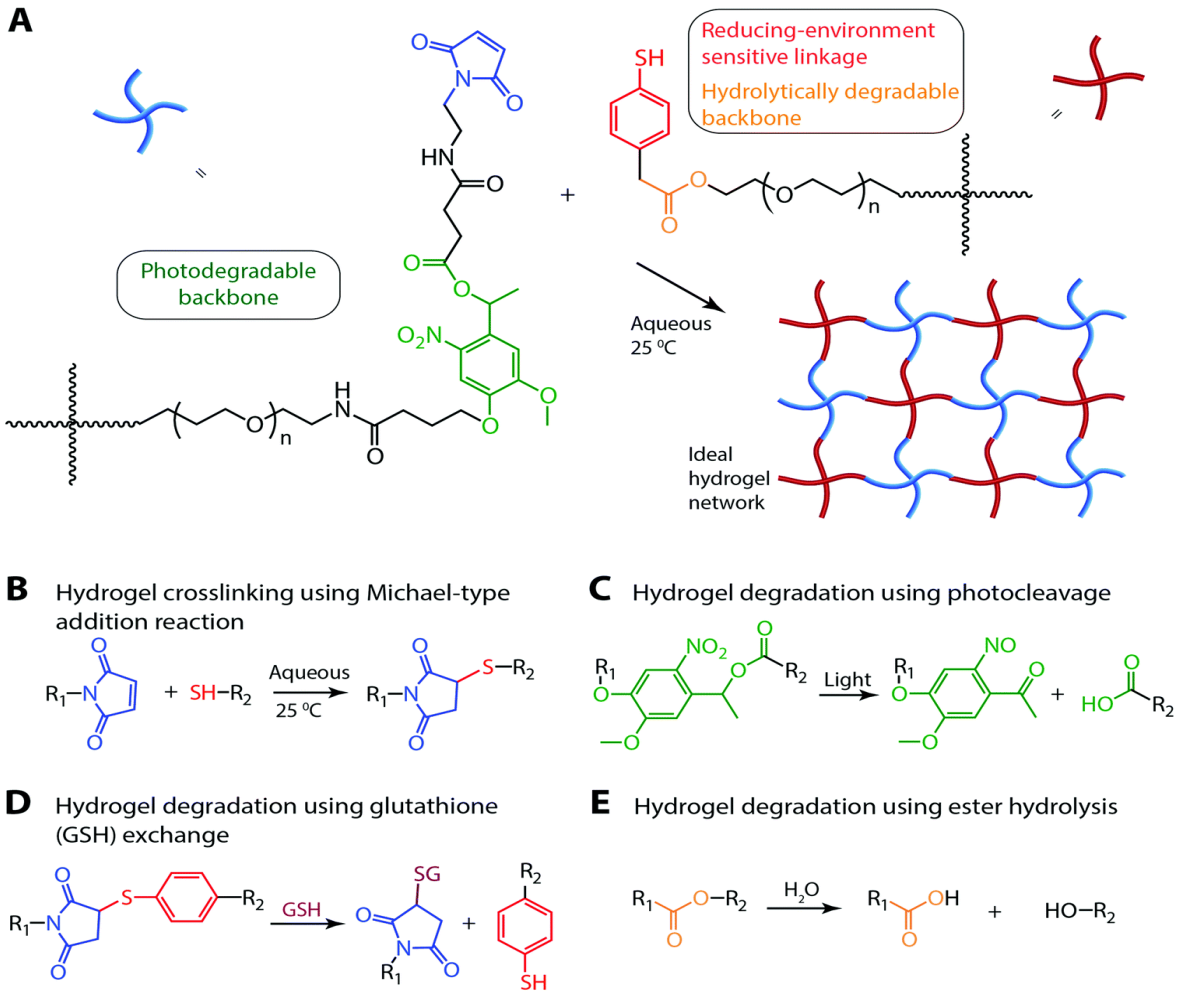

Figure 1.6. Hydrogels fabricated via Michael type click reaction of thiol-maleimide [34].

1.4. Hydrogels Synthesized via Diels-Alder Chemistry

In the DA reaction, a diene, an electron deficient molecule, and a dienophile, electron rich molecule, undergoes a [4+2]-cycloaddition reaction involving their 4 π-electrons and 2 π-electrons respectively to form cyclohexene ring in a single step (Figure 1.7). The driving force of this reaction is the stability of formed σ-bonds rather than the energetically less stable π-bonds. It is a thermoresponsive and biocompatible one-step "click" reaction that doesn't require a catalyst and doesn't produce side products [35]. This benign reaction conditions made the DA a suitable "click" reaction for synthesis of several polymeric networks [36,37].

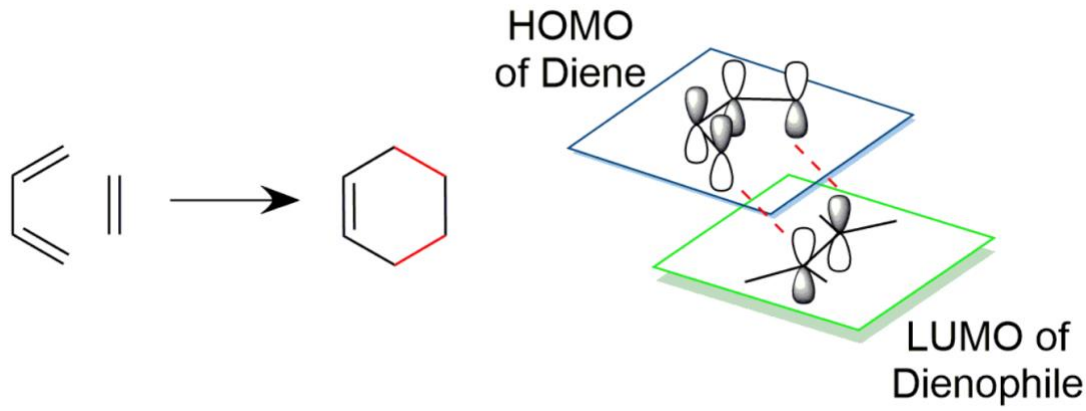

Figure 1.7. The DA reaction between a diene and a dienophile [35].

In the hydrogel preparation, the DA reaction became desirable approach due to its properties mentioned above. The polymers functionalized with desired diene and dienophile were used to synthesize hydrogels. Although there are several diene options, maleimide is mostly used dienophile since it is highly reactive and stable, as well as suitable to incorporate into polymeric materials. For the choice of diene, furan is a promising one since the cycloadduct formed between maleimide and furan are thermoreversible over a wide range of temperatures ranging from 50 to 100 °C depending the *endo*- or *exo*- stereochemistry of the cycloadduct [37]. In the literature, there are several examples of furan-maleimide hydrogels that have been fabricated for biomedical applications [38-42].

Lately, Altinbasak et al. developed a hydrogel system using the DA chemistry. In this system, the authors used a furan-containing copolymer and maleimide-containing cross-linker that also has a disulfide bond. While the reaction between furan and maleimide formed the hydrogels under benign reaction conditions, the disulfide bond in the cross-linker provided a redox-responsive system that can be degraded under reducing environment (Figure 1.8) [42]. In another example, Goepferich and co-workers prepared hydrogels through DA reaction between furfuryl and maleimide end groups of multi-armed poly (ethylene glycol)s (PEGs). Since the obtained hydrogels have *endo* DA cycloadducts in their network, they were readily degradable at body temperature. Therefore, the achieved hydrogel system could be used for protein delivery at body temperature via the retro DA reaction, in other way through bond rupture [43].

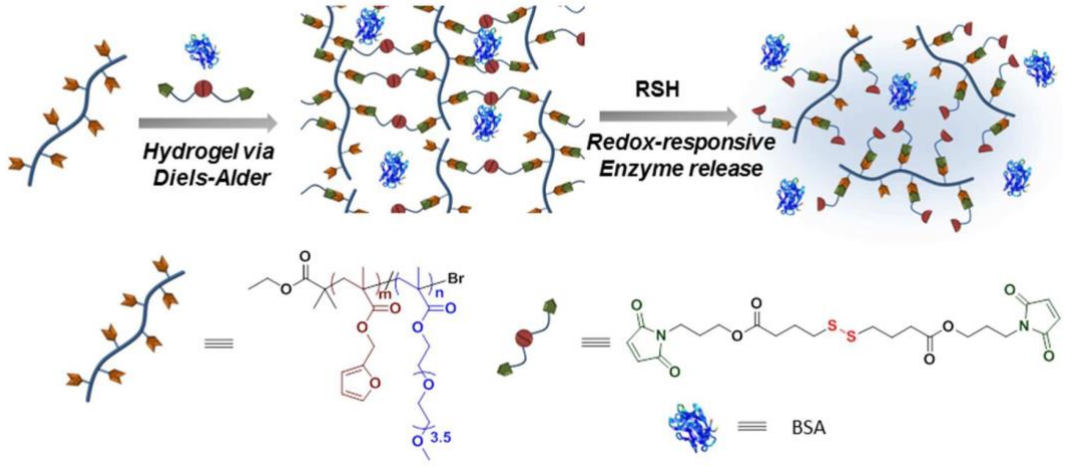

Figure 1.8. Schematic representation of synthesis and degradation of the redox-responsive DA hydrogel [42].

1.5. Hydrogels Synthesized via Thiol-Maleimide "Click" Chemistry

Thiol and maleimide functional groups undergoes a Michael addition type "click" reaction. In this reaction, the driving force derives from the release of ring strain when the product is formed, as well as the withdrawing effect of two activating carbonyls of maleimide. This process can be achieved in different mechanisms; base initiated one or nucleophile initiated one (Figure 1.9). In these mechanisms, a thiolate anion initiates reaction by attacking the double bond of maleimide and forms an enolate intermediate. The formed enolate deprotonates thiol to give the desired product [44]. It is a one-step reaction carried out under benign conditions with high conversion, as well as formation of no side products. Therefore, this reaction has been used to fabricate various polymeric networks [45-47].

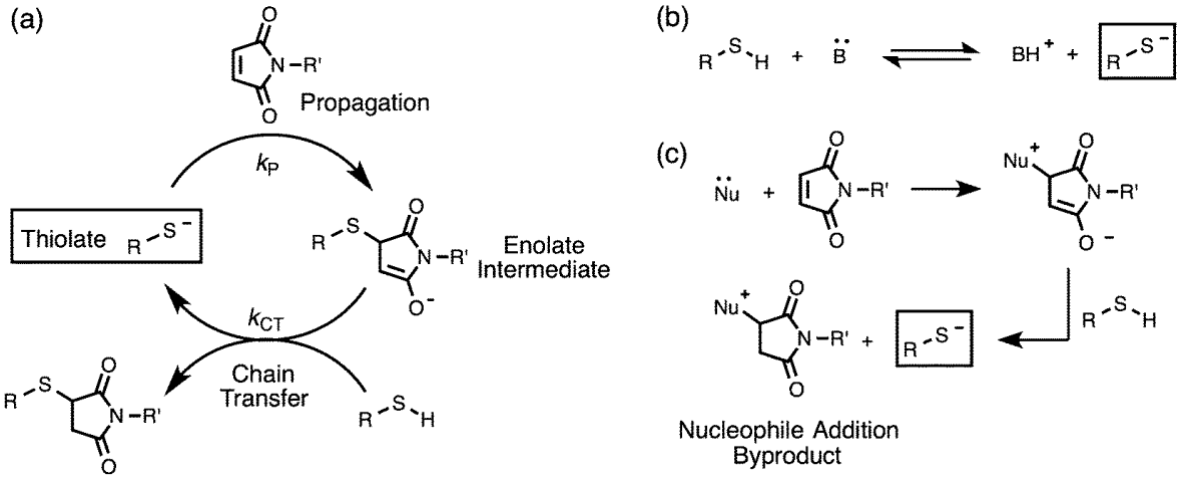

Figure 1.9. Thiol-maleimide "click" reaction mechanism [44].

Thiol-maleimide “click” chemistry has also used to fabricate hydrogels since the hydrogel system obtained with this chemistry gives a rapid gelation due to the fast kinetics of the reaction [48]. Apart from rapid gelation, there is another advantage of thiol-maleimide “click” chemistry; usually there is no need for another component. In other words, thiol and maleimide containing components starts gelation when they are mixed. Taking these into account, several examples of hydrogels obtained via thiol-maleimide “click” chemistry has been reported in literature recently [49,50].

Recently, Kloxin and co-workers developed a stimuli-responsive injectable hydrogel system via thiol-maleimide Michael addition reaction. They formed hydrogels by using heparin and PEG-based polymers via thiol-maleimide “click” reaction. In the developed system, they used o-nitrobenzyl aryl-thiol moiety containing PEGs and maleimide containing linear PEG, as well as maleimide-containing heparin to fabricate the gels. The o-nitrobenzyl group provides the responsivity to applied light, while the retro-Michael reaction provides degradability in the presence of reducing environment (Figure 1.10) [51].

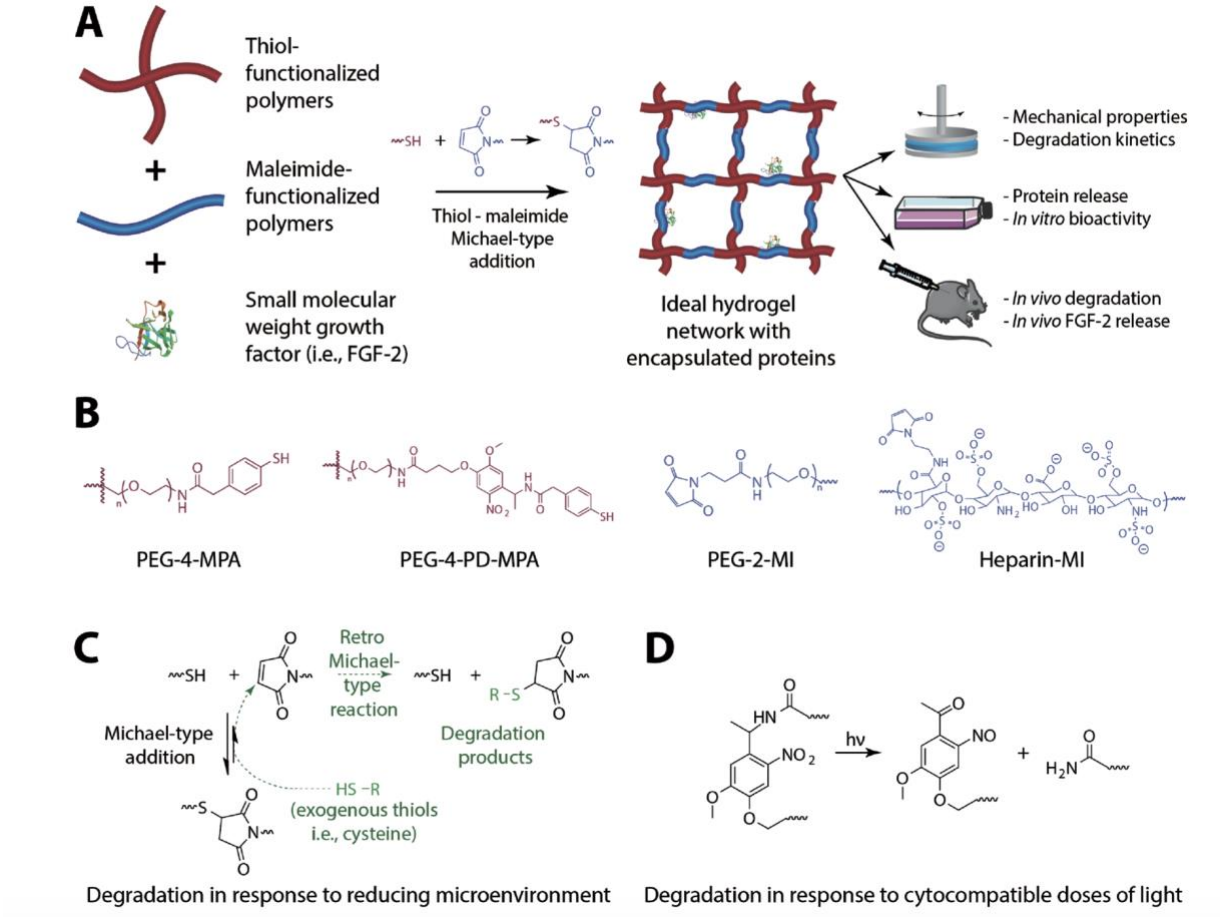

Figure 1.10. Schematic illustration of stimuli-responsive hydrogel system via thiol-maleimide "click" reaction [51].

1.6. Photothermally-Responsive Hydrogels

Among the biomedical hydrogels that are responsive to various types of external stimuli, NIR-responsive hydrogels have attracted a great interest since they exhibit a particular potential for localized biomolecule delivery since NIR light provides noninvasive remote control and cadence of drug releases [52]. To obtain these smart delivery systems, incorporation of photothermal agents such as gold nanostructures, carbon nanotubes, carbon nanoparticles, graphene, copper, black phosphorus is employed [53-59]. Incorporation of these agents enables the system to convert light energy into heat, thereafter, making the system photothermally responsive.

Lately, photothermally responsive hydrogels have been used in various areas such as photothermal therapy and drug delivery systems [60-65]. To achieve controlled release induced by photothermal effect, a general method is to combine thermal responsive components and NIR-absorbing photothermal agents. In this system, photothermal agents generate a photothermal effect via getting excited by a certain wavelength of light and converting the photon energy into localized heat [66,67]. Through this process, depending on the response of the mechanism release of cargo occurs.

Among photothermal agents, reduced graphene oxide shows an important role since it has a great property of stability and rapid light-to-heat conversion under NIR irradiation. By using rGO, various release systems; such as nanogels, nanocrystals, graphene sheets has been developed lately [66-71]. When a photothermal agent introduced into the hydrogel matrix, the interaction of hydrogel with light stimuli may differ according to the type and location of the photoresponsive moiety. The responses could be crosslinking, de-crosslinking, shrinking, swelling, degradation and so on [60]. For instance, in the release mechanism, rGO containing hydrogel converts light-to-heat and it can degrade the gel if a photo-labile bond is present in the hydrogel network (Figure 1.11). Also, sol-gel transition may also lead to release of loaded cargo.

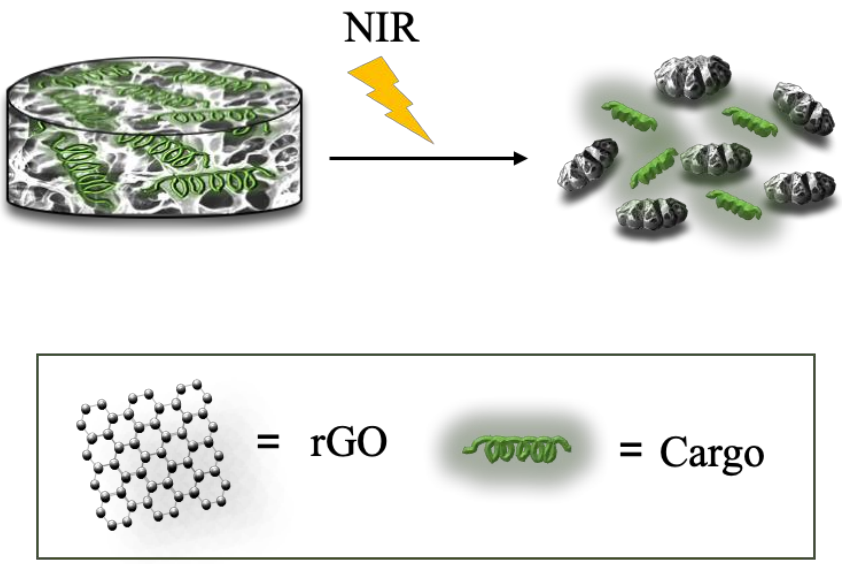

Figure 1.11. Cargo release from photothermally reactive hydrogel

Recently, Teodorescu *et al.* has developed an insulin delivery system from rGO modified hydrogels upon NIR irradiation. In the study, they have entrapped rGO into poly (ethylene glycol) dimethacrylate based hydrogels (PEGDMA-rGO), and managed to load insulin afterwards. Obtained hydrogels gave an efficient on-demand delivery platform for insulin under NIR irradiation due to photothermal effect of rGO (Figure 1.12) [72]. In another study, Wang et al. established a drug delivery system for Teriparatide, a drug used for osteoporosis, from rGO loaded chitosan hydrogels (CS/rGO) that are fabricated via electrodeposition. Upon NIR irradiation, light-to-heat conversion property of rGO enabled the biomimetic delivery of Teriparatide [73].

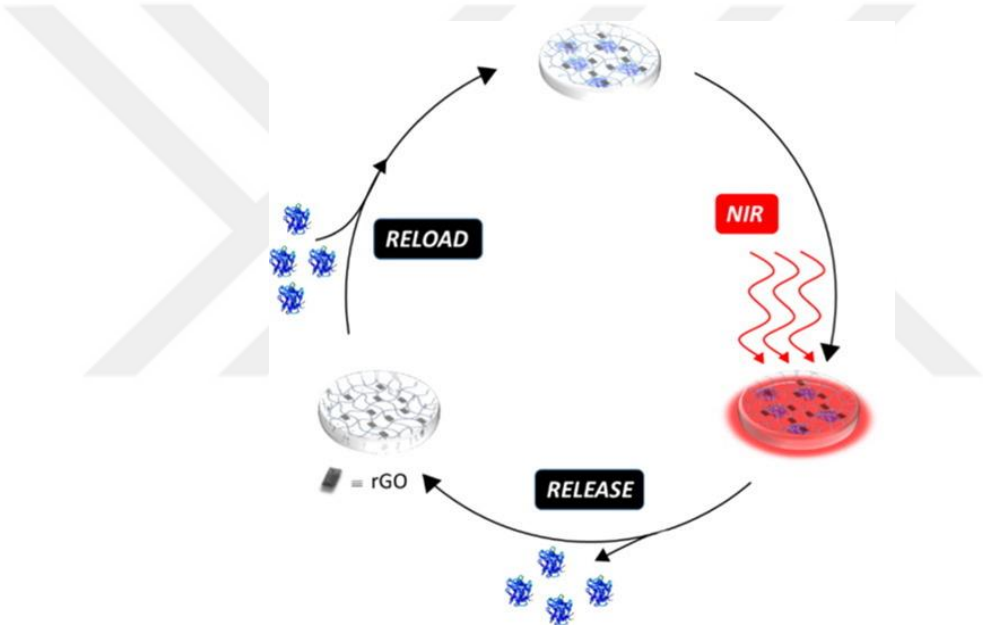

Figure 1.12. Illustration of on-demand insulin release from photothermally responsive rGO hydrogel [72].

2. PROTEIN RELEASE FROM PHOTOTHERMALLY RESPONSIVE HYDROGELS

2.1. Aim of the study

In this study, the aim is to develop a system in which on-demand protein release could be achieved from rGO containing photothermally responsive hydrogels (Figure 2.1). To this end, we first synthesized a 4-armed PEG-based polymer that has Diels-Alder cycloadduct of furan- maleimide in its structure. The reason for choosing PEG-based polymers was due to their biocompatibility, low toxicity, hydrophilicity and anti-biofouling effect. The DA reaction mechanism was chosen to introduce thermosensitivity into the hydrogel system since through the reaction two types of cycloadducts occurs; exo and endo. When the endo cycloadduct is in majority in the network of the obtained hydrogel, degradation of it could be achieved at lower temperatures than the one required for exo cycloadduct. To obtain hydrogels, we reacted DA cycloadduct containing PEG polymer with thiol bearing 4-armed PEG polymer through Michael addition type thiol-maleimide click reaction to obtain hydrogels. Here, thiol-maleimide click reaction was chosen to prepare hydrogels due to its fast kinetics. In this process, rGO was introduced into the gel matrices as well as three types of FITC-Dextrans of different molecular weights that similar of proteins. In the obtained hydrogels, to control the physical properties different w/v hydrogels prepared since the change in the w/v ratio leads to change in porosity of hydrogels as well as their release trend. Once the release trends of the dyes were analyzed passively, active releases of them under NIR irradiation have been analyzed. The aim here is to show that under NIR light rGO converts light to heat in a rapid way and the heated hydrogels start to degrade by going through retro-DA reaction. Thus, a protein can be released in a controlled way from photothermally responsive hydrogels.

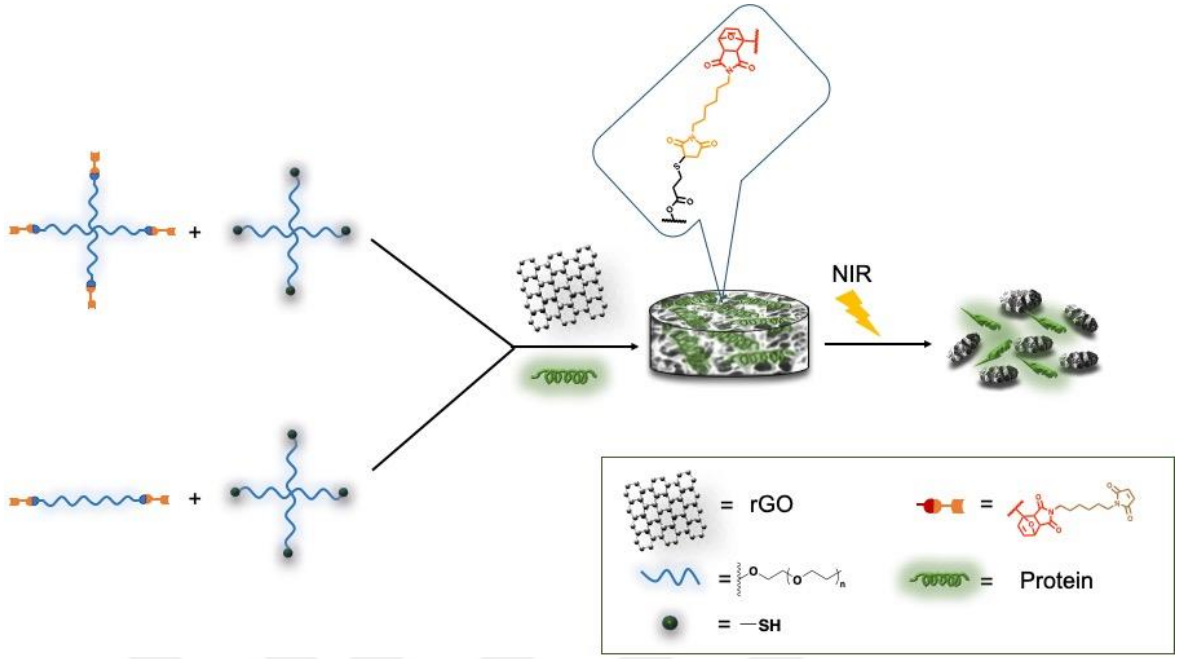

Figure 2.1. Illustration of aim of the project.

2.2. Experimental

2.2.1. Materials

3-Bromo-1-propene, methanol, chloroform, triethylamine and maleic anhydride were purchased from Merck. 1,6-Diaminohexane (>98%), p-toluenesulfonic acid (98%), 1,4-dithio-DL-threthiol (DTT) (98%) were purchased from Alfa Aesar. 2,2-Dimethoxy-2-phenylacetophenone (99%), 2-mercaptopropionic acid (>99%), furan (>99%), furfuryl methacrylate (97%), poly (ethylene glycol) (PEG, M_n 6k), sodium hydride (60% dispersed in mineral oil) were purchased from Sigma-Aldrich.

2.2.2. Instrumentation

Cross-linker and synthesized polymer characterizations was carried out with ^{1}H NMR spectroscopy (Varian 400 MHz). Microstructures of the hydrogels were investigated with JEOL NeoScope JCM-5000 scanning electron microscopy (SEM) instrument at an accelerating voltage of 10 kV. Hydrogel rheological behaviors were evaluated by measuring the loss (G”) and storage (G’) moduli of the hydrogel as a function of angular frequency and

time using Anton PAAR MCR 302 rheometer. ATR-FT-IR data were collected by attenuated total reflection Fourier transform infrared (ATR-FT-IR) spectroscopy (Nicolet 380, Thermo Scientific). UV spectrum were measured with a Varian Cary-100 UV-Vis Spectrophotometer.

2.2.3. Synthesis of Bismaleimide Crosslinker

A three-step synthesis route was followed to synthesize bismaleimide. First, furan protection of maleimide was performed. Second, protected bismaleimide synthesized and lastly retro-DA reaction performed to remove protection group according to literature procedure [74]. The obtained cross-linker was characterized using ^{1}H-NMR.

2.2.4. Synthesis of Linear PEG-based Allyl (PEG-Bis-A)

To obtain this polymer, S_N2 reaction was performed. In this process, NaH was used to dehydrogenate hydroxyl groups of PEG and 3-bromo-1-propene (allyl bromide) was added into the mixture to achieve S_N2. To achieve 100% conversion, NaH and allyl bromide was added excessively. To obtain PEG-Bis-allyl, Poly(ethylene glycol) (PEG, M_n 6kDa, 100 mg, 0.016 mmole) and solvent (THF, 5 mL) were added to a round bottom flask. NaH (8.83 mg, 0.128 mmole) was added into PEG solution. After obtaining a turbid solution with removal of H_2 gas 3-bromo-1-propene (33.74 µL, 0.4 mmole) was added to PEG solution. Reaction was left stirring for 24h under N_2 atmosphere. To remove excess NaH, reaction mixture was filtered; and for further purification, the product was concentrated on a rotary evaporator and precipitated in cold diethyl ether. The resulting polymer was dried in high vacuum. ^{1}H NMR (400 MHz, $CDCI_3$, δ, ppm2), 5.90 (m, 1H, CH_2=C*H*-), 5.15 (d, 2H, C*H*-H=CH-), 4.02 (d, 2H, CH-*H*=CH-).

2.2.5. Synthesis of 4-PEG-Allyl (PEG-Tetra-A)

To obtain these polymers, S_N2 reaction was performed. In this process, NaH was used to dehydrogenate 4-PEG-OH and 3-bromo-1-propene (allyl bromide) was added into the mixture to achieve S_N2. To achieve 100% conversion, NaH and allyl bromide was added excessively. Firstly, 4-armed PEG-OH (M_n 10kDa, 500 mg, 0.050 mmole) was dissolved in

anhydrous THF (5mL) and NaH (30 mg, 0.800 mmole) was added to the dissolved polymer slowly. After obtaining a turbid mixture, allyl bromide (202.47 μL, 2.4 mmole) was added to the mixture and the reaction mixture was left stirring overnight at 37 °C. The resulting polymer mixture was filtered to remove precipitates and obtained solution was concentrated via rotary evaporation. Concentrated crude was precipitated in cold diethyl ether for further purification. The resulting polymer was dried in vacou. ^{1}H NMR was used to characterize the resulting polymer. ^{1}H NMR (400 MHz, $CDCl_3$, δ, ppm), 5.90 (m, 2H, CH_2=C*H*-), 5.15 (d, 4H, C*H*-H=CH-), 4.02 (d, 4H, CH-*H*=CH-).

2.2.6. Synthesis of furan containing linear polymer (PEG-Bis-F)

To obtain this polymer, thiol-ene click chemistry was performed between PEG-Bis-A and furane-2-methyl thiol. Briefly, linear PEG-Bis-A (60.82 mg, 0.01 mmole) was dissolved in 50 μL dry THF and oxygen is removed by using N_2. 2,2-Dimethoxy-2-phenylacetophenone (DMPA, 2.05 mg, 0.008 mmole) and 2-Furanmethanethiol (98% purity, 19.02 μL, 0.2 mmole) were added into PEG solution. Reaction mixture is left to react under 365 nm UV light for 3h. The product was concentrated on a rotary evaporator and precipitated in cold ether for further purification. ^{1}H NMR (400 MHz, $CDCI_3$, δ, ppm), 7.35 (s, 2H, CH=C*H*O), 6.30 (d, 2H, furan H's), 6.15 (d, 2H, furan H's), 2.55 (t, 4H, -C*H*$_2$-OCH_2-).

2.2.7. Synthesis of furan containing four-armed PEG (PEG-Tetra-F)

To obtain PEG-Tetra-F, thiol-ene click chemistry was performed between PEG-Tetra-A and furane-2-methyl thiol. Briefly, PEG-Tetra-A (100 mg, 0.01 mmole) was dissolved in 100 μL anhydrous THF in a sealed vial and purged with nitrogen gas. Later on, DMPA (2.04 mg, 0.008 mmole) and furan-2-methyl thiol (38 μL, 0.4 mmole) were added to the polymer solution. The reaction mixture was left stirring under 365 nm UV light. The resulting polymer, PEG-Tetra-F, was precipitated in cold diethyl ether for purification. The precipitate was dried in *vacuo* and characterized using ^{1}H NMR. ^{1}H NMR (400 MHz, $CDCI_3$, δ, ppm), 7.35 (s, 4H, CH=C*H*O), 6.30 (d, 4H, furan H's), 6.15 (d, 4H, furan H's), 2.55 (t, 8H, -C*H*$_2$-OCH_2-).

2.2.8. Synthesis of maleimide containing linear polymer (PEG-Bis-M)

To achieve this polymer, Diels-Alder cycloaddition reaction was performed between furan functional group of and maleimide group of bismaleimide. To obtain PEG-Bis-M, 1,6-Bismaleimidohexane (69.07 mg, 0.25 mmole) and furan containing linear PEG (150 mg, 0.025 mmole) were dissolved in 2 mL $CHCl_3$ and added into a round bottom flask. Reaction mixture was left stirring for 72 h at 37 °C to obtain endo product. For exo product, same amount of ingredients were dissolved in toluen and left stirring at 110 °C for 24h. The product obtained was concentrated on a rotary evaporater and precipitated in cold ether for further purification. ^{1}H NMR (400 MHz, $CDCI_3$, δ, ppm), 6,67(s, 4H, maleimide), 6,50 (s, 2H, cycloadduct H's), 6,40 (d, 1H, cycloadduct H's), 6,30 (d, 1H, cycloadduct H), 6,20-6,25 (s,d, 2H, cycloadduct H).

2.2.9. Synthesis of maleimide containing four-armed polymer (PEG-Tetra-M)

To achieve this polymer, Diels-Alder cycloaddition reaction was performed between furan functional group of and maleimide group of bismaleimide. For PEG-Tetra-M synthesis, PEG-Tetra-F (200 mg, 0.020 mmole) was dissolved in 2 mL chloroform. Synthesized bismaleimide (110.52 mg, 0.4 mmole) was added into the PEG-Tetra-F solution. Reaction mixture was left stirring for 72h at 37 ºC. For purification, resulting polymer was precipitated in cold diethyl ether. The obtained polymer was dried in vacou and characterized using ^{1}H NMR. ^{1}H NMR (400 MHz, $CDCI_3$, δ, ppm), 6.67 (s, 8H, maleimide H), 6.50 (s, 4H, cycloadduct H's), 6.40 (d, 2H, cycloadduct Hs), 6.30 (d, 2H, cycloadduct H), 5,20-5.25 (s, d, 4H), 2.70 (p, 8H), 1,80 (p, 8H).

2.2.10. Synthesis of tetra thiol (4-TSH)

4-armed poly (ethylene glycol) (260 mg, 0.026 mmole) was dissolved in 20 mL dry toluene. 3-mercaptopropionic acid (1.84 mL, 1.4 mmole) and p-toluensulfonic acid (1.97 mg, 0.014 mmole) added into PEG solution. Reaction mixture was left stirring for 48h at 110 °C under by using Dean-Stark. The product was concentrated on a rotary evaporator and precipitated

in cold ether. For further work-up, 4-TSH (200 mg,0.02 mmole) was treated with 1,4-dithio-DL-threthiol (DTT, 98% purity, 3.11 mg, 0.02 mmole) to reduce oxidized thiol groups. After the product was concentrated on a rotary evaporator, it was precipitated in cold ether to obtain the final product. The resulting polymer was dried under high vacou and characterized via 1H-NMR. 1H NMR (400 MHz, CDCI3, δ, ppm), 4,30 (t, 8H), 2,75 (t, 8H), 2,65 (t, 8H).

2.2.11. Synthesis of rGO

GO (150 mg, 3 mg mL^{-1}) was sonicated for three hours. To obtained GO suspension, hydrazine hydrate (50 μL, 1.03 mmole) was added drop-wise. Reaction mixture was left stirring for 24 hours at 100 °C. The resulting black precipitate was filtered through poly (vinylidene fluoride) membrane (45 μm pore size). The residue was washed with distilled water (20 mLx5) and methanol (20 mLx5) respectively. Lastly, the resulting rGO was dried in the vacuum oven at 65 °C. Obtained rGO was characterized by using FT-IR and UV.

2.2.12. Synthesis of Bis-PEG Hydrogels (w/o rGO)

Bis-PEG hydrogels were prepared with three different w/v % concentrations as 5% and 10% w/v by dissolving respective polymers of PEG-Bis-M (11 mg, 0.1 mmole) and 4-TSH (10 mg, 0.1 mmole) in required amount of water with a SH:MI ratio fixed to 1:1. The two polymers were mixed at room temperature and left 24 h for complete gelation. The hydrogels were rinsed with distilled water to remove unreacted polymers.

2.2.13. Synthesis of PEG-Tetra Hydrogels (w/o rGO)

PEG-Tetra hydrogels were prepared with three different w/v % concentrations as 10% w/v, 20% w/v and 30% w/v by dissolving respective polymers of 4-PEG-M (10 mg, 0.1 mmole) and 4-TSH (5 mg, 0.05 mmole) in required amount of water with a SH:MI ratio fixed to 1:1. The two polymers were mixed at room temperature and left 24 h for complete gelation. The hydrogels were rinsed with distilled water to remove unreacted polymers.

2.2.14. Synthesis of Bis-PEG rGO-Hydrogels

Bis-PEG hydrogels containing rGO were prepared similar to the ones without rGO. Briefly, hydrogels were prepared with three different w/v % concentrations as 10% w/v and 30% w/v by dissolving respective polymers of PEG-Bis-M (10 mg, 0.1 mmole) and 4-TSH (10 mg, 0.1 mmole) in required amount of rGO dispersion (0.1%) with a SH:MI ratio fixed to 1:1. The two polymers were again mixed at room temperature and left 24 h for complete gelation. The hydrogels were rinsed with distilled water to remove unreacted polymers.

2.2.15. Synthesis of PEG-Tetra rGO-Hydrogels

PEG-Tetra hydrogels containing rGO were prepared similar to the ones without rGO. Briefly, hydrogels were prepared with three different w/v % concentrations as 10% w/v, 20% w/v and 30% w/v by dissolving respective polymers of PEG-Tetra-M (11 mg, 0.1 mmole) and 4-TSH (10 mg, 0.1 mmole) in required amount of rGO dispersion (0.1%) with a SH:MI ratio fixed to 1:1. The two polymers were again mixed at room temperature and left 24 h for complete gelation. The hydrogels were rinsed with distilled water to remove unreacted polymers.

2.2.16. Characterization of Hydrogels

Gelation yields of hydrogels**. -** For calculation of the gelation yield of hydrogels gravimetric analysis is used. After 24h, hydrogels were washed with distilled water to remove unreacted polymers and cross-linkers. Later on, water inside the hydrogels were removed by using lyophilizer. To calculate yield of hydrogels, dried masses of hydrogels (W_{dry}) was used by using equation (W_{dry}/W_{p+c})*100 where W_{p+c} was the total mass of polymer (p) and crosslinker (c).

Swelling studies. - For swelling test, lyophilized hydrogels (20 mg) were dipped in deionized water at room temperature and each hydrogel was weighed after removal of water from the surface at periodic time intervals. Until no weight increase was observed, water uptake experiment was performed. For each hydrogel, three sets of experiment performed to

calculate degree of swelling. For the calculation, $(M_s/M_{dry})*100$ equation was used where M_s and M_{dry} refers to weight of swollen and dry hydrogels, respectively.

Imaging of microstructure. – Microstructure of hydrogels were investigated using SEM at an accelerating voltage of 10 kV. Porosity of the hydrogels were investigated and compared for all gels.

2.2.17. Determination of Remaining Thiol Groups in Hydrogels

To determine unreacted thiol groups inside the hydrogels, Ellman's test has been performed. 5,5-dithiobis-(2-nitrobenzoic acid), the Ellman's reagents, is known to give an absorbance peak at 412 nm in the presence of free thiols. Later, by using extinction coefficient of Ellman's reagent, the amounts of free thiols inside the hydrogels were calculated to investigate % conversion of hydrogels.

2.2.18. Rheological Studies

To investigate the effect of concentration variance on physical properties of hydrogels, Anton Paar MCR 302 rheometer was used. 15 mm diameter plate was used as the test geometry. For rheological analysis, prepared disk-shaped hydrogels were immersed in distilled water. After swelling of hydrogels completed, to check the linear-viscoelastic limit regime (LVR), strain sweep test was performed between values of 0.01 to 100% at an angular frequency of 10 rad/s at 25°C. To determine the lower frequency limit of hydrogel behavior, frequency sweep test with suitable strain value was performed between values of 0.1 to 100 rad/s at a fixed strain value of 1% at 25°C. In these tests, G' (storage modulus) and G'' (loss modulus) were recorded.

2.2.19. Loading FITC-Dextran to Hydrogels

FITC-Dextran (M_n= 70 kDa) was encapsulated into hydrogel matrix in the gel preparation process. For this purpose, the total of 100 μg FITC-dextran was added into rGO/water dispersion that was used to dissolve polymers to achieve homogenous mixture. After gelation completed, the hydrogels were washed with distilled water to remove FITC-dextran from the surface. Later on, to determine removed FITC-dextran UV measurement was done.

2.2.20. Passive Release from rGO-Hydrogel

To investigate the passive release of FITC-dextran from rGO containing hydrogels, UV spectroscopy was used since FITC-dextran gives an absorbance peak at 490 nm. Firstly, FITC-loaded rGO containing hydrogels were synthesized. After gelation, gels were washed with PBS to remove the dye from the surface. The absorbance of the collected solution was measured in UV. After the washing, hydrogels were immersed into 1 mL PBS buffer and every hour PBS solution was measured in UV to determine % release of the hydrogels.

2.2.21. Active Release from rGO-Hydrogels

To investigate the active release of FITC-Dextran from PEG-Tetra-M-HG-rGO_{30}, the hydrogel was heated up to 70 °C under NIR (980 nm, 1.2 W) for 15 minutes intervals for four times. Firstly, 100 μg FITC-dextran containing PEG-Tetra-M-HG-rGO_{30} was synthesized. After gelation, the gel was washed with PBS to remove the dye from the surface as well as to remove the unreacted PEGs. When the washing was done, the gel was soaked into 1 mL PBS. After the gel was heated the absorbance at 495 nm was measured and waited to cool down. After the gel cooled, the absorbance was measured again in the UV.

2.2.22. NIR Heating Experiment of rGO-Hydrogel

To investigate photothermal responsivity of rGO containing hydrogel, PEG-Tetra-M-HG-rGO_{30} was heated to 70 °C with NIR laser (1.2 W, 980 nm) for 15 minutes time intervals for four times. After each interval, the gel was taken and storage modulus was measured in rheometer.

2.3. Results and Discussion

2.3.1. Synthesis and characterization of BMI

Three steps reaction was performed to obtain BMI. Firstly, maleic anhydride was protected with furan via DA reaction. Secondly, a diamine was used to obtain a molecule that has maleimide at both ends. Lastly, retro-DA reaction was performed to remove furan ring that was used to protect maleimide at first step (Figure 2.2).

First step reaction was obtained with a yield of 55%. When furan protected maleic anhydride was characterized by ^{1}H-NMR, three peaks were observed belonging to DA cycloadduct at 6.50, 5.25 and 3.45 ppm (Figure 2.3). Second step was obtained with a yield of 22.32% and ^{1}H-NMR characterization showed three additional peaks at 2.75, 1.50 and 1.25 ppm belonging to hexyl group of diamine (Figure 2.4). Last step obtained with 100% yield resulting in unprotected BMI. In ^{1}H-NMR, peaks belonging to cycloadduct were removed and a new peak emerged at 6.67 ppm indicating successful retro-DA reaction (Figure 2.5).

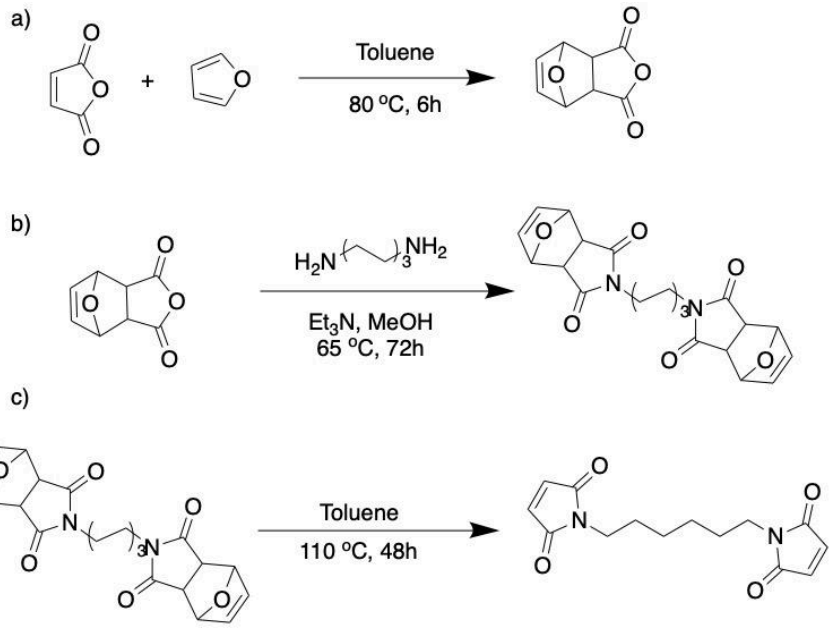

Figure 2.2. Synthesis of BMI.

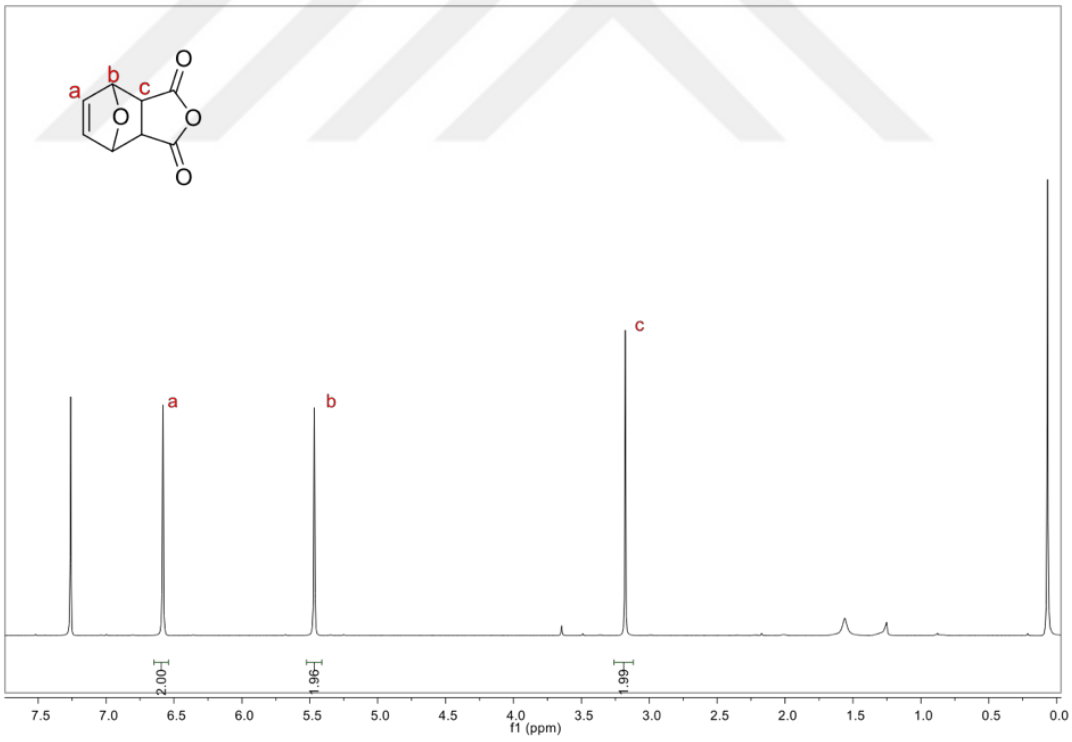

Figure 2.3. ^{1}H-NMR spectrum of protected maleic anhydride.

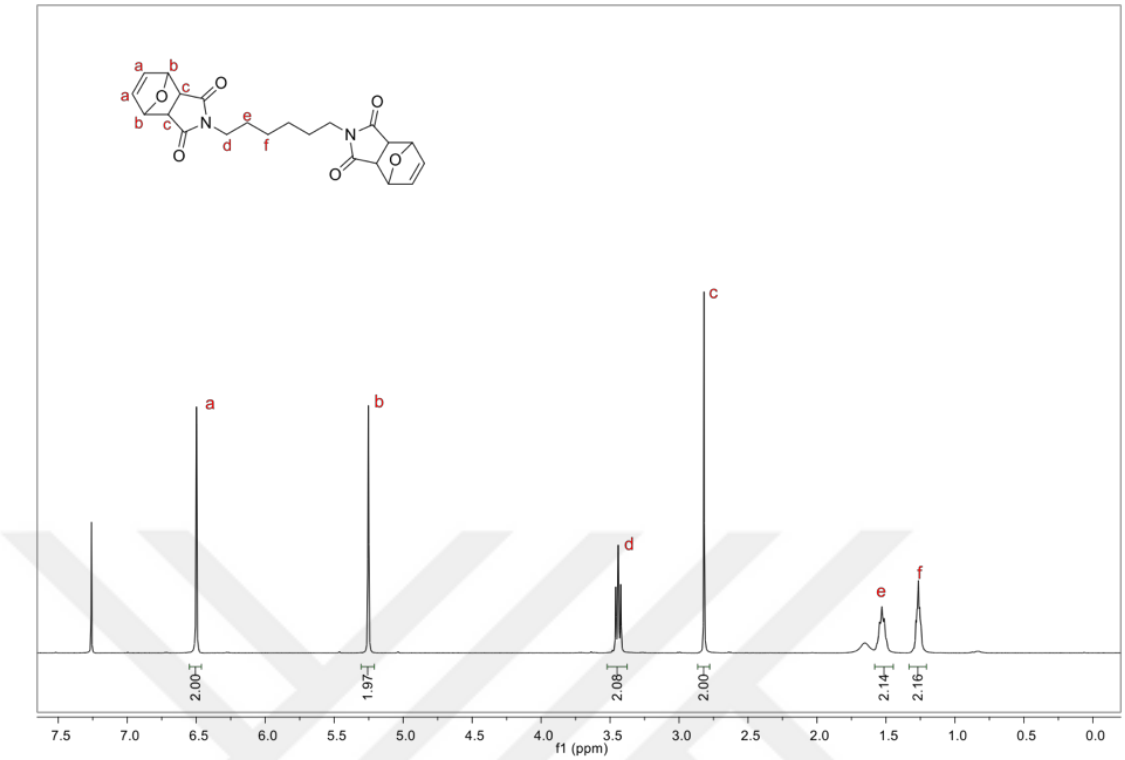

Figure 2.4. ^{1}H-NMR spectrum of protected BMI.

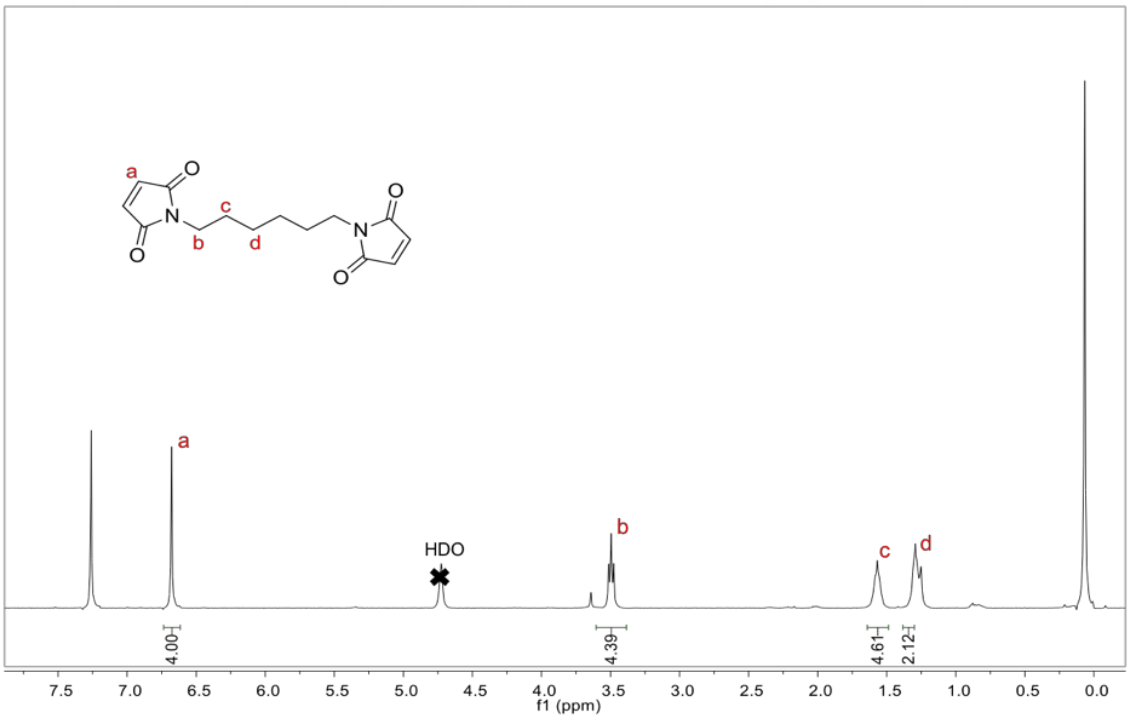

Figure 2.5. ^{1}H-NMR spectrum of BMI.

2.3.2. Synthesis and characterization of PEG-Bis-A

In the synthesis process of PEG-Bis-A, hydroxyl groups of linear PEG were converted into negatively charged nucleophile with the help of NaH. After dehydrogenation of PEG, allyl bromide and PEG were reacted to result in allylation of hydroxyl groups via S_N2 reaction (Figure 2.6).

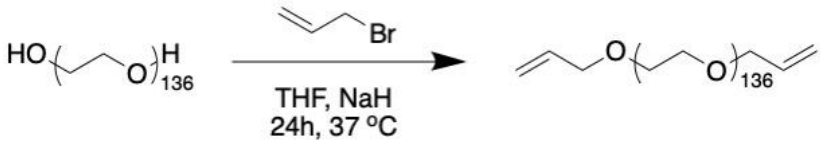

Figure 2.6. Synthesis of PEG-Bis-A.

After the calculation, the yield for PEG-Bis-A was found to be 94%. In ^{1}H-NMR characterization, the peaks appeared in 5.90, 5.15 and 4.20 ppm belonging to allyl functional groups at the end of PEG (Figure 2.7). The appearances of these peaks and their integrations showed that S_N2 reaction was achieved with 100% conversion.

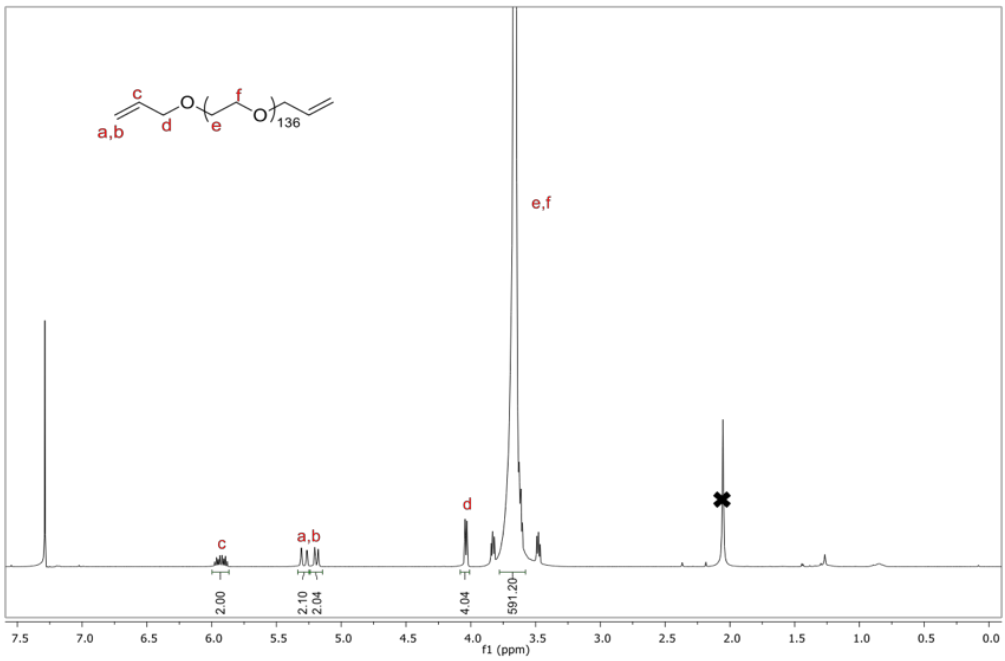

Figure 2.7. ^{1}H-NMR of PEG-Bis-A.

2.3.3. Synthesis and characterization of PEG-Tetra-A

In the synthesis process of PEG-Tetra-A, hydroxyl groups of four-armed PEG were converted into negatively charged nucleophile with the help of NaH. After dehydrogenation of PEG, allyl bromide and PEG were reacted to result in allylation of hydroxyl groups via S_N2 reaction (Figure 2.8).

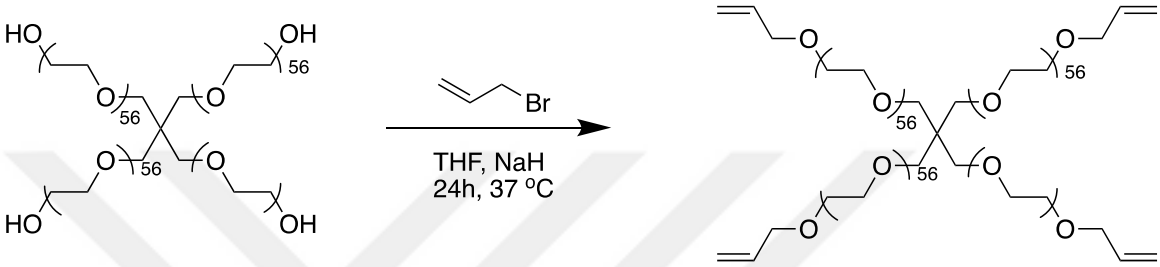

Figure 2.8. Synthesis of PEG-Tetra-A.

After the calculation, the yield for PEG-Tetra-A was found to be 94.3%. In ^{1}H-NMR characterization, the peaks appeared in 5.90, 5.15 and 4.20 ppm belonging to allyl functional groups at the end of PEG (Figure 2.9). The appearances of these peaks and their integrations showed that S_N2 reaction was achieved with 100% conversion.

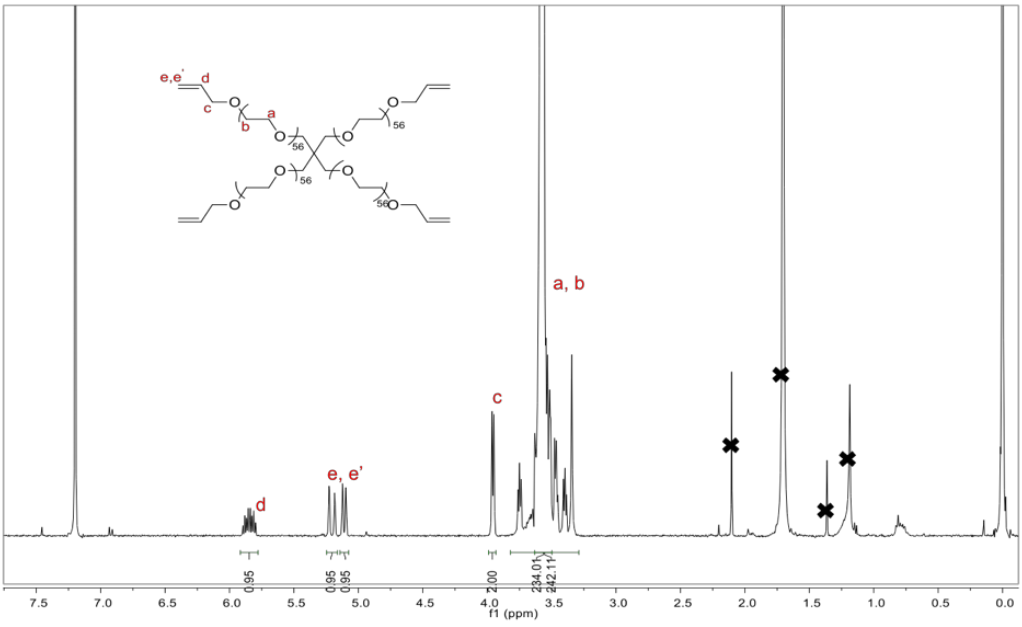

Figure 2.9. ^{1}H-NNMR of PEG-Tetra-A.

2.3.4. Synthesis and characterization of furan containing polymer (PEG-Bis-F)

Once the PEG-Bis-A was obtained, its allyl functional groups were used to add furfuryl thiol into PEG structure via thiol-en click reaction in the presence of a photo-initiator DMPA under 365 nm UV light (Figure 2.10). The reason for incorporating furan group into PEG structure is to introduce DA cycloaddition ring into the hydrogel structure. PEG is chosen due to its hydrophilicity here. The thiol-ene reaction is sensitive to oxygen. Thereafter, in order to convert all of allyl groups to furan groups different amounts of furfuryl thiol have been used to adjust suitable reaction condition (Table 2.1).

Table 2.1. Optimization of thiol-ene "click" reaction.

PEG-Bis-A	DMPA	Furan-2-metil tiyol	% Dönüşüm
0.01 mmol	0.008 mmol	0.04 mmol	64
0.01 mmol	0.008 mmol	0.1 mmol	87
0.01 mmol	0.008 mmol	0.2 mmol	100

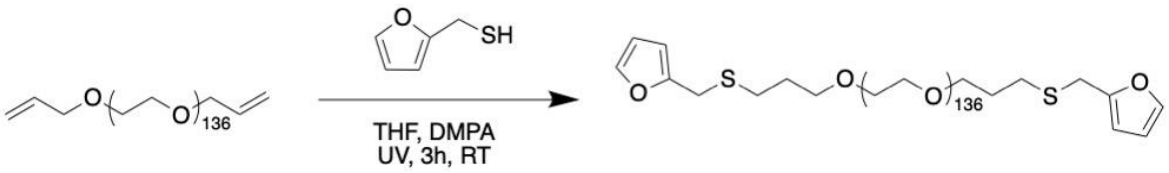

Figure 2.10. Synthesis of PEG-Bis-F.

Calculated yield was found to be 95% after thiol-ene click reaction for PEG-Bis-F. In ^{1}H-NMR, the peaks belonging to allyl at 5.90, 5.15 and 4.20 disappeared and new furan peaks emerged at 7.35, 6.30, 6.15, 2.55 and 1.80 ppm (Figure 2.11). Three peaks coming at 7.35, 6.30 and 6.15 ppm belong to furan ring whereas the peaks coming at 2.55 and 1.80 ppm belong to ethylene groups next to sulfur.

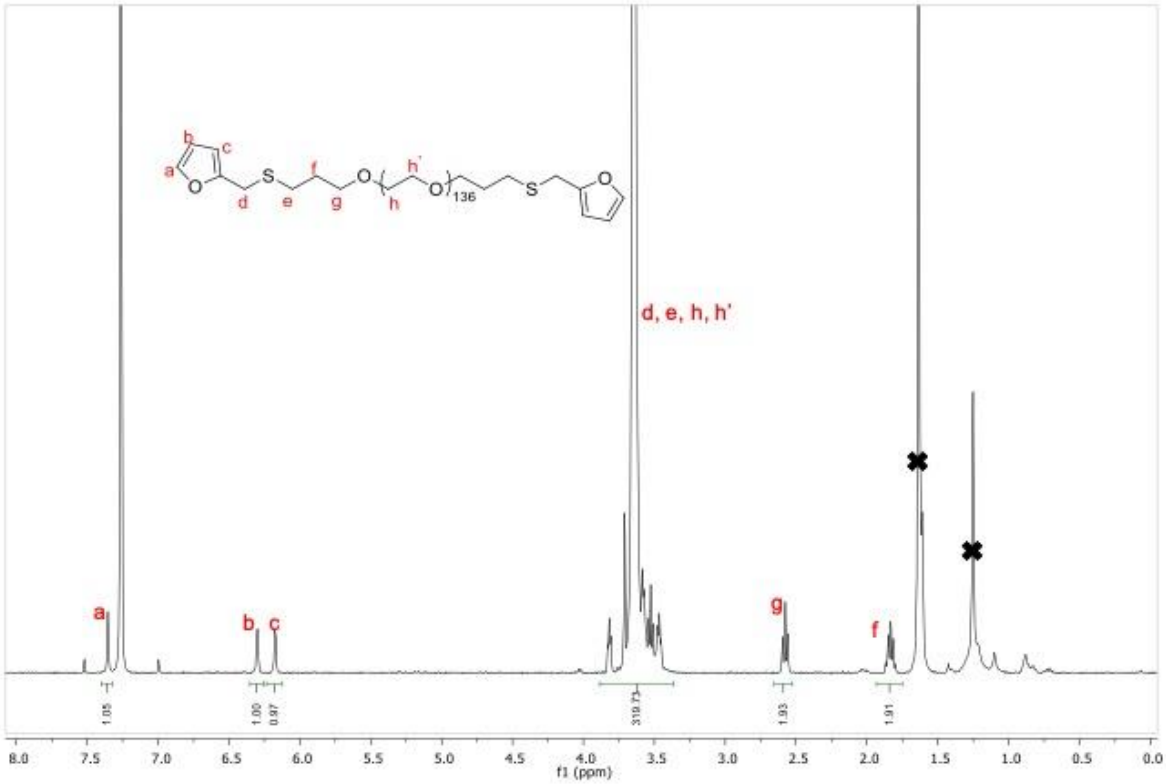

Figure 2.11. ^{1}H-NMR spectrum of PEG-Bis-F.

2.3.5. Synthesis and characterization of furan containing four-armed polymer (PEG-Tetra-F)

Once the PEG-Tetra-A was obtained, its allyl functional groups were used to add furfuryl thiol into PEG structure via thiol-en click reaction in the presence of a photo-initiator DMPA under 365 nm UV light (Figure 2.12). The reason for incorporating furan group into PEG structure is to introduce DA cycloaddition ring into the hydrogel structure. PEG is chosen due to its hydrophilicity here.

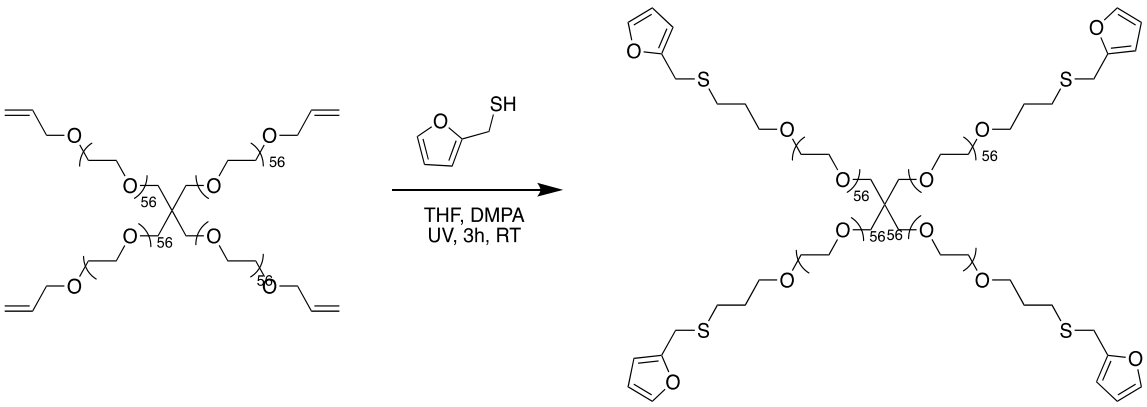

Figure 2.12. Synthesis of PEG-Tetra-F.

Calculated yield was found to be 81% after thiol-ene click reaction for PEG-Tetra-F. In ^{1}H-NMR, the peaks belonging to allyl at 5.90, 5.15 and 4.20 disappeared and new furan peaks emerged at 7.35, 6.30, 6.15, 2.55 and 1.80 ppm (Figure 2.13). Three peaks coming at 7.35, 6.30 and 6.15 ppm belong to furan ring whereas the peaks coming at 2.55 and 1.80 ppm belong to ethylene groups next to sulfur.

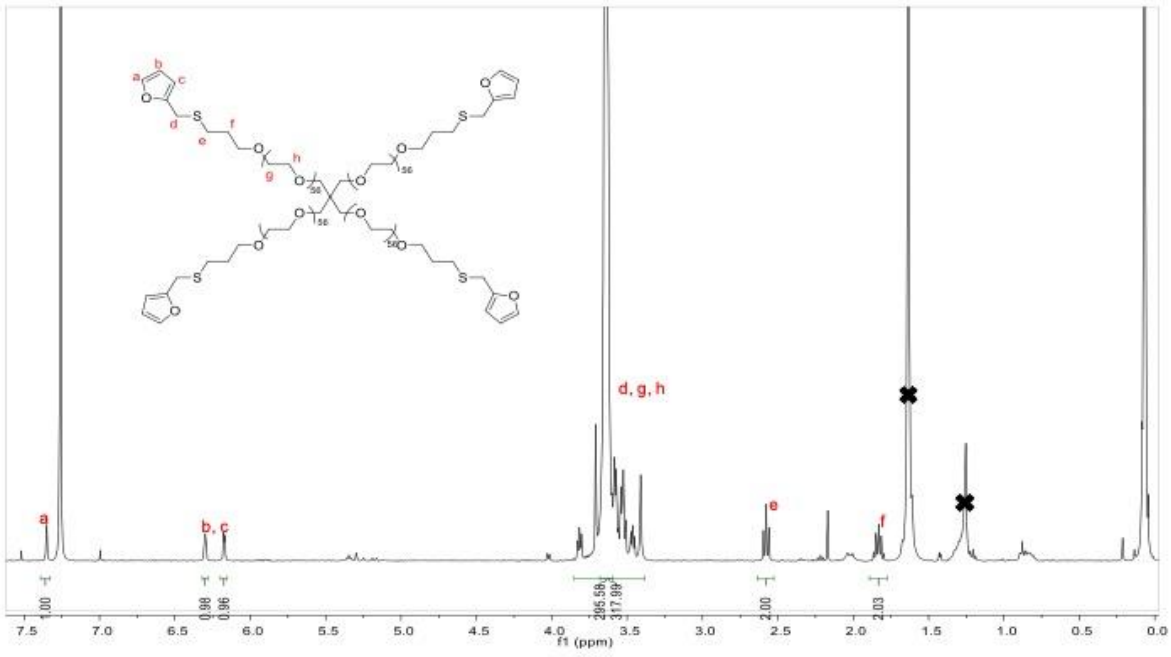

Figure 2.13. ^{1}H-NMR spectrum of PEG-Tetra-F.

2.3.6. Synthesis and characterization of maleimide containing polymers (PEG-Bis-M)

This polymer that are going to be used to synthesize hydrogels were synthesized via DA cycloaddition chemistry (Figure 2.14). The reason for choosing the DA reaction is to introduce a thermoresponsive junction point into hydrogel matrix. In the synthesis process, obtained polymers were both containing exo and endo cycloadducts. The presence of endo cycloadduct enables the degradation of hydrogels at lower temperatures than the one required for exo cycloadduct.

After the synthesis, the yield of PEG-Bis-M was calculated 88%. In the ^{1}H-NMR spectrum, the peaks belonging to furan at 7.35, 6.30 and 6.15 ppm were disappeared as well as new peaks belonging to furan-maleimide cycloadduct appeared at 6.50, 6.40, 6.30 and 6.20-6.25 ppm. The peaks coming at 6.20-6.25 ppm were used to calculate endo:exo ratio as 1:1. Also, free maleimide peak observed at 6.67 ppm (Figure 2.15).

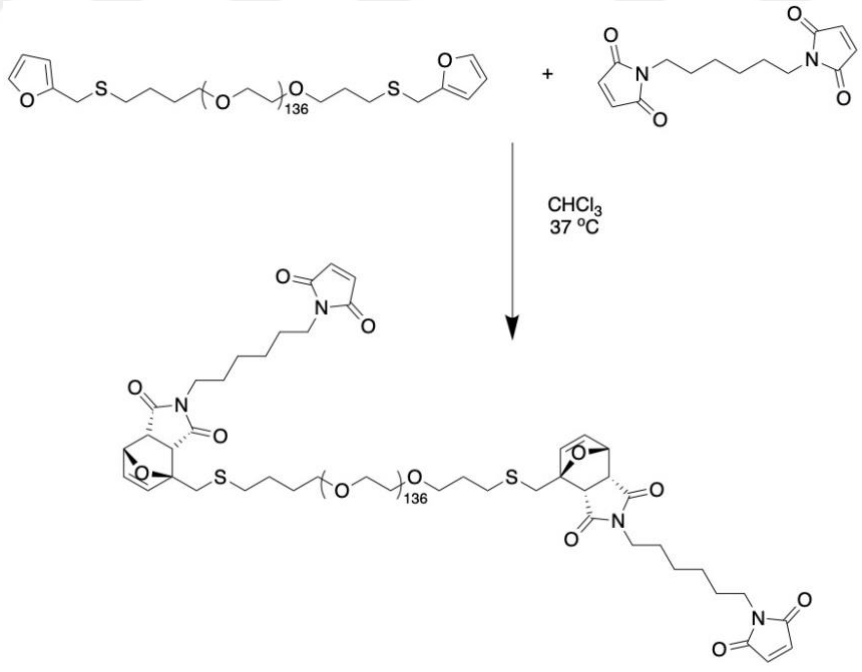

Figure 2.14. Synthesis of PEG-Bis-M.

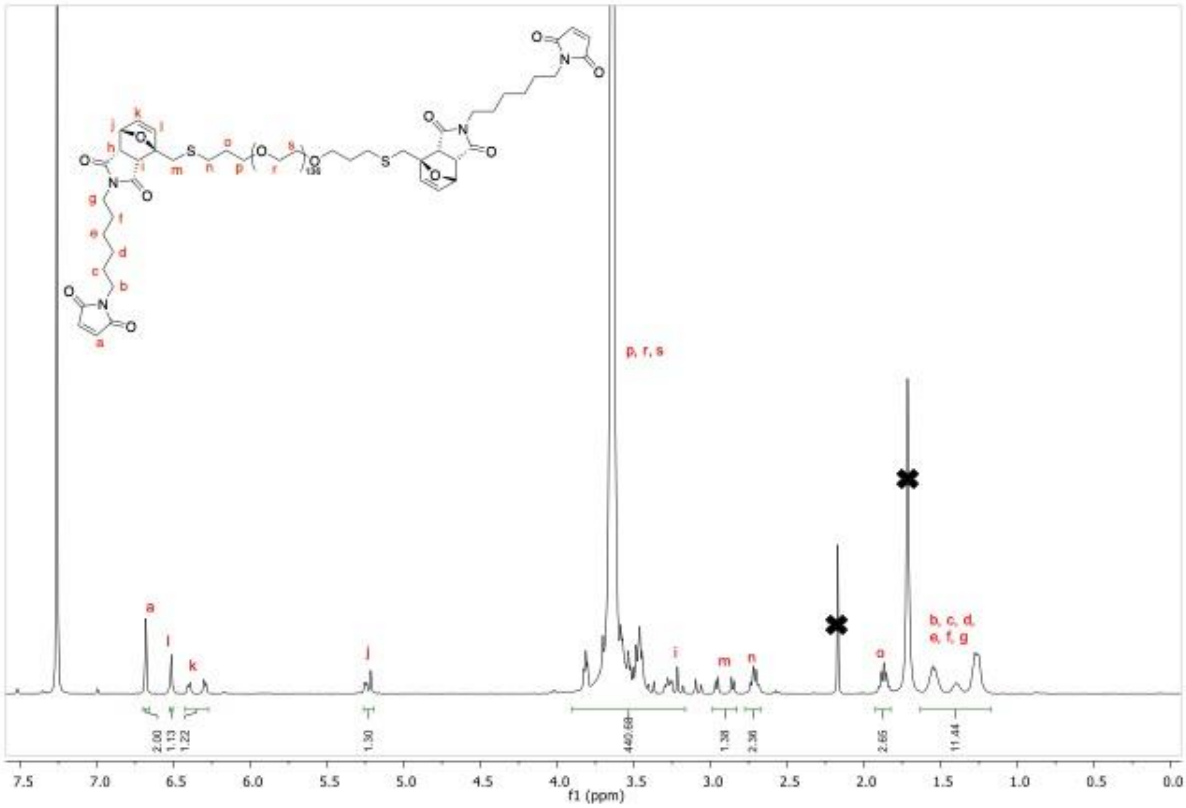

Figure 2.15. 1H-NMR of PEG-Bis-M.

2.3.7. Synthesis and characterization of maleimide containing polymers (PEG-Tetra-M)

This polymer that are going to be used to synthesize hydrogels were synthesized via DA cycloaddition chemistry (Figure 2.16). The reason for choosing the DA reaction is to introduce a thermoresponsive junction point into hydrogel matrix. In the synthesis process, obtained polymers were both containing exo and endo cycloadducts. The presence of endo cycloadduct enables the degradation of hydrogels at lower temperatures than the one required for exo cycloadduct.

After the synthesis, the yield of PEG-Tetra-M was calculated 86%. In the ^{1}H-NMR spectra of both polymers, the peaks belonging to furan at 7.35, 6.30 and 6.15 ppm were disappeared as well as new peaks belonging to furan-maleimide cycloadduct appeared at 6.50, 6.40, 6.30 and 6.20-6.25 ppm. The peaks coming at 6.20-6.25 ppm were used to calculate endo:exo ratio as 1:1. Also, free maleimide peak observed at 6.67 ppm (Figure 2.17).

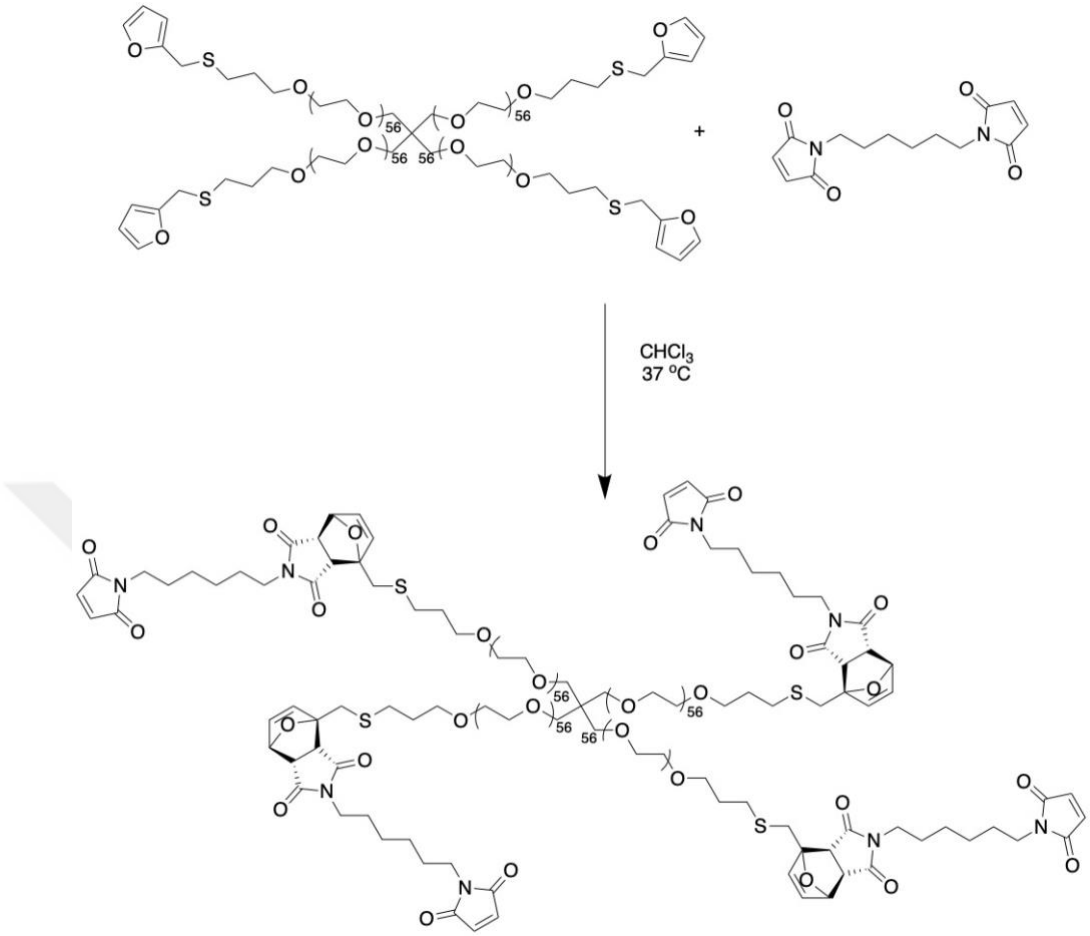

Figure 2.16. Synthesis of PEG-Tetra-M.

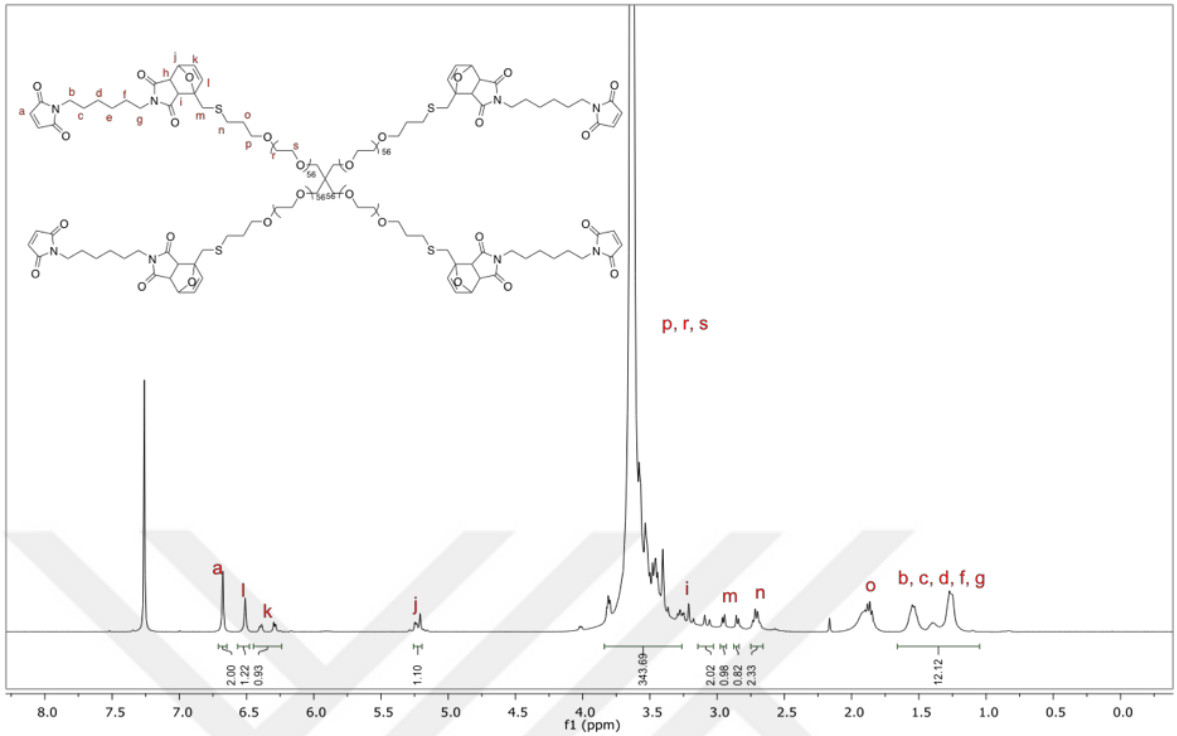

Figure 2.17. ^{1}H-NMR of PEG-Tetra-M.

2.3.8. Synthesis of 4-TSH

This esterification reaction (Figure 2.18) is known to be water sensitive; therefore, dean-stark set-up was used in this reaction to remove water that formed as a byproduct. After the reaction completed, DTT treatment was required to reduce possible disulfide bonds in the polymer structure. After purification, the yield of the reaction was calculated 70%. In ^{1}H-NMR, additional triplets at 4.30, 2.75 and 2.65 ppm were observed (Figure 2.19). These peaks and the integration of PEG hydrogens indicate 100% conversion of four-armed PEG into TSH.

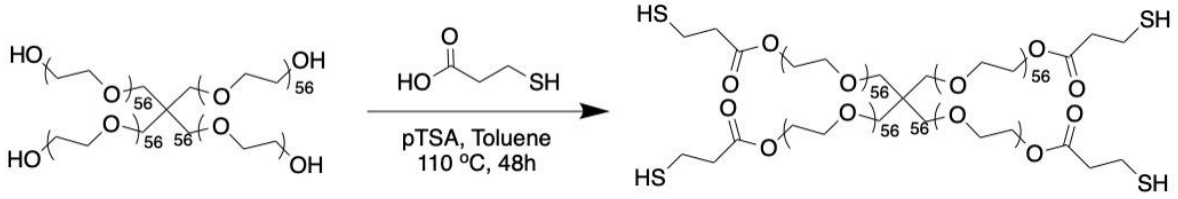

Figure 2.18. Synthesis of 4-TSH.

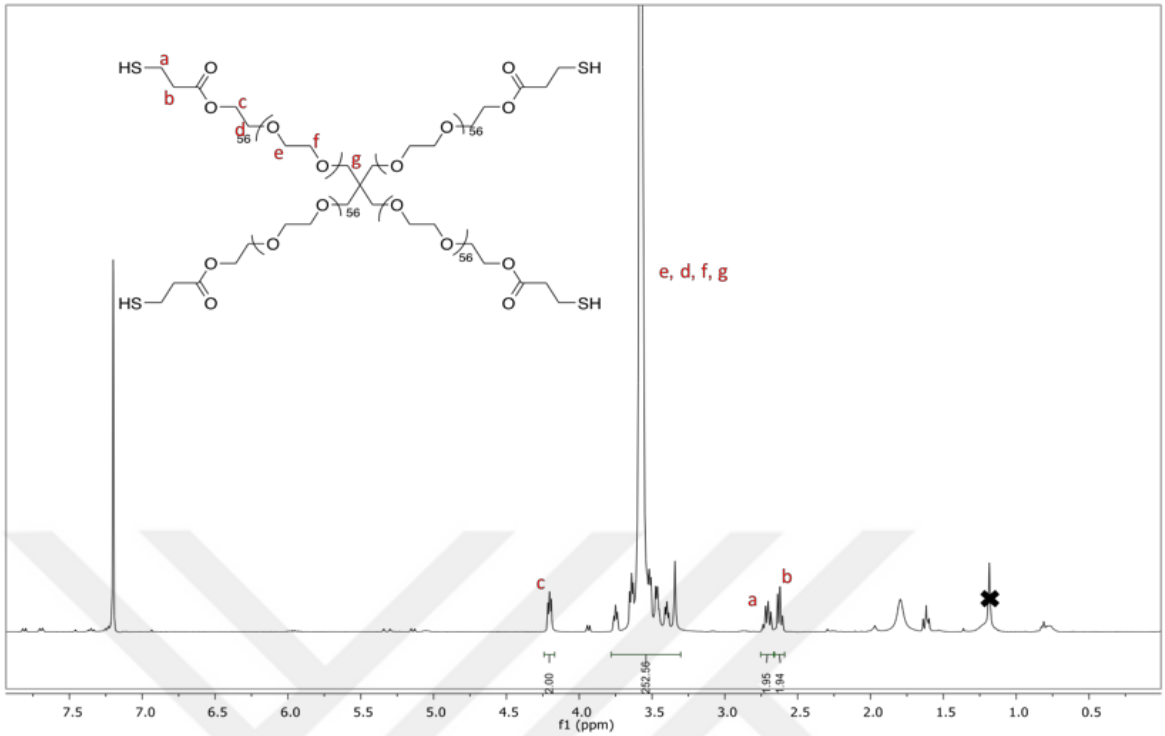

Figure 2.19. H-NMR spectrum of 4-TSH.

2.3.9. Synthesis and characterization of rGO

In the synthesis process of rGO, GO was reduced to rGO by using a strong reducing agent hydrazine hydrate. In this process, most functional groups of GO were reduced to hydroxyl and carboxylic acid groups. In FT-IR data, it is seen that –OH stretching peak (3424 cm^{-1}) has disappeared after reduction (Figure 2.20). In the UV, the peaks at 230 belonging C=C π-π and C=O n-π electronic transition peaks have shifted to 260 nm after reduction (Figure 2.21) as well as a color change of dispersion from brown to black. UV and IR data are in correlation with literature data [75,76]. In Raman data, specific D and G band peaks to rGO were observed at 1338 cm^{-1} and 1567 cm^{-1} respectively (Figure 2.20) [77,78].

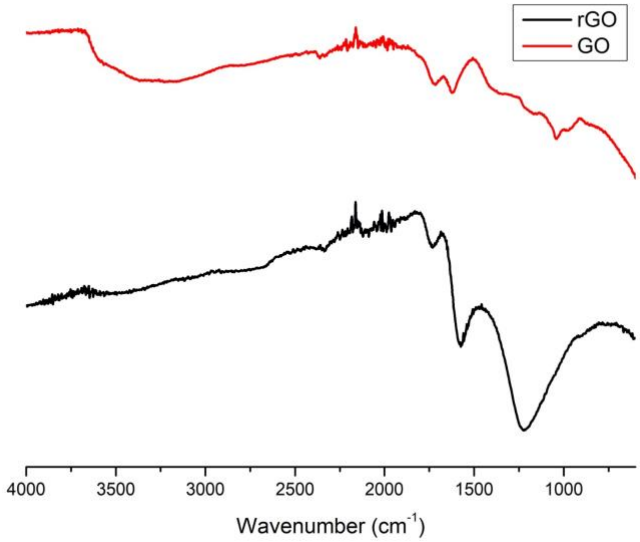

Figure 2.20. ATR-FTIR spectra of rGO and GO.

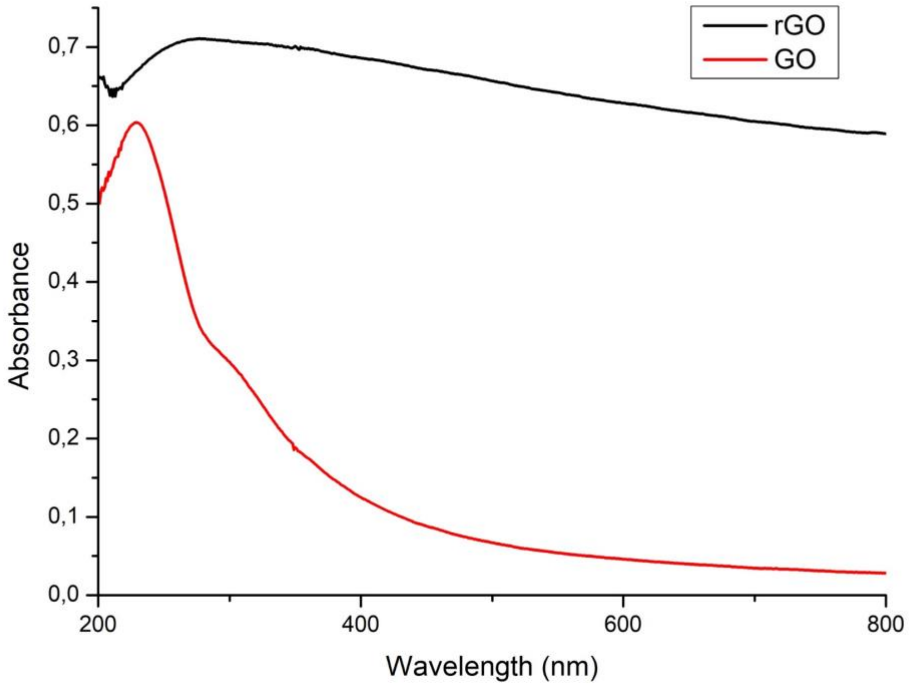

Figure 2.21. UV spectra of rGO and GO.

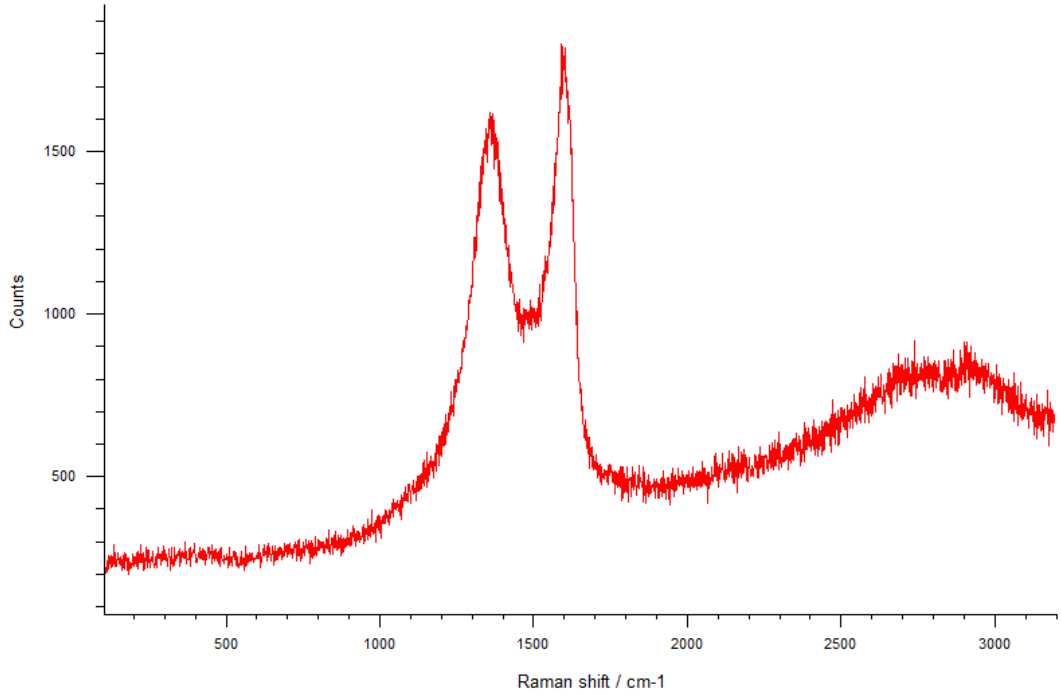

Figure 2.22. Raman spectrum of rGO.

2.3.10. Synthesis and characterization of Bis-PEG Hydrogels (w/o rGO)

In the synthesis of hydrogels, thiol-maleimide "click" reaction was used due to the reaction's fast kinetics between TSH (M_n=10 kDa) and PEG-Bis-M (M_n= 6 kDa). However, in the gel preparation water was used instead of PBS to increase gelation time in order to obtained homogenous hydrogel structure. In the fabrication of hydrogels, 5% w/v and 10% w/v concentrations were chosen.

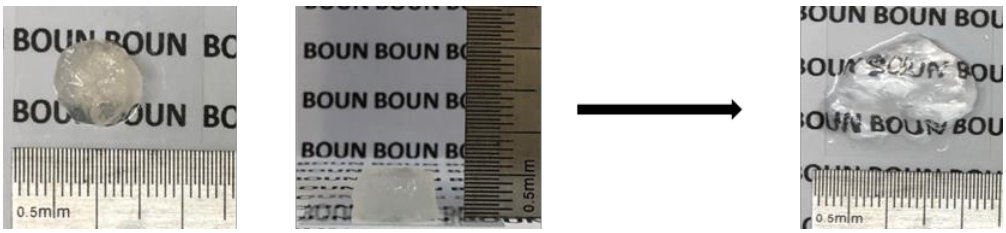

Figure 2.23. PEG-Bis-M-HG$_5$ after synthesis (left) and after swelling (left).

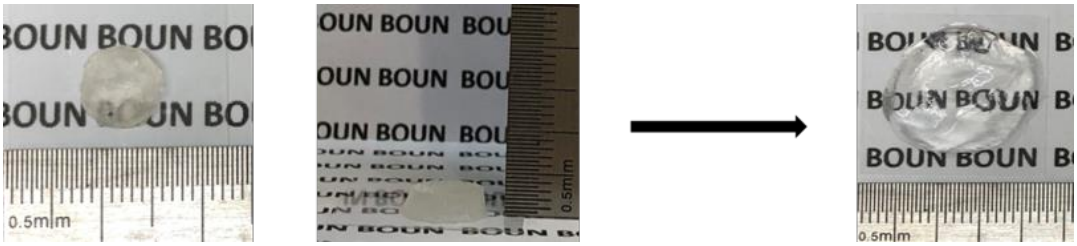

Figure 2.24. PEG-Bis-M-HG$_{10}$ after synthesis (left) and after swelling (right).

PEG-Bis-M-HG$_5$ and PEG-Bis-M-HG$_{10}$ corresponds to hydrogels prepared using Bis-Peg-M with 5% w/v and 10% w/v respectively. SEM was used to investigate the microstructure of hydrogel. Since PEG-Bis-M-HG$_5$ has lower w/v concentration, it is supposed to have larger pore size than PEG-Bis-M-HG$_{10}$. The obtained SEM images indicates the larger porosity for PEG-Bis-M-HG$_5$ (Figure 2.25). When the Ellman's test performed, 99.6% of thiol groups found to be reacted with PEG-Bis-M.

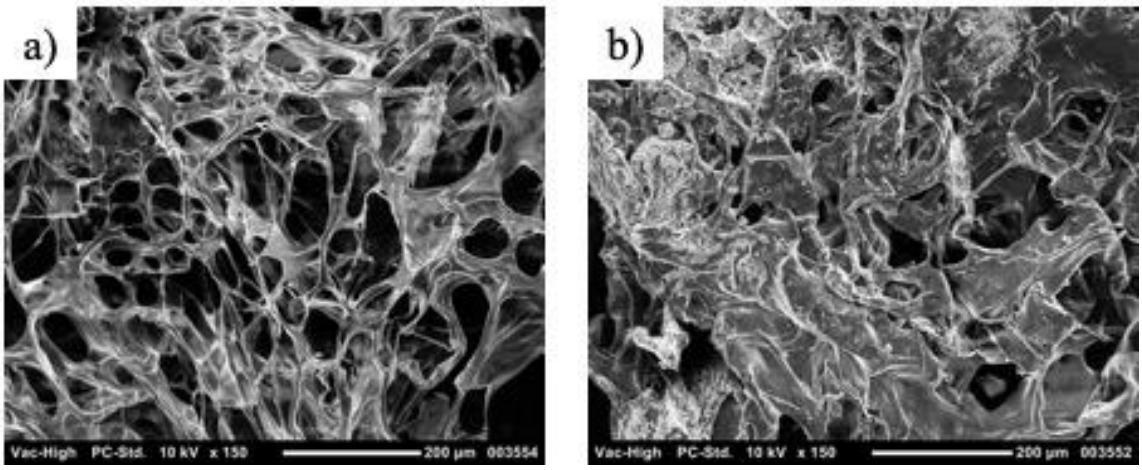

Figure 2.25. SEM images of a) PEG-Bis-M-HG$_5$ and b) PEG-Bis-M-HG$_{10}$ in the scale bar 200 μm.

After the morphological analysis done, swelling profiles of PEG-Bis-M-HG$_5$ and PEG-Bis-M-HG$_{10}$ were investigated. However, due to mechanical instability, obtaining swelling capacity for PEG-Bis-M-HG$_5$ wasn't possible since the gel ruptured upon swelling. On the other hand, PEG-Bis-M-HG$_{10}$ reached an equilibrium around 3000 in 3 minutes (Figure 2.26). After the Ellman's test, the reacted thiol groups were calculated up to 99.32%.

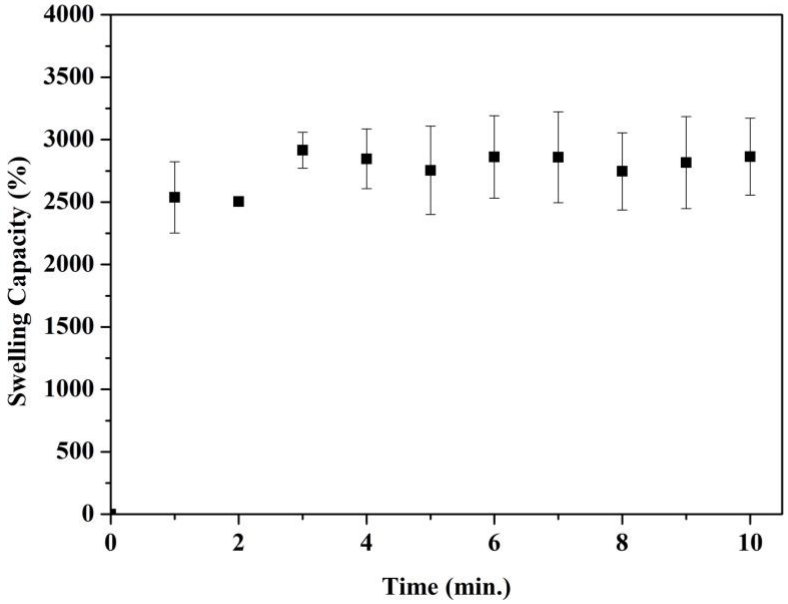

Figure 2.26. Swelling data of PEG-Bis-M-HG$_{10}$.

The w/v concentration also effects the viscoelastic properties of hydrogels. The difference in the viscoelastic properties were investigated via rheological analysis. In this process, frequency sweep test and amplitude sweep tests were performed on PEG-Bis-M-HG$_5$ and PEG-Bis-M-HG$_{10}$. However, the mechanical properties of PEG-Bis-M-HG$_5$ wasn't strong enough to obtain rheological data. Thereafter, only PEG-Bis-M-HG$_{10}$ rheological analysis will be given.

The linear viscoelastic region (LVE) of PEG-Bis-M-HG$_{10}$ was determined through amplitude sweep test. It was stable until 10% strain. Therefore, the frequency sweep test was performed at this strain. From the frequency sweep test, the G' value was found to be between 10 and 100 Pa. This low value of PEG-Bis-HG$_{10}$ indicates that the obtained gel didn't have a good stability (Figure 2.27).

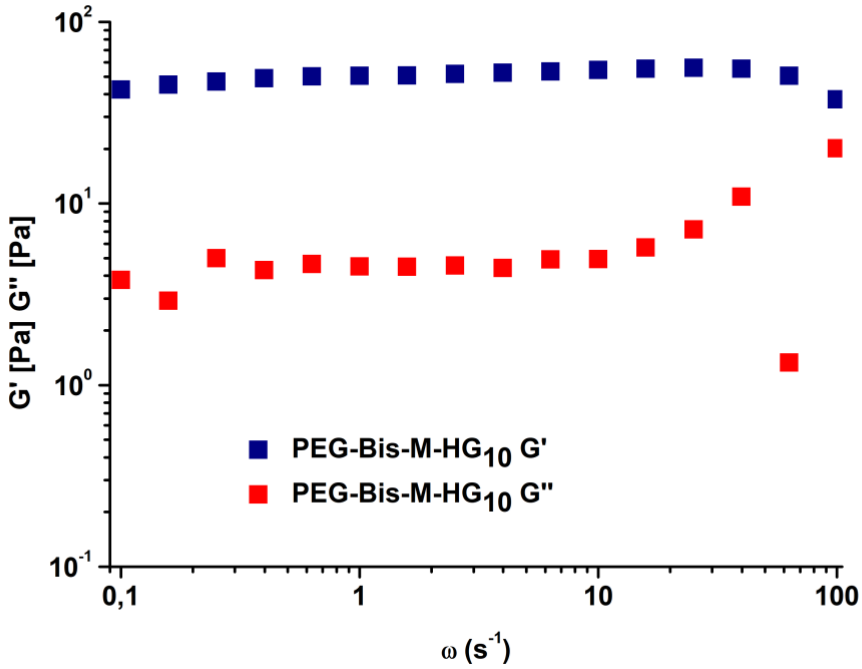

Figure 2.27. Frequency sweep test of PEG-Bis-HG$_{10}$.

2.3.11. Synthesis and characterization of rGO-containing Bis-PEG Hydrogels

In the synthesis of hydrogels, thiol-maleimide "click" reaction was used due to the reaction's fast kinetics between 4-TSH (M_n=10 kDa) and PEG-Bis-M (M_n= 6 kDa). However, in the gel preparation water was used instead of PBS to increase gelation time in order to obtained homogenous hydrogel structure. In the fabrication of hydrogels, 10% w/v and 30% w/v concentrations were chosen since 5% w/v concentration wasn't mechanically strong.

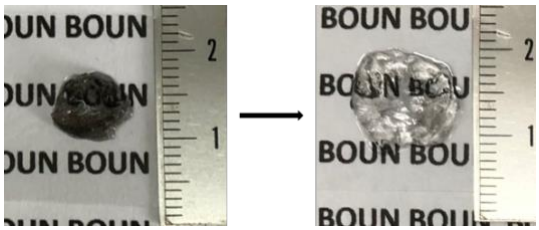

Figure 2.28. PEG-Bis-M-HG-rGO$_{10}$ after fabrication (left) and after swelling (right).

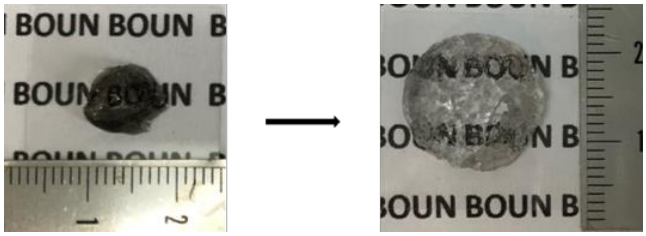

Figure 2.29. PEG-Bis-M-HG-rGO$_{30}$ after fabrication (left) and after swelling (right).

For the microstructure analysis, SEM was used. Since PEG-Bis-M-HG-rGO$_{10}$ has lower w/v concentration, it is supposed to have larger pore size than PEG-Bis-M-HG-rGO$_{30}$. However, due to PEG's hydrophilicity obtaining a clear image for PEG-Bis-M-HG-rGO$_{10}$ couldn't be managed. On the other hand, large pore size in PEG-Bis-M-HG-rGO$_{30}$ was observed (Figure 2.30). The Ellman's test gives the result of almost 100% of reacted thiol groups for both hydrogels.

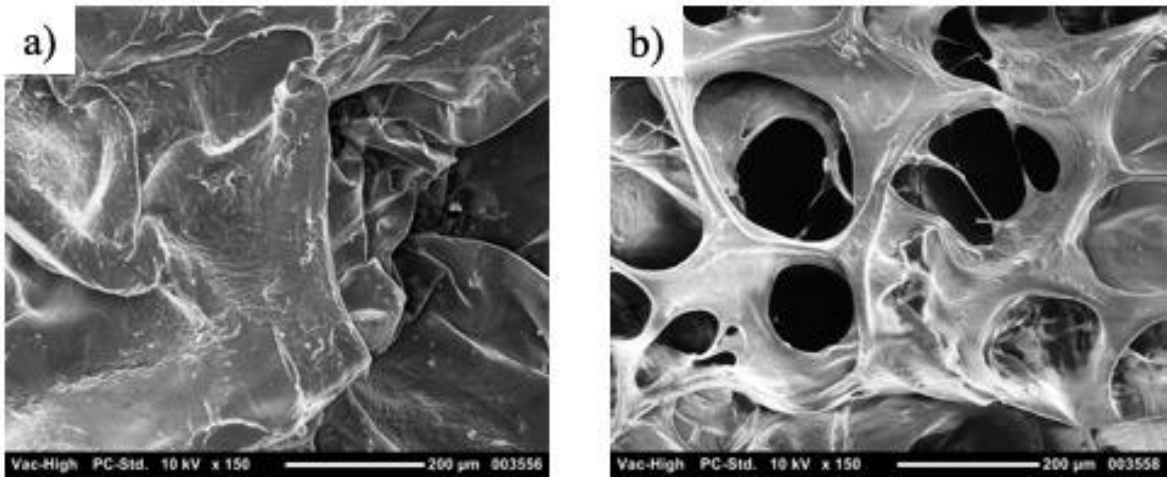

Figure 2.30. SEM images of a) PEG-Bis-M-HG-rGO$_{10}$ and b) PEG-Bis-M-HG-rGO$_{30}$ in sacle of 200 μm.

When the swelling profiles of PEG-Bis-M-HG-rGO$_{10}$ and PEG-Bis-M-HG-rGO$_{30}$ were investigated, PEG-Bis-M-HG-rGO$_{30}$ has reached the swelling capacity equilibrium of 2000 in 1 minute (Figure 2.31). However, PEG-Bis-M-HG-rGO$_{10}$ wasn't stable enough to obtain swelling data since the gel ruptured in water.

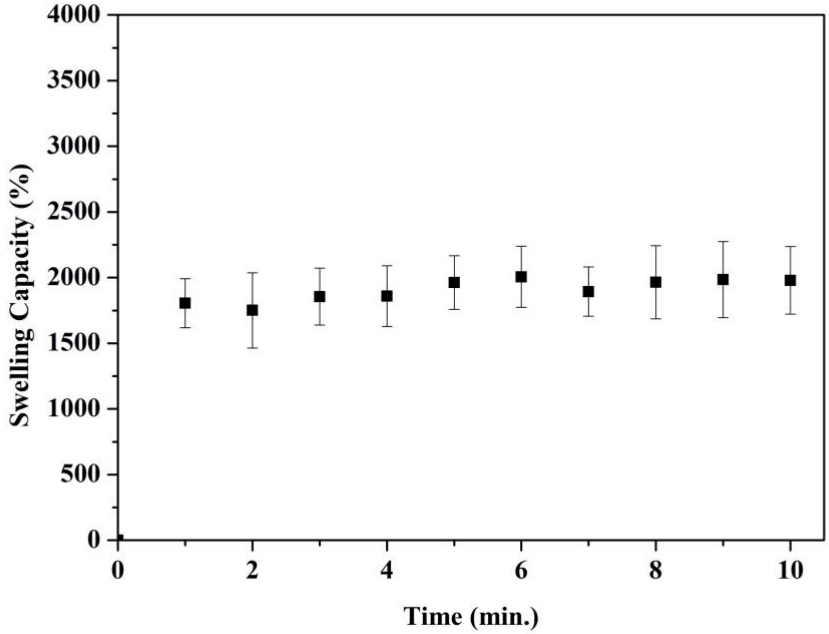

Figure 2.31. Swelling profile of PEG-Bis-M-HG-rGO$_{30}$.

For the rheological analysis, obtained hydrogels weren't mechanically stable enough to perform amplitude sweep and frequency sweep test. Also, high swelling capacities of these PEG-Bis-M-HGs weren't suitable enough for the purpose of protein release. Thereafter, the project mainly focuses on hydrogels prepared with TSH and PEG-Tetra-M.

2.3.12. Synthesis and characterization of PEG-Tetra-M hydrogels (w/o rGO)

In the synthesis of hydrogels, thiol-maleimide "click" reaction was used due to the reaction's fast kinetics between TSH (M_n=10 kDa) and PEG-Tetra-M (M_n= 10 kDa). However, in the gel preparation water was used instead of PBS to increase gelation time in order to obtained homogenous hydrogel structure. In the fabrication of hydrogels, 10% w/v, 20% w/v and 30% w/v concentrations were chosen.

The microstructures of hydrogels were investigated via SEM. As the w/v concentration of the hydrogels increases the porosity of hydrogels should decrease since there will be more bulk density in same amount of water. From swelling profiles, it was

observed that PEG-Tetra-M-HG$_{10}$ has the largest pore size since it has the least bulk density among the other two gels (Figure 2.32).

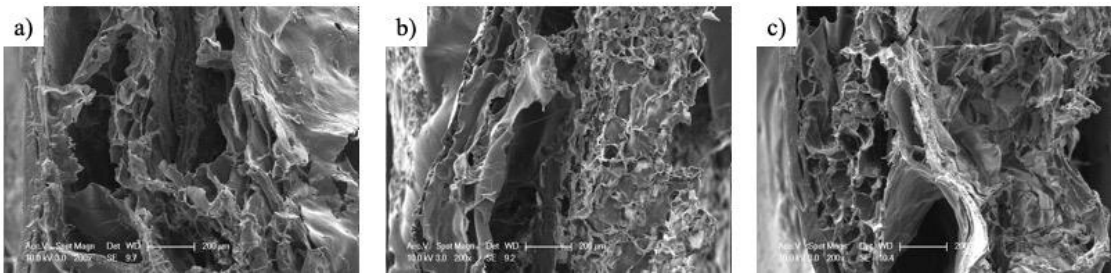

Figure 2.32. SEM images of a) PEG-Tetra-M-HG10 b) PEG-Tetra-M-HG20 and c) PEG-Tetra-M-HG30 in scale bar of 200 μm.

The swelling profiles of the hydrogels were also investigated. These hydrophilic gels were found to be reach swelling equilibrium in less than 3 minutes. As expected, the results indicate that there is a correlation between w/v concentration of hydrogels and their swelling capacities. Among the PEG-Tetra-M-HGs, the one with the least concentration (PEG-Tetra-M-HG$_{10}$) had the highest swelling capacity while PEG-Tetra-M-HG$_{30}$ had the lowest swelling capacity (Figure 2.33). When the Ellman's test performed, reacted thiol groups were calculated 99.7%, 99.7%, 98.9% and 98.6% for PEG-Tetra-M-HG-rGO$_5$, PEG-Tetra-M-HG-rGO$_{10}$, PEG-Tetra-M-HG-rGO$_{20}$ and PEG-Tetra-M-HG-rGO$_{30}$ respectively.

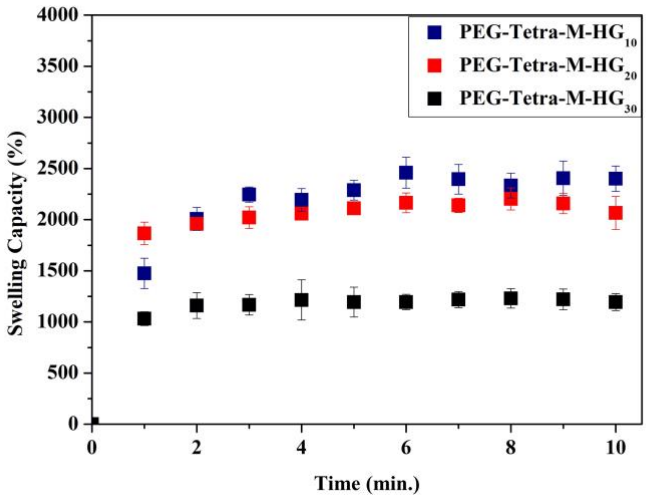

Figure 2.33. Comparison of Swelling Capacities of PEG-Tetra-M-HGs.

The w/v concentration also affects the viscoelastic properties of hydrogels. Thereafter, to investigate viscoelastic properties of hydrogels rheological analysis was performed. Mechanical stabilities of the hydrogels were analyzed by performing the amplitude sweep test as well as frequency sweep test on rheometer.

To start with, amplitude sweep test was used to determine the linear viscoelastic (LVE) regions of hydrogels. In this test, the inversion of G' and G'' indicates the rupture of bonds in the hydrogel matrix. This inversion point occurs after the critical strain point and in amplitude test PEG-Tetra-M-HG$_{10}$ (Figure 2.34), PEG-Tetra-M-HG$_{20}$ (Figure 2.36) and PEG-Tetra-M-HG$_{30}$ (Figure 38) were observed to be resistant under high oscillatory strains. Also, G' values being higher than G'' values in the frequency sweep tests indicate that PEG-Tetra-M-HG$_{10}$ (Figure 2.35), PEG-Tetra-M-HG$_{20}$ (Figure 2.37) and PEG-Tetra-M-HG$_{30}$ (Figure 2.39) preserve their viscoelastic solid structures. As expected, hydrogel with the highest % w/v concentration (PEG-Tetra-M-HG$_{30}$) had the highest G' value that is more than 1000 Pa while the one with the least w/v concentration had the lowest G' value (Figure 2.40). These results indicate that, the viscoelastic properties of these hydrogels can be adjusted for suitable biological applications without altering the polymer

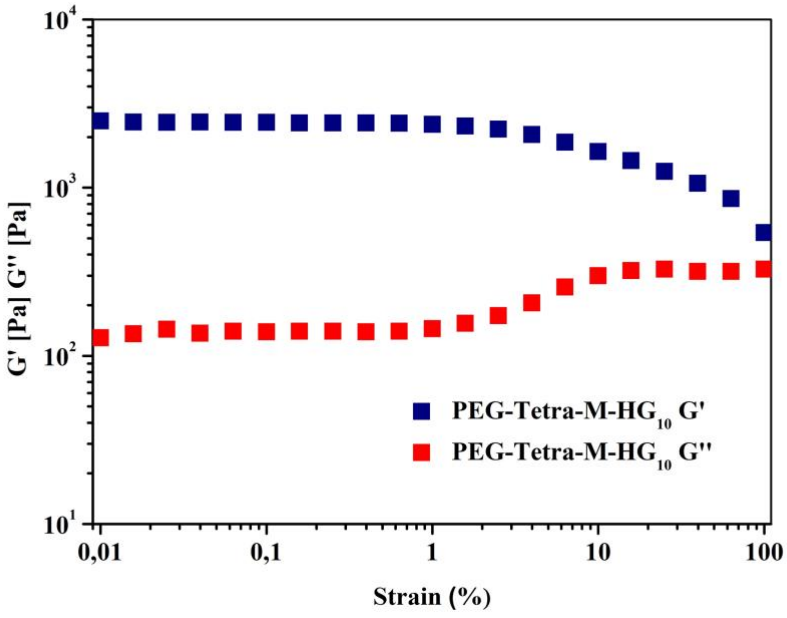

Figure 2.34. Amplitude Sweep Test of PEG-Tetra-M-HG$_{10}$.

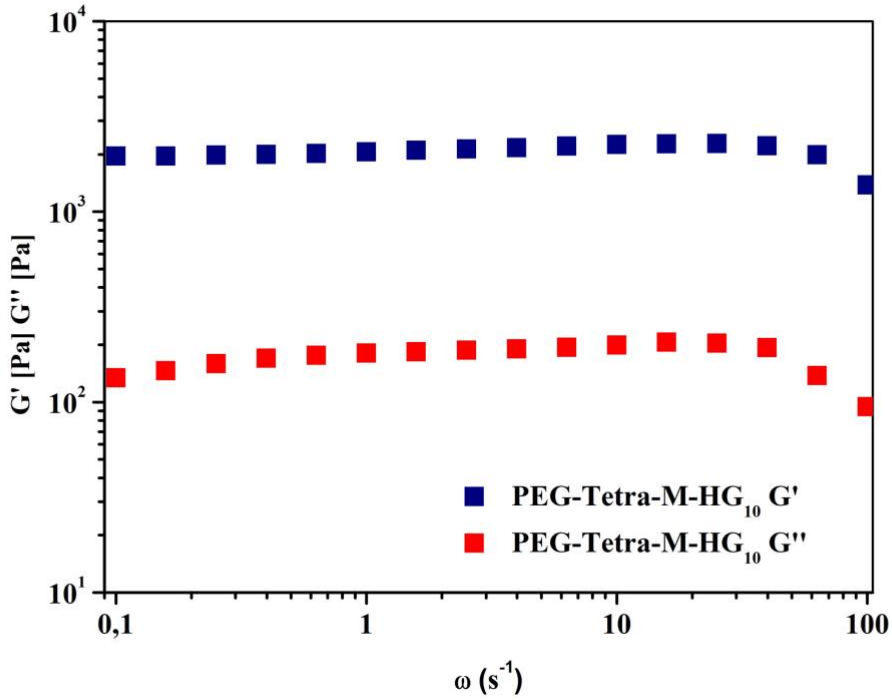

Figure 2.35. Frequency Sweep Test of PEG-Tetra-M-HG10.

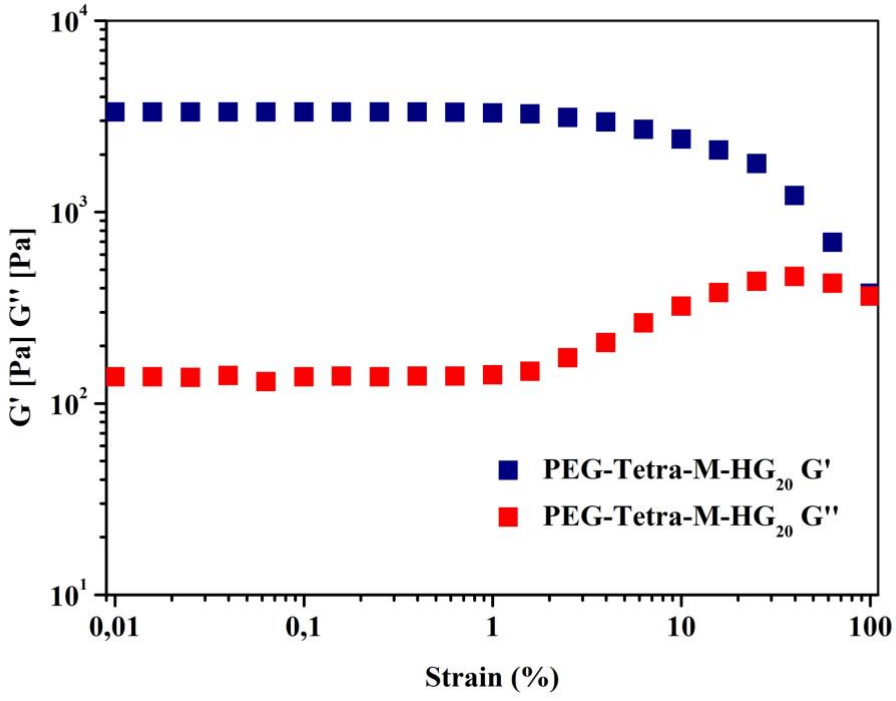

Figure 2.36. Amplitude Sweep Test of PEG-Tetra-M-HG20.

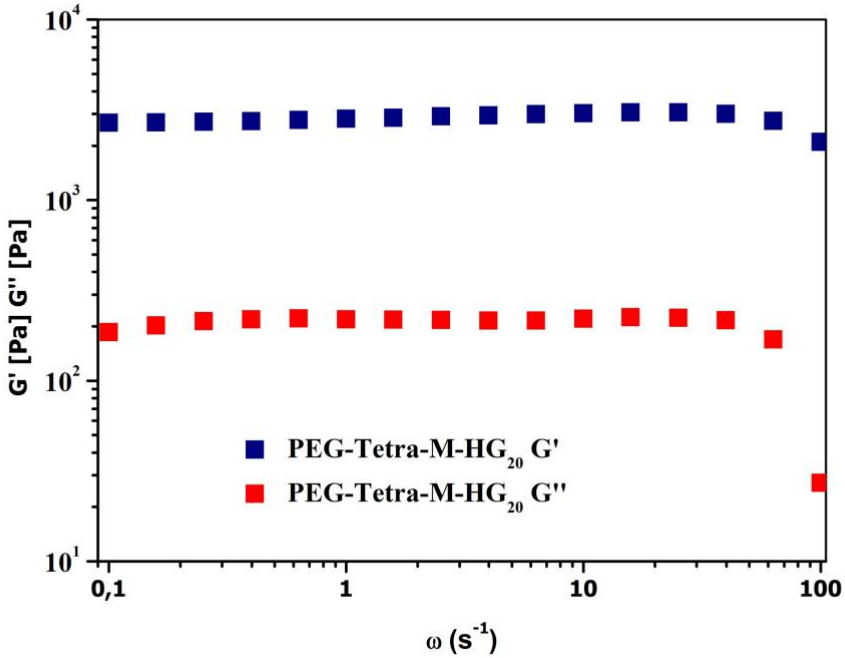

Figure 2.37. Frequency Sweep Test of PEG-Tetra-M-HG$_{20}$.

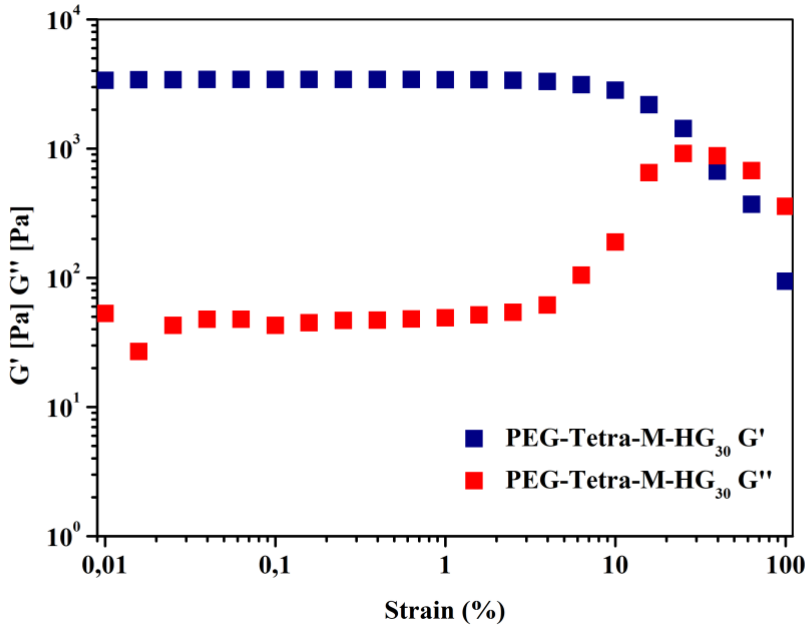

Figure 2.38. Amplitude Sweep Test of PEG-Tetra-M-HG$_{30}$.

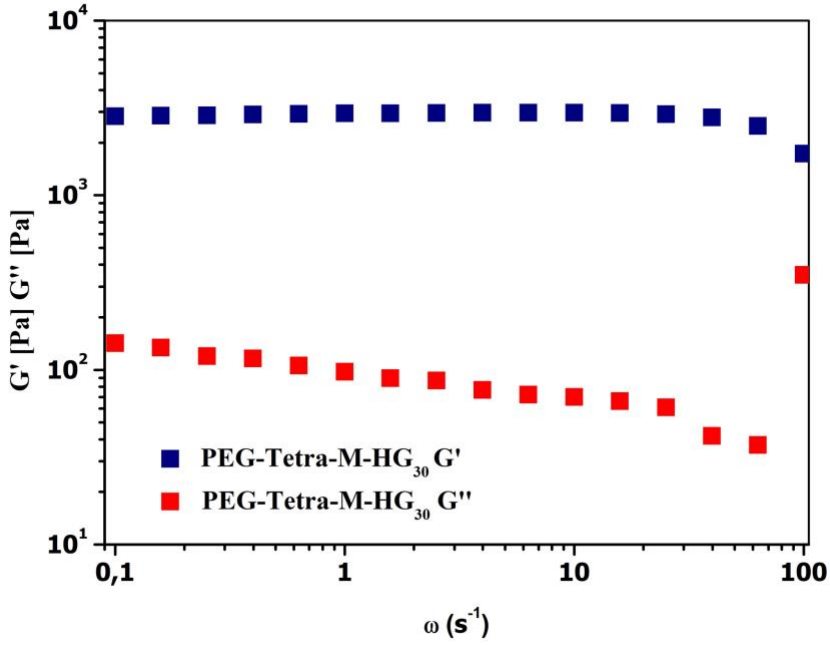

Figure 2.39. Frequency Sweep Test of PEG-Tetra-M-HG30.

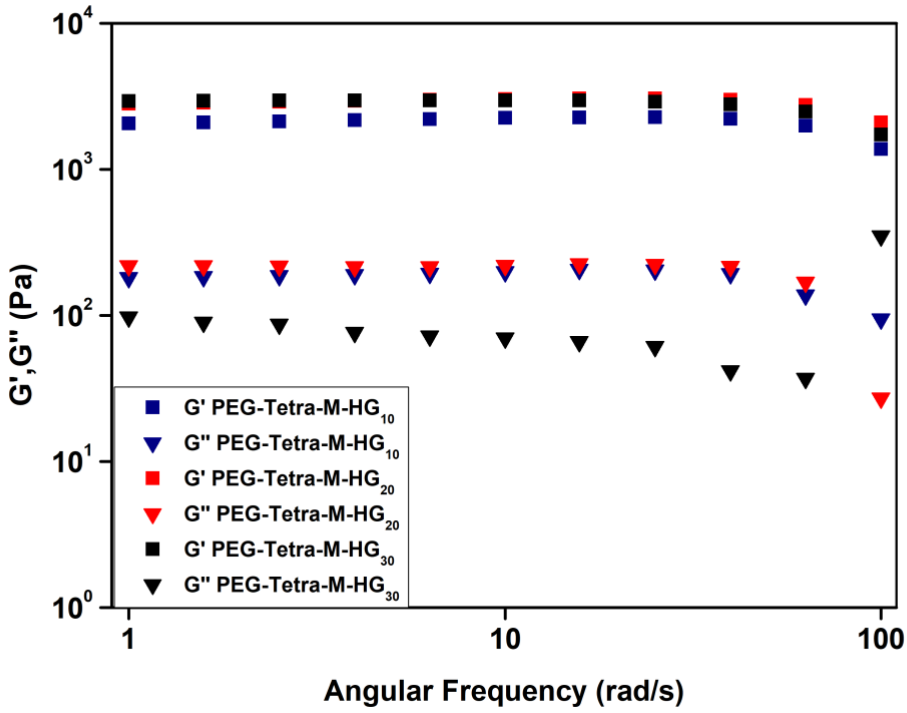

Figure 2.40. Comparison of the G' values of PEG-Tetra-M-HGs.

2.3.13. Synthesis and characterization of rGO containing PEG-Tetra-M hydrogels

In the synthesis of hydrogels, thiol-maleimide "click" reaction was used due to the reaction's fast kinetics between TSH (M_n=10 kDa) and PEG-Tetra-M (M_n= 10 kDa). However, in the gel preparation water was used instead of PBS to increase gelation time in order to obtained homogenous hydrogel structure. In the fabrication of hydrogels, 10% w/v, 20% w/v and 30% w/v concentrations were chosen.

The microstructures of hydrogels were investigated via SEM. As the w/v concentration of the hydrogels increases the porosity of hydrogels should decrease since there will be more bulk density in same amount of water. From swelling profiles, it was observed that PEG-Tetra-M-HG-rGO$_{10}$ has the largest pore size since it has the least bulk density among the other two gels (Figure 2.41).

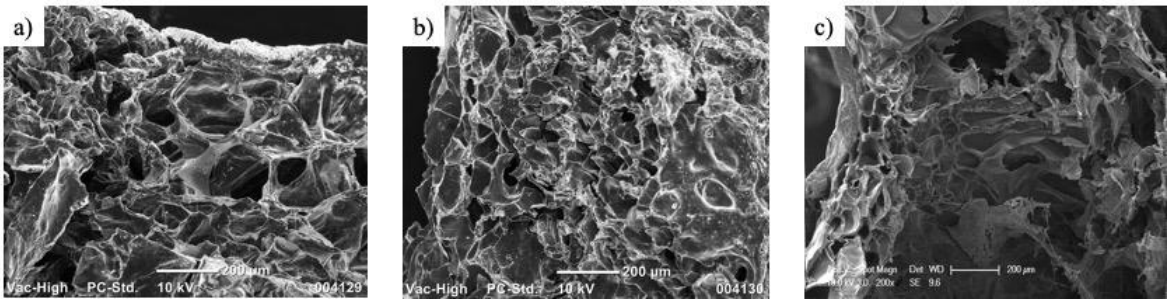

Figure 2.41. SEM images of (a) PEG-Tetra-M-HG-rGO$_{10}$, (b) PEG-Tetra-M-HG-rGO$_{20}$ and (c) PEG-Tetra-M-HG-rGO$_{30}$.

The swelling profiles of the hydrogels were also investigated. These hydrophilic gels were found to be reach swelling equilibrium in less than 3 minutes. As expected, the results indicate that there is a correlation between w/v concentration of hydrogels and their swelling capacities. Among the PEG-Tetra-M-HG-rGOs, the one with the least concentration (PEG-Tetra-M-HG-rGO$_{10}$) had the highest swelling capacity while PEG-Tetra-M-HG-rGO$_{30}$ had the lowest swelling capacity (Figure 2.42).

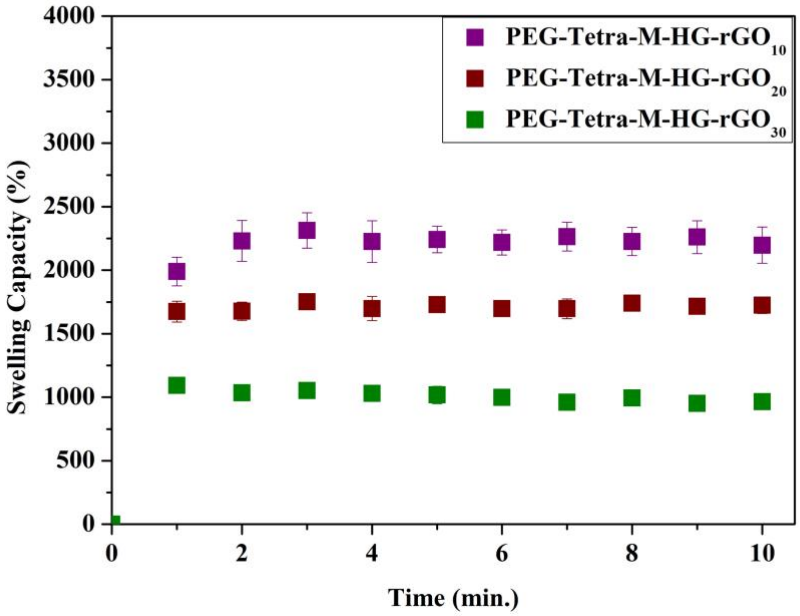

Figure 2.42. Swelling Profiles of PEG-Tetra-M-HG-rGOs.

The rheological analysis of PEG-Tetra-M-HG-rGO$_{10}$ and PEG-Tetra-M-HG-rGO$_{30}$, both hydrogels were investigated through frequency sweep test to measure LVE regions of hydrogels. Even at 100 rad/s, the inversion of G' and G'' didn't observed indicating the resistance of hydrogels under high oscillatory strains. When the G' values of these hydrogels were compared PEG-Tetra-M-HG-rGO$_{30}$ was found out to have a larger value than that of PEG-Tetra-M-HG-rGO$_{10}$ (Figure 2.43).

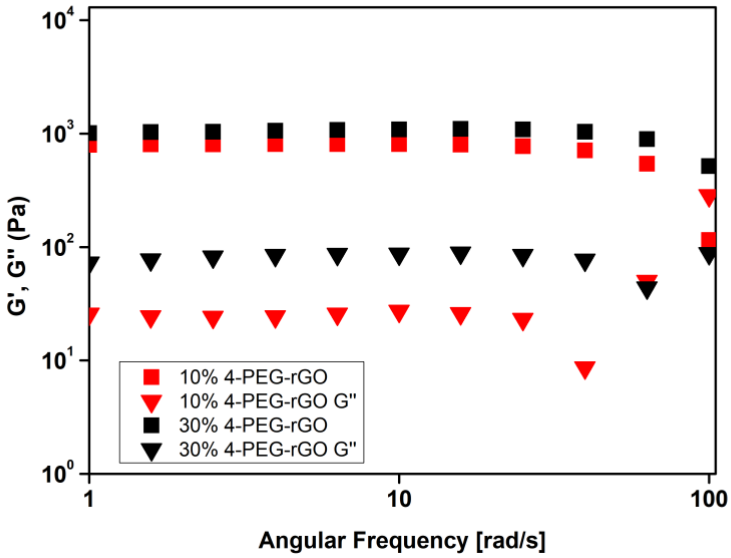

Figure 2.43. Frequency Sweep Tests of PEG-Tetra-M-HG-rGOs.

2.3.14. Passive Release of FITC-Dextran from rGO containing PEG-Tetra-M-HG-rGO

Passive release studies of FITC-Dextran (M_n= 70 kDa) from PEG-Tetra-M-HG-rGOs were performed in physiological (PBS=7.4) condition. FITC-Dextran with molecular weight of 70 kDa was chosen due to its similarity to FITC-BSA (M_n= 66 kDa), a model protein. Without NIR irradiation, the release of FITC-Dextran was expected to be low. For this purpose, PEG-Tetra-M-HG-rGO$_{10}$, PEG-Tetra-M-HG-rGO$_{20}$ and PEG-Tetra-M-HG-rGO$_{30}$ were loaded with 100 μg FITC-Dextran for total of 30 mg polymer. Each hydrogel was soaked into 1 mL PBS and UV measurement of PBS was done at different durations at 495 nm.

The varying w/v concentrations of hydrogels should result in a change at release profiles due to the difference in the microstructures of the hydrogels. As expected PEG-Tetra-M-HG-rGO$_{10}$ had the highest release percentage due to the fact that it has the smallest pore size among other gels. On the other hand, from PEG-Tetra-M-HG-rGO$_{30}$ that has the smallest pore size, the lowest release of FITC-Dextran was observed (Figure 2.44).

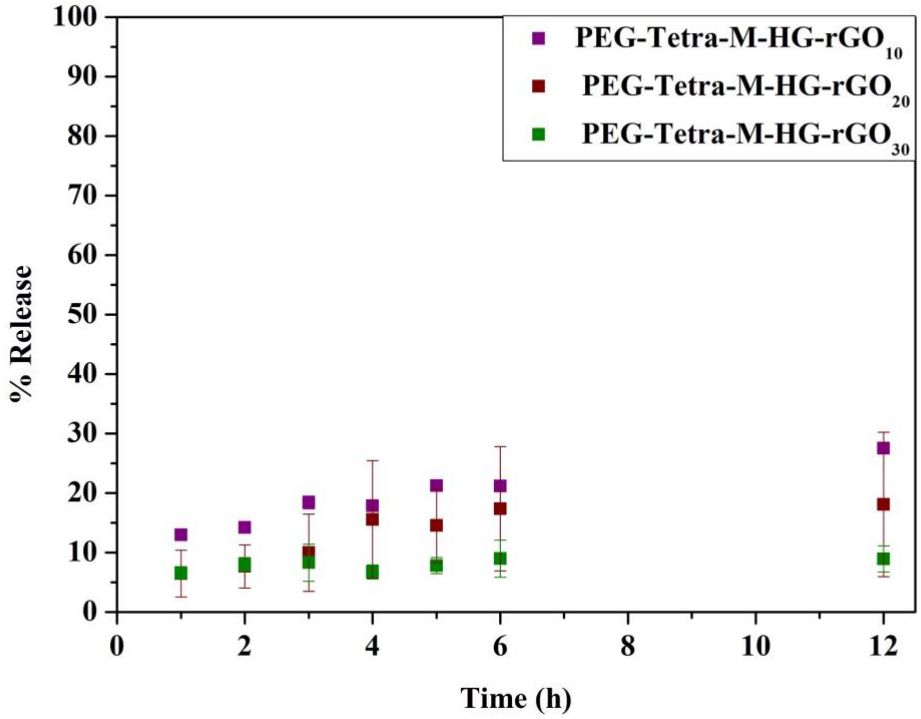

Figure 2.44. Release Profiles of PEG-Tetra-M-HG-rGOs.

2.3.15. Active Release of FITC-Dectran from rGO-containing Hydrogels

rGO as a photothermal agent has a rapid light-to-heat conversion property. The rGO incorporation into hydrogels makes the system photothermally responsive and the resulting hydrogels can be heated up to 70 °C under NIR light (980 nm). This temperature enables the release of desired cargo upon bond rupture by the retro-DA reaction. To this end, PEG-Tetra-M-HG-rGO$_{30}$ with 100 µg FITC-dextran (M_n= 70 kDA) was prepared. The active release of this hydrogel was done under NIR (980 nm, 1.2 W). 30% w/v rGO hydrogels was chosen for this purpose due to its swelling profile.

Between NIR irradiation sets, the gel was cooled down and its absorbance was measured in order to check whether the release of protein stops or continues. In each set of NIR irradiation, the gel releases FITC-dextran and stops when the gel was cooled. At the end of four NIR irradiation, the release of FITC from PEG-Tetra-M-HG-rGO$_{30}$ was up to 60%, much more than the one of passive release (Figure 2.45).

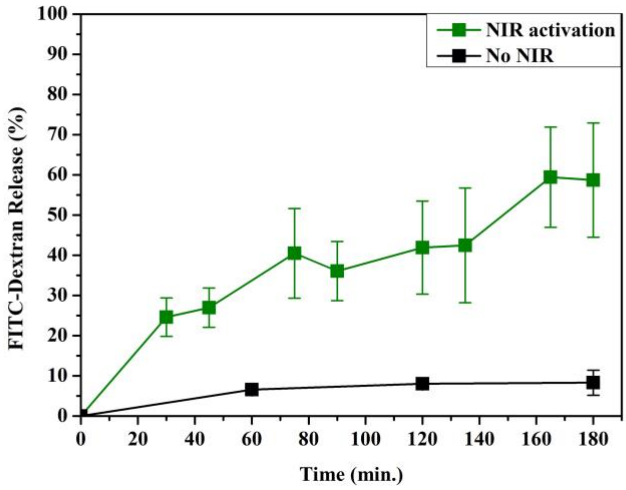

Figure 2.45. Active release of FITC-Dextran from PEG-Tetra-M-HG-rGO$_{30}$ under NIR light.

2.3.16. NIR Heating Experiment of rGO-Hydrogel

Since the obtained hydrogels contains thermoresponsive bonds in their network, an increase in temperature should lead to some decrease in the mechanical stability of the hydrogels. Under NIR irradiation, G' value of PEG-Tetra-M-HG-rGO$_{30}$ decreases in each time interval since the thermoresponsive DA cycloadduct bond ruptures at high temperatures (Figure 2.47).

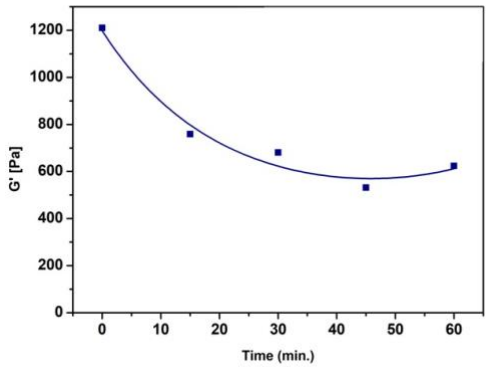

Figure 2.46. Rheology data of NIR heating experiment of PEG-Tetra-M-HG-rGO$_{30}$.

2.4. Conclusion

In this project, a hydrogel system for ‘on-demand’ protein release was developed by using rGO incorporated thermoresponsive hydrogels. The obtained hydrogels could be heated up to 80 °C under NIR irradiation leading to the rupture of thermoresponsive bonds in the hydrogel network. As a result, as gels degrade the protein release occurs in an ‘on-demand’ manner in each NIR irradiation. For this purpose, first a four-armed polymer and a linear polymer containing thermoresponsive Diels-Alder cycloadduct in the polymer chain and a free maleimide at the end were synthesized to introduce thermosensitivity to the hydrogels. Later on, another four-armed PEG with a thiol end group was synthesized. And the maleimide functional groups bearing and thiol functional groups bearing polymers were used to synthesize hydrogels via thiol-maleimide “click” chemistry with varying w/v percentages. In microstructure investigation, the hydrogel with the lowest w/v concentration showed the largest porosity leading to the highest swelling capacity. The hydrogels obtained with PEG-Bis-M and TSH were mechanically the least stable hydrogels whereas the hydrogels obtained with PEG-Tetra-M and TSH were mechanically much more stable. Thereafter, the release studies of the project were done by using PEG-Tetra-M-HG-rGO$_{30}$, hydrogel with the lowest swelling capacity. In the NIR irradiation experiment, the mechanical properties such as swelling capacity and storage moduli of PEG-Tetra-M-HG-rGO$_{30}$ were changed after NIR irradiation. In the passive release studies of FITC-Dextran (M_n= 70 kDa) from PEG-Tetra-M-HG-rGOs, the hydrogel with the lowest w/v concentration was observed to have the highest release percentage due to its larger pores. Since the developed hydrogel system contains rGO, a photothermal agent, and a thermoresponsive bonds, it can be a promising system for “on-demand” protein release. The active and passive release studies of rGO containing hydrogels need to be further investigated with FITC-Dextrans of different molecular weights as well as a protein like FITC-BSA.

3. FUNCTIONALIZATION OF RGO VIA DISULFIDE CHEMISTRY

3.1. Aim of Study

In this study, the aim is to functionalize rGO reversibly via disulfide exchange mechanism. For this purpose, a small molecule pyrene pyridyl disulfide (PPD) and a PEG-based polymer (PDS-PEG-Py) that has pyrene and PDS groups were synthesized. After obtaining these ligands, pyrene functional groups of PDS-PEG-Py and PPD were used to functionalize rGO via π-π stacking. After modification of rGO, PDS group was used for the post-modification of rGO via disulfide exchange reaction. Due to the reversibility of disulfide exchange reaction, physically functionalized rGO could also be functionalized chemically in the presence of other thiols. To this end, rGO was first modified with PPD physically and after characterizations via XPS, UV and IR were done, other thiol containing molecules were used for modification of rGO. Once the modifications with small molecules were done, PDS containing PEG was used to modify rGO and the solubility of rGO in water was investigated after functionalization with PEG. Since the direct functionalization of rGO chemically is not a very efficient process, the developed system will give a solution to this problem. Also, this system can be used in biological applications such as delivering thiolated proteins or drugs since PDS-PEG-modified rGO will be water soluble as well as can be modified reversibly (Figure 3.1).

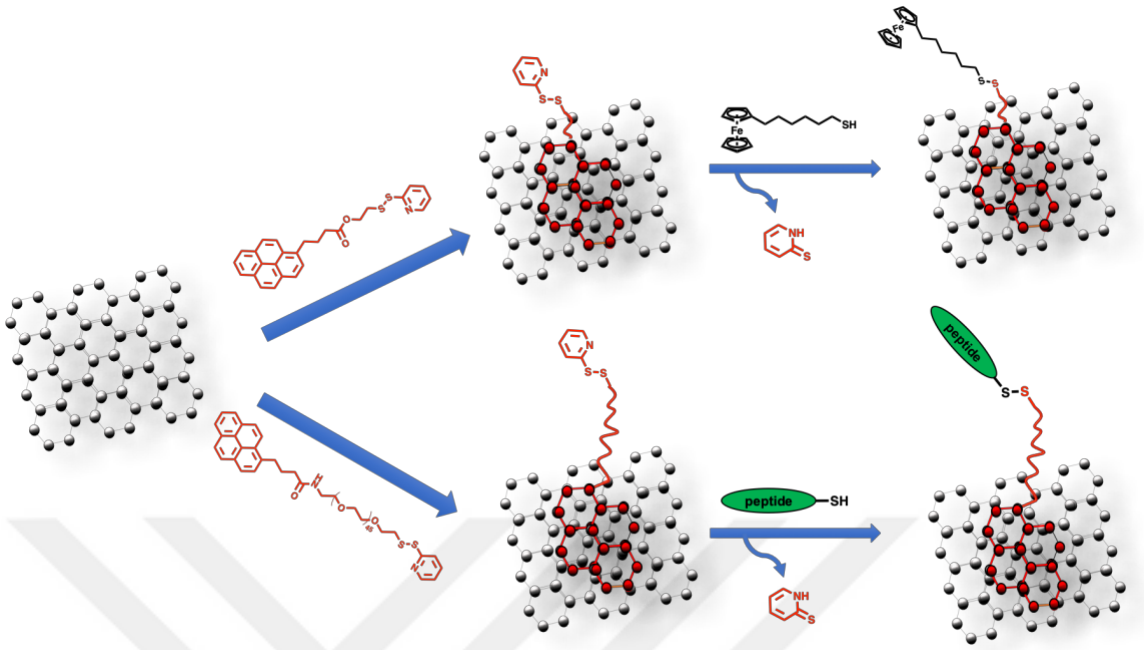

Figure 3.1. Schematic representation of the project.

3.2. Experimental

3.2.1. Materials

4-Pyrenebutyric acid purchased from Acros Organics.1-(3-Dimethyl-aminopropyl)-3-ethylcarbodiimide hydrochloride (EDCI), 1,4-dithio-DL-threthiol (DTT) (98%), N-hydroxysuccinimide (NHS) (98%+) and 4-(Dimethylaminno)pyridine (DMAP) were purchased from Alfa Aesar. 2,2'-Dipyridyl disulfide was obtained from TCI Chemicals. SH-PEG-NH_2 (M_n=2000) was purchased from JennKem USA. 6-(Ferrocenyl)hexanethiol was purchased from Sigma-Aldrich. Anhydrous CH_2Cl_2 was obtained from SciMatCo purification system.

3.2.2. Instrumentation

Small molecule (PPD) and polymer characterizations was carried out with ^1H NMR spectroscopy (Varian 400 MHz). Stacking of small molecules onto rGO were characterized by X-ray photon spectroscopy, XPS, (K-Alpha, Thermo Scientific) and by attenuated total reflection Fourier transform infrared (ATR-FT-IR) spectroscopy (Nicolet 380, Thermo

Scientific). UV spectrum were measured with a Varian Cary-100 UV-Vis Spectrophotometer.

3.2.3. Synthesis of Pyrene Pyridyl Disulfide Ester (PPD)

This ester was synthesized as an adaptation to the literature procedure [79]. PDS-alcohol (0.160 g, 0.85 mmol), EDCI (0.164 g, 0.85 mmol) and DMAP (0.02 g, 0.17 mmol) were dissolved in anhydrous CH_2Cl_2 (6 mL). To this mixture was added 4-pyrenebutyric acid (0.296 g, 1.03 mmol) dissolved in anhydrous CH_2Cl_2 (4 mL). The mixture was stirred for 24 h at room temperature under N_2 atmosphere. Thereafter, CH_2Cl_2 (25 mL) was added into the reaction mixture and organic phase was washed with saturated $NaHCO_3$ (100 mL X 3). Organic layers were combined and dried over anhydrous Na_2SO_4, and solvent was removed under reduced pressure. Obtained residue was purified using column chromatography on SiO_2 (Hexane: EtOAc 1 : 1) affording 0.290 g (74% yield) PPD as a colorless oil. ^{1}H NMR ($CDCl_3$, δ, ppm): 8.44 (d, 1H); 8.29 (d, 1H); 8.17 (d, 2H); 8.11 (d, 2H); 8.03-7.98 (m, 3H); 7.86 (d, 1H); 7.64 (d, 1H); 7.54 (t, 1H); 7.03 (m, 1H); 4.34 (t, 2H); 3.4 (t,2H); 3.02 (t, 2H); 2.45 (t, 2H); 2.23-2.16 (m, 2H). ^{13}C NMR ($CDCl_3$, δ, ppm): 173.5, 160.0, 150.0, 137.3, 135.9, 131.7, 131.2, 130.3, 129.1, 127.8, 127.78, 127.73, 127.1, 126.2, 125.4, 125.3, 125.3, 125.1, 125.1, 123.6, 121.1, 120.1, 62.5, 37.7, 34.0, 33.0, 27.0.

3.2.4. Synthesis of PDS-PEG-Amine

For the synthesis of PDS-PEG-Amine, thiol group of HS-PEG-amine was converted to pyridyl disulfide group via disulfide exchange mechanism. Firstly, MeOH used in this reaction was deoxygenated under N_2 atmosphere for 20 minutes. In separate vials thiol-PEG-amine (100 mg, 0.05 mmole) was dissolved in 0.2 mL MeOH and aldrithiol (22.02 mg, 0.11 mmole) was dissolved in 0.2 mL MeOH. The catalytic amount of acetic acid (0.012 mmole) was added into polymer mixture. Lastly, the aldrithiol was added into the polymer and the reaction was left stirring for 4 hours. After the reaction completed, the reaction mixture was precipitated in cold diethyl ether. The white precipitate was filtered and dried under high vacou. ^{1}H-NMR (400 MHz, $CDCl_3$, δ, ppm), 8.46 (d, 1H), 8.1-7.85 (br, 2H), 7.76 (d, 1H), 7.65 (t, 1H), 7.08 (t, 1H), 3.0 (t, 2H).

3.2.5. Synthesis of Pyrene-PEG-PDS (PDS-PEG-Py)

For the synthesis of this polymer, two steps synthetic route has been followed. Firstly, NHS activation of 4-pyrenebutyric acid was done according to literature procedure [80]. Later on, NHS-activated pyrenebutyric acid (3.85 mg, 0.01 mmole) was dissolved in 0.1 mL THF and PDS-PEG-amine (20 mg, 0.01 mmole) was dissolved in 0.1 mL THF. Both mixtures were mixed and the reaction mixture was left stirring overnight at room temperature. For purification, the resulting polymer was precipitated in cold diethyl ether and the precipitate was filtered. The obtained polymer was dried under vacou. ^{1}H-NMR (400 MHz, $CDCl_3$, δ, ppm) 8.46 (d, 1H), 8.34 (d, 1H), 8.16-8.10 (m, 5H), 7.95-8.05 (m, 4H), 7.76 (d, 1H), 7.65 (d, 1H), 7.08 (t, 1H), 3.0 (t, 2H).

3.2.6. Preparation of rGO/PPD

rGO (1.5 mg/mL) was dispersed in THF and PPD (60 mg, 0.13 mmole) was dissolved in 0.5 mL THF. PPD was added into rGO dispersion dropwise and ultrasonicated for 3 hours. The resulting rGO/PPD was collected by centrifugation at 13000 rpm and washed several times with THF to remove unstacked PPD. Lastly, the functionalized rGO was dried under high vacou.

3.2.7. Functionalization of rGO/PPD with small compounds via Thiol-disulfide Exchange Reaction

Once the rGO was functionalized physically via pi-pi interaction with PPD, it was further functionalized with thiolated compounds via thiol-disulfide exchange reaction. Briefly, dispersion of rGO/PPD in THF (1mg/mL) was mixed with 6-(ferrocenyl)hexanethiol (3.96 mg, 0.013 mmole) and sonicated for 4h at room temperature and left stirring for 24 hours. The product was again collected via centrifugation at 13000 rpm. Unreacted ferrocenyl-thiol was washed away with THF. Similarly, the functionalization of rGO/PPD with 1H,1H,2H,2H-perfluorodecanthiol was also achieved with the same procedure.

3.2.8. Fuctionalization of rGO/PPD with thiolated-PEG

As well as modifying rGO/PPD with small molecules, it was also modified with a PEG-SH (M_n= 5 kDa) to check thiol-disulfide exchange reaction. To this end, previously prepared rGO/PPD was dispersed in water (1 mg/mL) and to this disperstion PEG-SH (10 mg, 0.05 mmole) was added. The mixture was left stirring for 24 hours at room temperature. The resulting functionalized rGO was collected via centrifugation at 13000 rpm. The obtained rGO was dried under high vacou.

3.2.9. Functionalization of rGO/PPD with PEG via Thiol-disulfide Exchange Reaction

After the modification of rGO/PPD with small compounds like 1H,1H,2H,2H-perfluorodecanthiol, 6-(ferrocenyl)hexanethiol and PEG-SH the next step was to modify rGO itself with a hydrophilic compound such as PEG since the dispersibility of rGO in water is a major problem for biomedical application. However, using PDS-containing PEG to functionalize rGO, this problem can be overcome. Thereafter, Py-PEG-PDS was used to modify rGO surface. For this purpose, rGO was dispersed in water (1 mg/mL) and Py-PEG-PDS (30 mg, 0.015 mmole) was added into rGO dispersion. The mixture was ultrasonicated for 4 hours at room temperature. The resulting functionalized rGO was collected via centrifugation at 13000 rpm. Unstacked polymer was washed with water. The resulting modified rGO was dried under vacou.

3.2.10. DTT Treatment of rGO/PPD

DTT is a reagent that cleaves disulfide bond by giving a cyclic structure as a byproduct. rGO/PPD was treated with DTT to characterize functionalization of rGO. To this end, rGO/PPD dispersion (1 mg/mL) was mixed with DTT (10 mM) and left stirring in magnetic stirrer for 30 minutes. The DTT treated rGO/PPD was collected via centrifugation at 13000 rpm. The resulting rGO was washed with distilled water and dried under high vacou.

3.2.11. DTT and GSH Treatment of Functionalized rGO/PPD

Since the thiol-disulfide exchange reaction is a reversible reaction to characterize functionalization, ferrocenyl-thiol modified rGOs was treated with DTT whereas 1H,1H,2H,2H-Perfluorodecanthiol modified rGO was treated with DTT and glutathione (GSH) separately. For this purpose, ferrocenyl-thiol modified rGO was dispersed in THF (1 mg/mL). to the rGO dispersion DTT (10 mM) was added and the mixture was sonicated for 30 minutes. The DTT treated modified rGO was collected by centrifugation at 13000 rpm and the resulting rGO was dried in vacou.

1H,1H,2H,2H-Perfluorodecanthiol modified rGO was treated with GSH and DTT separately. To this end, 1H,1H,2H,2H-Perfluorodecanthiol modified rGO was dispersed in THF (1 mg/mL) and GSH (10 mM) was added into rGO dispersion. The mixture lest stirring for 24 hours at room temperature and the resulting rGO was collected via centrifugation at 13000 rpm. Unreacted GSH was washed with THF and rGO was dried under high vacou.

1H,1H,2H,2H-Perfluorodecanthiol modified rGO again dispersed in THF (1 mg/mL) and DTT (10 mM) was added into rGO dispersion. The mixture was sonicated for 30 minutes and rGO was collected via centrifugation at 13000 rpm after reaction was completed. The resulting rGO was washed with THF to remove unreacted DTT and dried in high vacou.

3.3. Results and Discussion

3.3.1. Synthesis and Characterization of PPD

In this esterification reaction DMAP coupling was used to obtain PPD (Figure 3.2). Characterization of the compound was done by using ^{1}H-NMR. In the ^{1}H-NMR, specific peaks at 8.44 ppm, 7.54 ppm and 7.03 belonging to PDS ring were observed. In addition to that, pyrene ring peaks were also observed at 8.29 ppm, 8.17 ppm, 8.11 ppm, 8.03-7.98 ppm, 7.86 ppm and 7.64 ppm were observed with fitting integrals (Figure 3.3). In ^{13}C-NMR, 27 carbons of PPD were observed in their fitting places (Figure 3.4).



Figure 3.2. Synthesis of PPD.

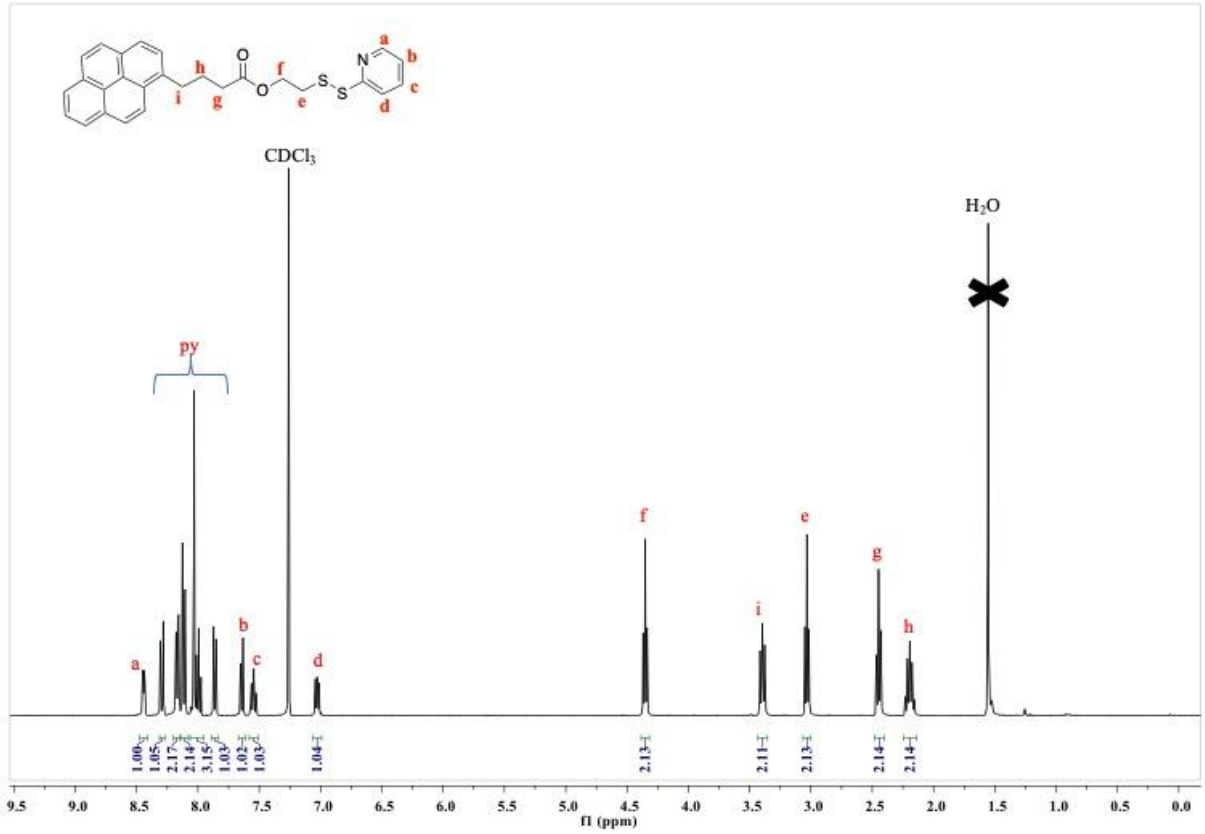

Figure 3.3. ^{1}H-NMR spectrum of PPD.

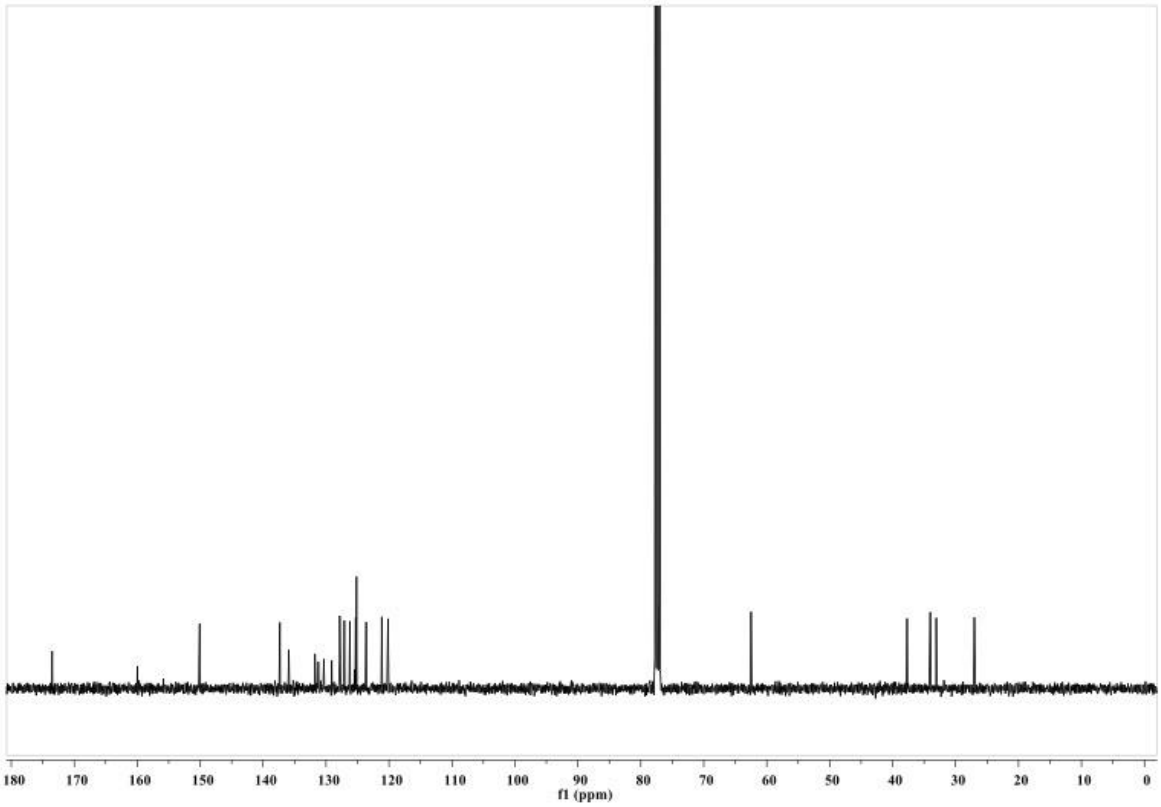

Figure 3.4. ^{13}C-NMR of PPD.

3.3.2. Synthesis and Characterization of PDS-PEG-Amine

The synthesis of PDS-PEG-amine was achieved through thiol-disulfide exchange reaction between thiol group of thiol-PEG-amine and disulfide bond of aldrithiol (Figure 3.5). The characterization of the resulting polymer was done by ^{1}H-NMR. In the ^{1}H-NNMR spectrum, specific peaks belonging to PDS ring were observed at 8.46 ppm, 7.76 ppm, 7.64 ppm and 7.08 ppm were observed. In addition to that, two hydrogens of ethyl group next to sulfur was observed as a triplet at 3.00 ppm (Figure 3.6).

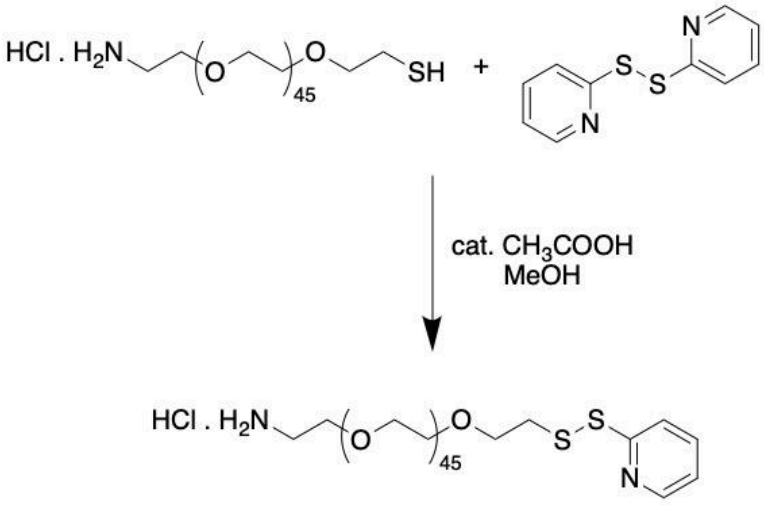

Figure 3.5. Synthesis of PDS-PEG-Amine.

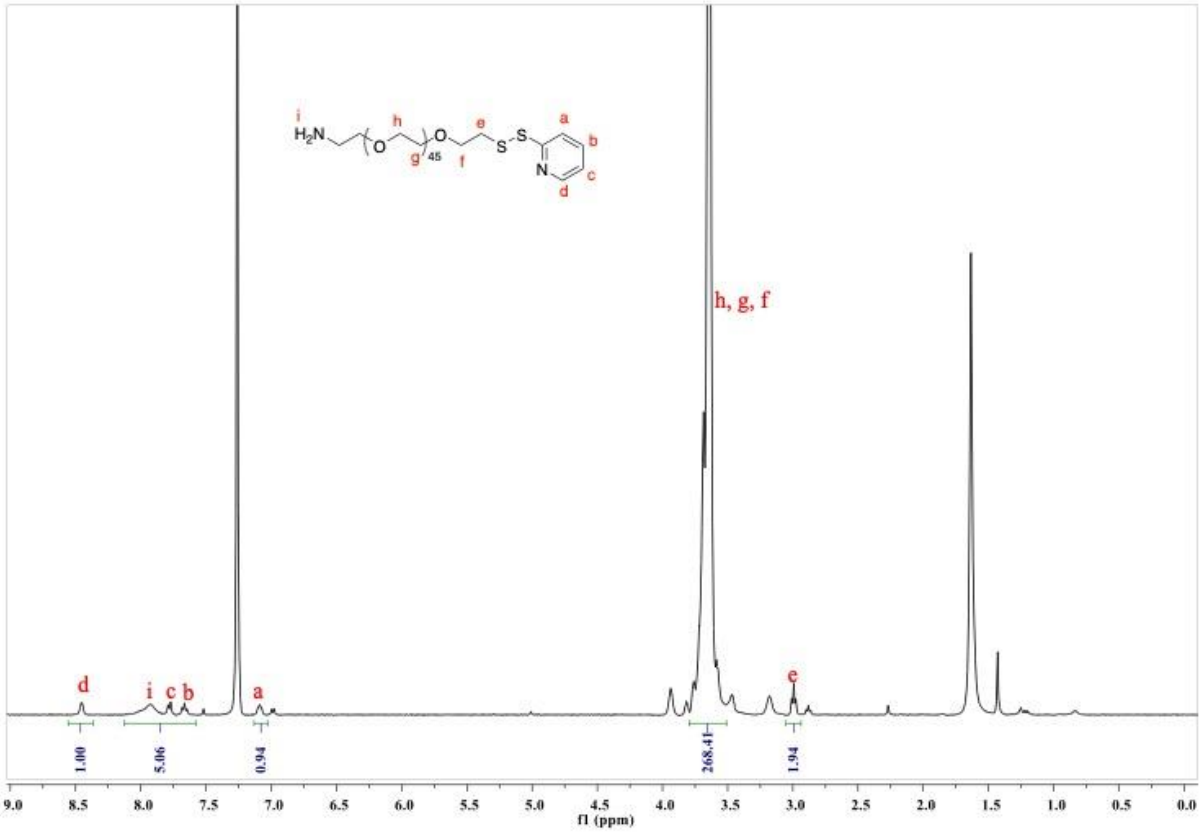

Figure 3.6. ^{1}H-NMR Spectrum of PDS-PEG-Amine.

3.3.3. Synthesis and Characterization of PDS-PEG-Py

In the synthesis of this polymer, amidation reaction was performed between NHS-activated pyrenebutyric acid and amine group of PDS-PEG-amine (Figure 3.7). The characterization of the polymer was done by ^{1}H-NMR. In the ^{1}H-NMR, specific peaks at 8.46 ppm, 7.76 ppm, 7.65 ppm and 7.08 belonging to PDS ring were observed. In addition to that, pyrene ring peaks were also observed at 8.34 ppm, 8.16-8.10 pmm, 8.05-7.95 ppm, were observed with fitting integrals as well as peak at 3.0 ppm belonging to ethyl group next to sulfur (Figure 3.8).

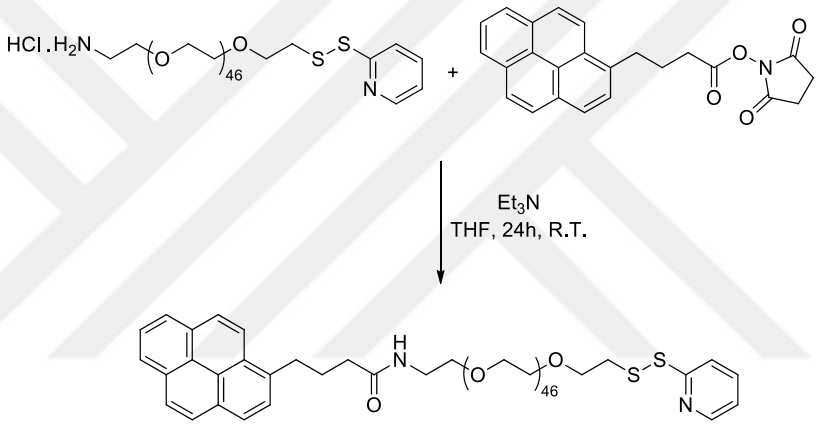

Figure 3.7. Synthesis of PDS-PEG-Py.

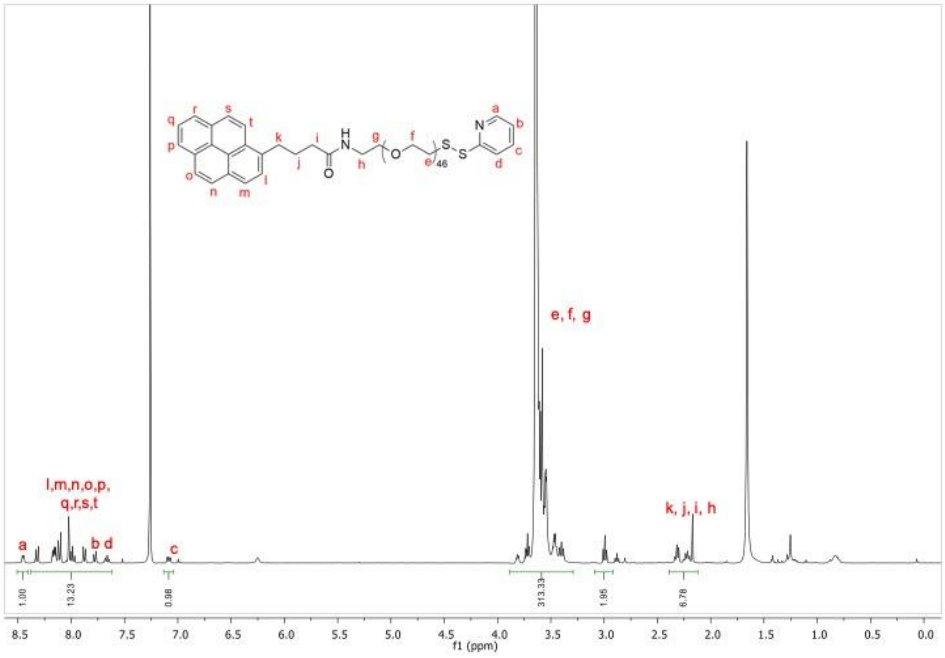

Figure 3.8. ^{1}H-NMR of PDS-PEG-Py.

3.3.4. Characterization of rGO/PPD

rGO can be physically functionalized via different non-covalent interactions and π-π stacking is one of the widely used method to functionalize rGO physically. Thereafter, we synthesized a small compound that has a pyrene group in its structure. Then, we functionalized rGO by using this pyrene group (Figure 3.9). In addition to that, this small molecule PPD also has a PDS group that enables it to undergo thiol-disulfide exchange reaction which is reversible. After the functionalization with PPD was achieved characterization of rGO/PPD was investigated by using XPS, cyclic voltammetry (CV) and FT-IR. In FT-IR, C=O peaks belonging to PPD was also observed in rGO/PPD (Figure 3.10). In XPS, there is an increase in nitrogen peak (originally coming from reduction of rGO) at 164.8 eV and new appereance of sulfur peak at 164 eV (Figure 3.12). In CV, the reduction and oxidation peaks belonging to glassy carbon electrode were decreased since the stack PPD prevents redox reaction between the electrode and the electrolyte (Figure 3.14).

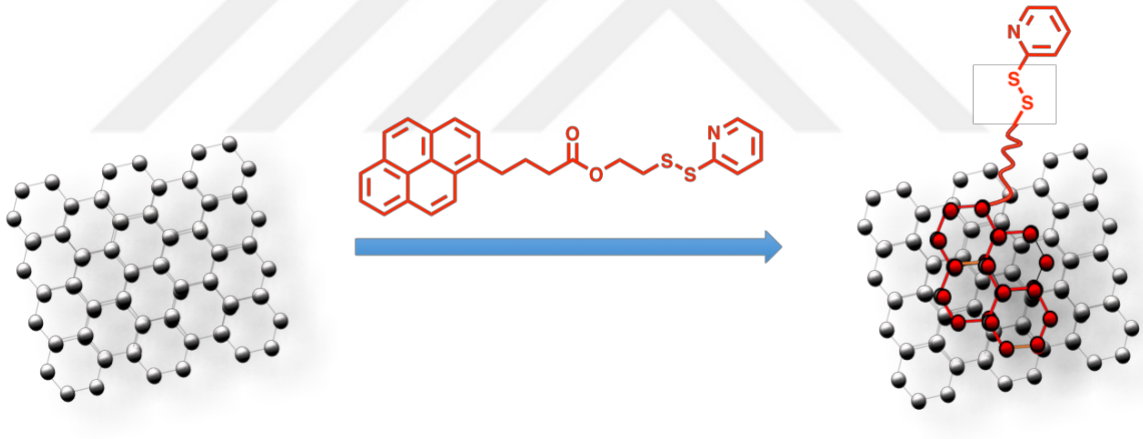

Figure 3.9. Illustration of rGO/PPD stacking.

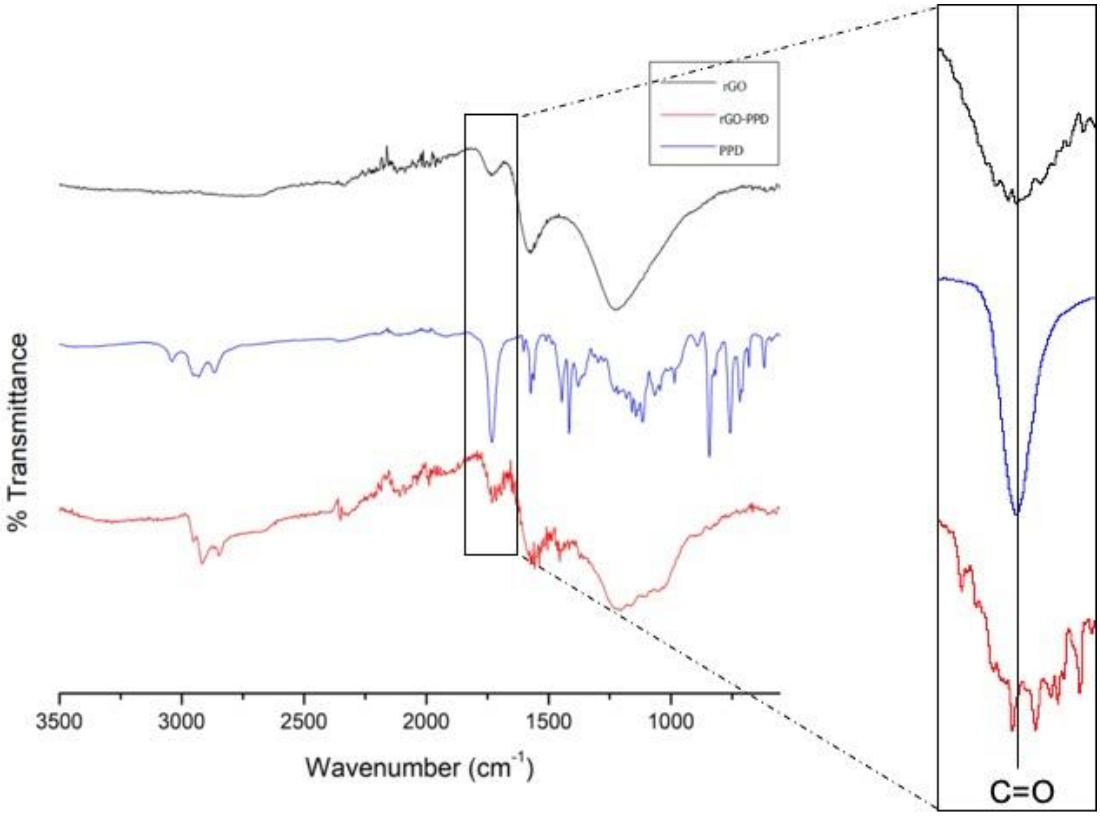

Figure 3.10. ATR-FT-IR of rGO, PPD and rGO/PPD.

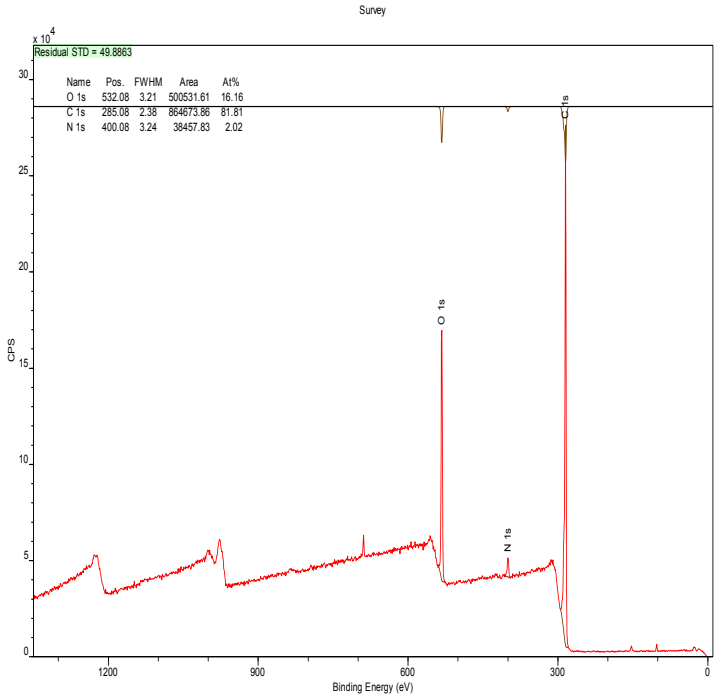

Figure 3.11. XPS of rGO.

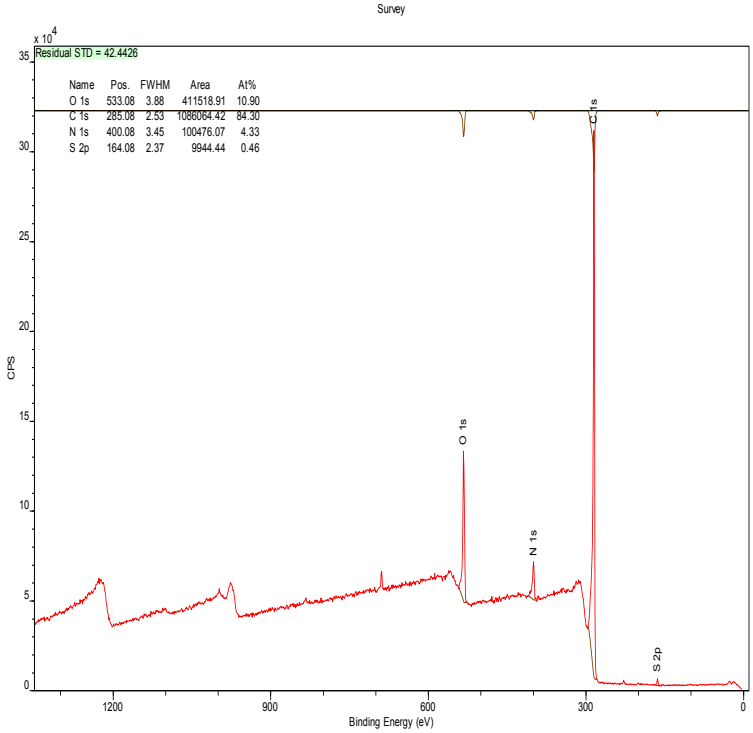

Figure 3.12. XPS of rGO/PPD.

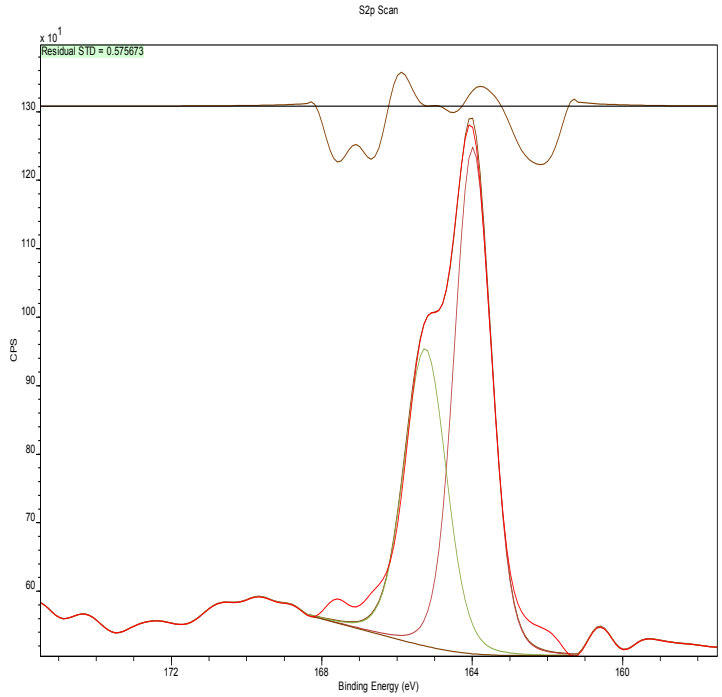

Figure 3.13. S_{2p} Scan of rGO/PPD.

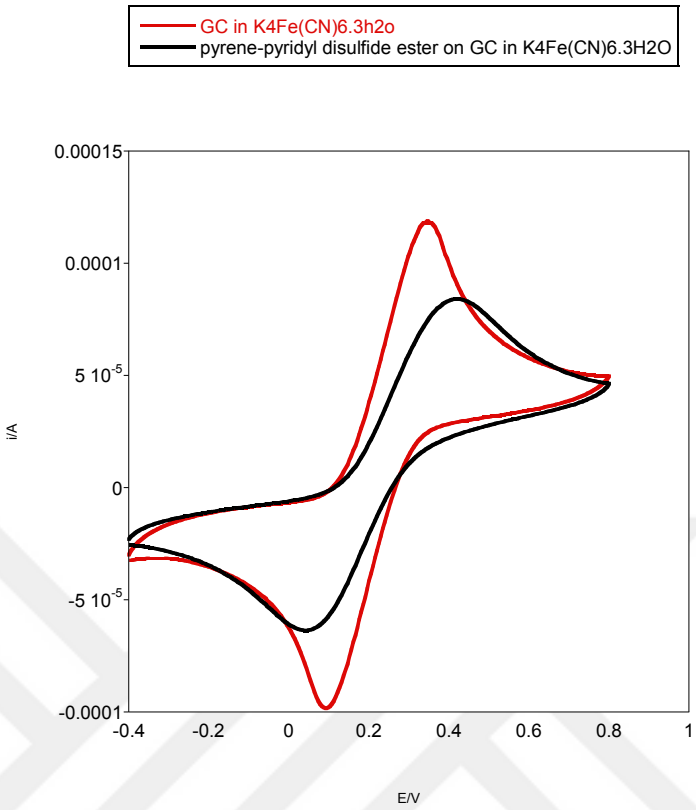

Figure 3.14. CV data of PPD Stacking.

3.3.5. Functionalization of rGO/PPD with small compounds via Thiol-disulfide Exchange Reaction

rGO can be modified physically and in some cases chemically as mentioned before. However, a system in which rGO was modified physically and chemically at the same time hasn't been developed yet. In our developed system, after physically functionalized rGO with PDS through its pyrene group, we used PDS functional group for post-modification of rGO via thiol-disulfide exchange chemistry. For this purpose, we used two different thiolated molecules; 6-(ferrocenyl)hexanethiol and 1H,1H,2H,2H-Perfluorodecanthiol. After the thiol-disulfide reaction has been performed, the characterization of the chemical functionalization was done by XPS.

Firstly, 6-(ferrocennyl)hexanethiol was used to modify rGO chemically (rGO/PPD-FeSH) (Figure 3.15). While the characterization of the chemical functionalization was done by XPS. In the XPS, two peaks belonging to Fe 2p ½ and Fe 2p, 2p 3/2 were observed at 723 eV and 710 eV respectively (Figure 3.16).

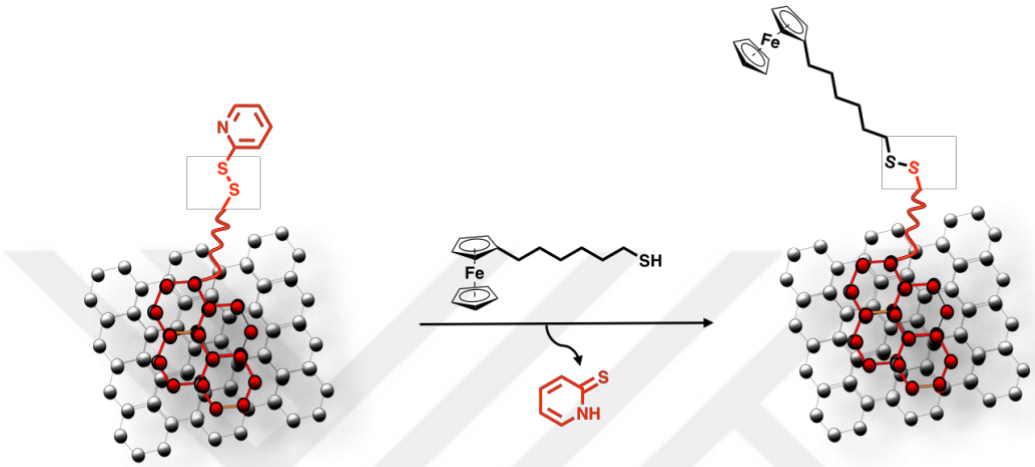

Figure 3.15. Schematic illustration of modification of rGO/PPD with 6-(Ferrocenyl)hexanethiol.

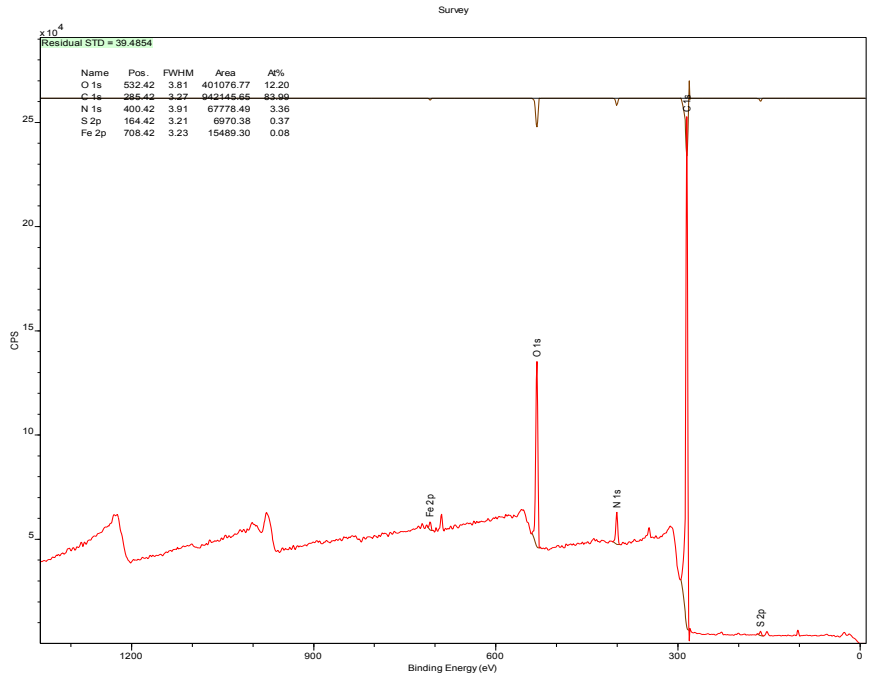

Figure 3.16. XPS data of rGO/PPD-FSH.

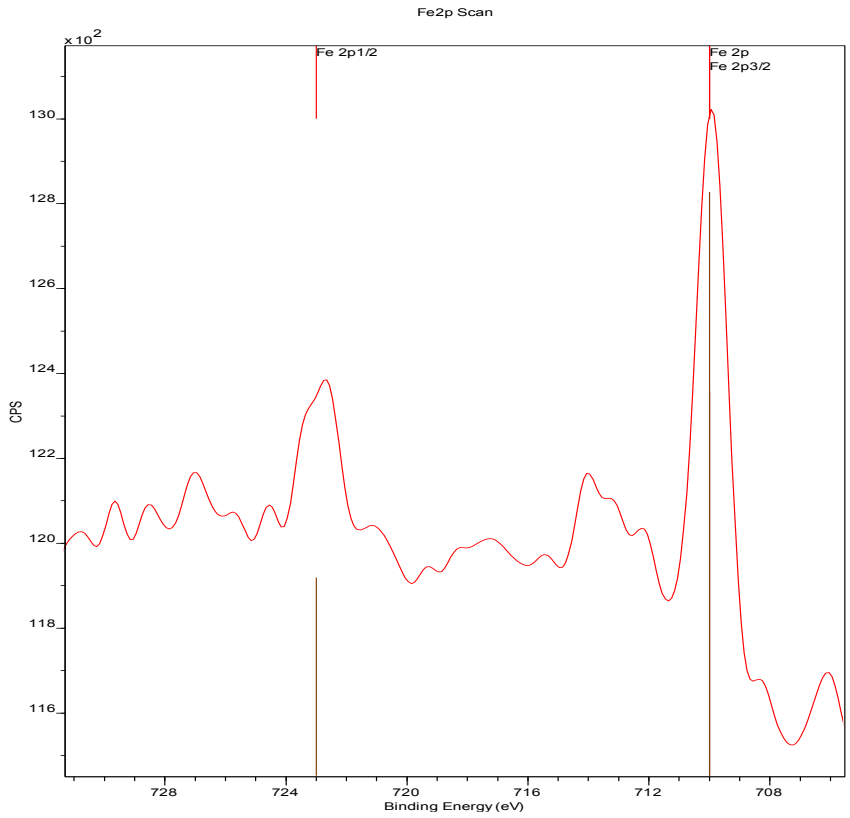

Figure 3.17. XPS of Fe 2p electron.

After the modification of rGO/PPD with ferrocenyl thiol, 1H,1H,2H,2H-Perfluorodecanthiol was used to chemically modify rGO/PPD via thiol-disulfide exchange reaction (rGO/PPD-FSH) (Figure 3.18). The characterization of the modification was done via XPS. In XPS, the fluorine peak was very distinguishable indicating successful thiol-disulfide exchange reaction (Figure 3.19).

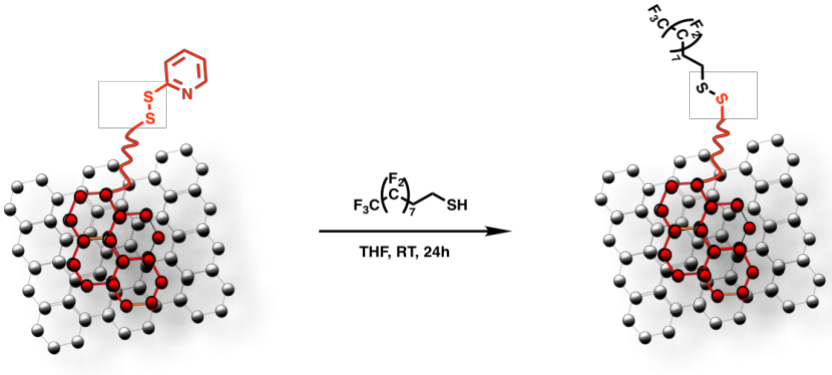

Figure 3.18. Schematic illustration of exchange reaction between rGO/PPD and 1H,1H,2H,2H-Perfluorodecanthiol.

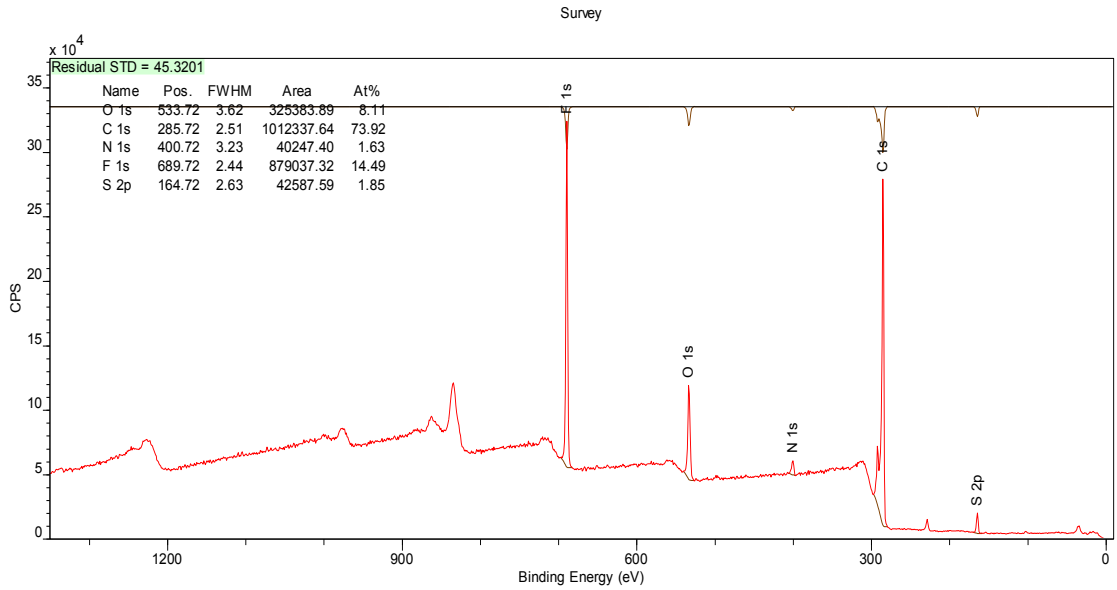

Figure 3.19. XPS data of rGO/PPD-FSH.

3.3.6. Functionalization and Characterization of rGO/PPD with PEG-SH via Thiol-disulfide Exchange Reaction

Even though rGO was modified with PPD physically and later on with two different thiolated molecules chemically via disulfide exchange reaction, the dispersibility of rGO in water was a problem since these small molecules used to modify rGO physically or chemically are water insoluble. Thereafter, rGO was modified with a hydrophilic compound (PEG-SH) in order to increase dispersibility of rGO in water (Figure 3.20). After the exchange reaction, the solubility of the obtained rGO was checked. As a result, the thiol-disulfide exchange reaction provided an increase in dispersibility time of rGO in water up to 12 hours whereas rGO precipitated in water after 12 hours (Figure 3.21). In FT-IR, specific peak belonging to C-O stretching band at 1030 was observed after thiol-disulfide exchange reaction. Also, treating rGO/PPD-PEG with DTT resulted in disappearance of this C-O banding peak since DTT removes PEG part by cleaving disulfide bond (Figure 3.22).

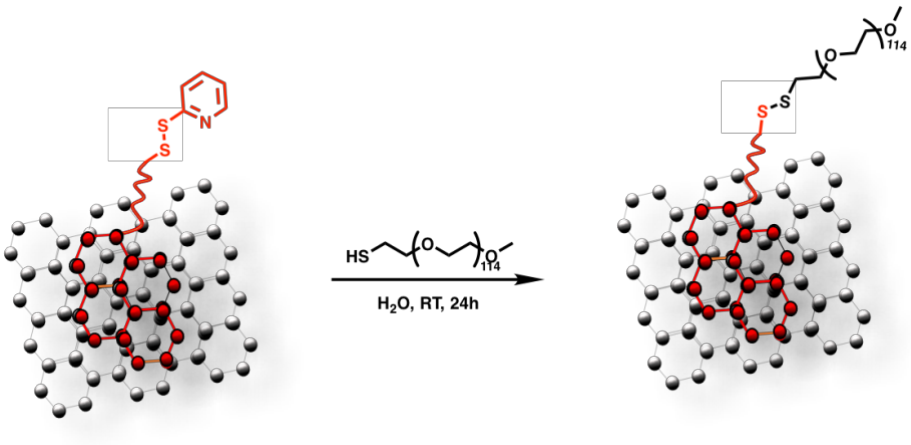

Figure 3.20. Schematic Illustration of modification of rGO/PPD with PEG-SH.

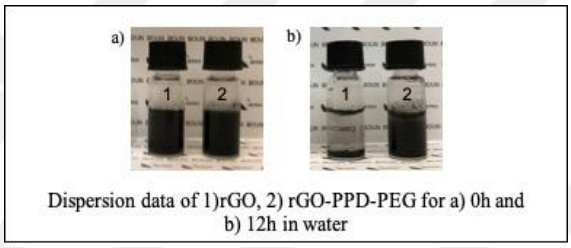

Figure 3.21. Water Solubility Experiment of rGO/PPD-PEG.

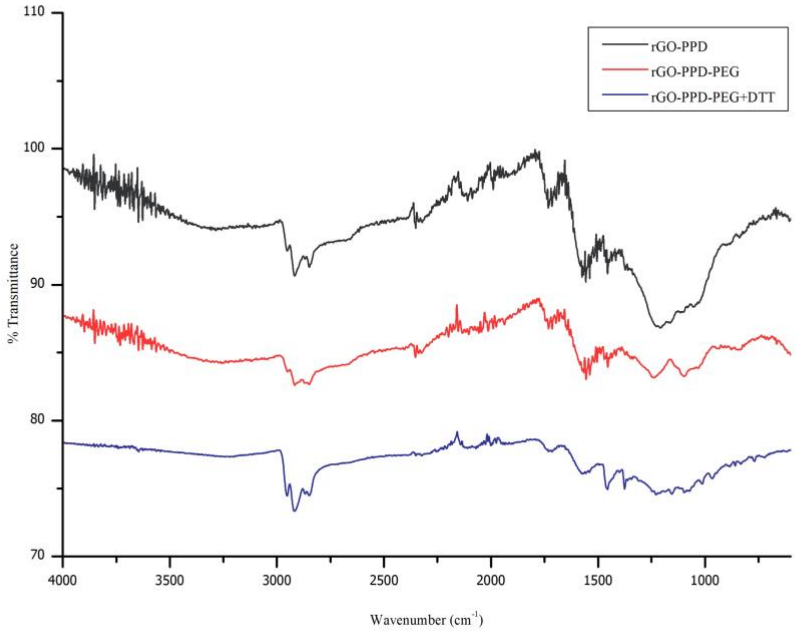

Figure 3.22. ATR-FT-IR Data of rGO/PPD-PEG Stacking and DTT Treatment.

3.3.7. Functionalization and Characterization of rGO with PDS-PEG-Py via Thiol-disulfide Exchange Reaction

Once the functionalization of rGO/PPD with PEG-SH increased the dispersibility of rGO in water, the idea of mimicking this nature directly by using pyrene and PDS containing PEG came to mind. While the pyrene unit was used to modify rGO physically, the PDS group will enable the post-modification of rGO via thiol-disulfide exchange reaction. After performing the exchange reaction, solubility experiment of modified rGO was performed. As a result, the dispersion time of modified rGO in water increased up to 12 hours (Figure 3.23).

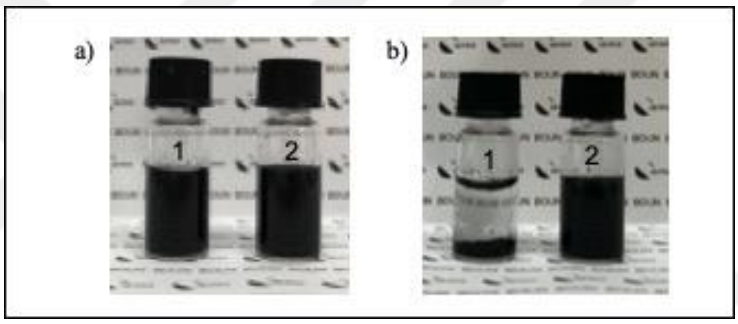

Figure 3.23. Dispersion data of (a) rGO, (b) rGO-PEG-PDS for (1) 0h and (b) 12h in water.

3.3.8. DTT Treatment and Characterization of rGO/PPD

In order to show that the modification of rGO with PPD was achieved via π-π stacking, a simple experiment, cleaving disulfide bond of rGO/PPD was performed since the release of pyridinethione can be observed in the UV (Figure 3.24). For this purpose, rGO/PPD was treated with DTT and after the precipitation of DTT treated rGO/PPD, the UV of solution was measured. As a result, specific absorption peak belonging to pyridinethione at 343 nm was observed in a time dependent manner (Figure 3.25). The presence of the peak at 343 nm indicates the release of pyridinethione from rGO/PPD with the treatment of DTT and the successful functionalization of rGO with PPD.

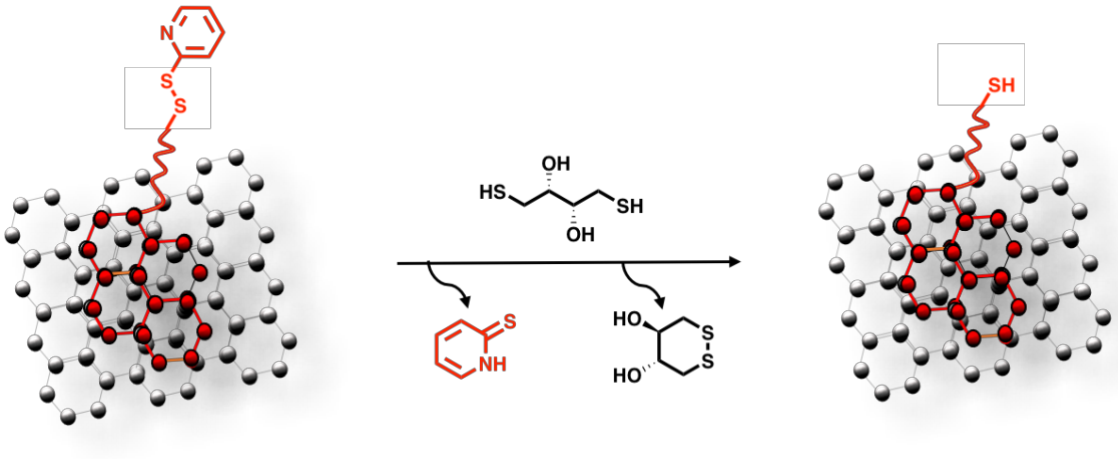

Figure 3.24. Illustration of DTT Treatment of rGO/PPD.

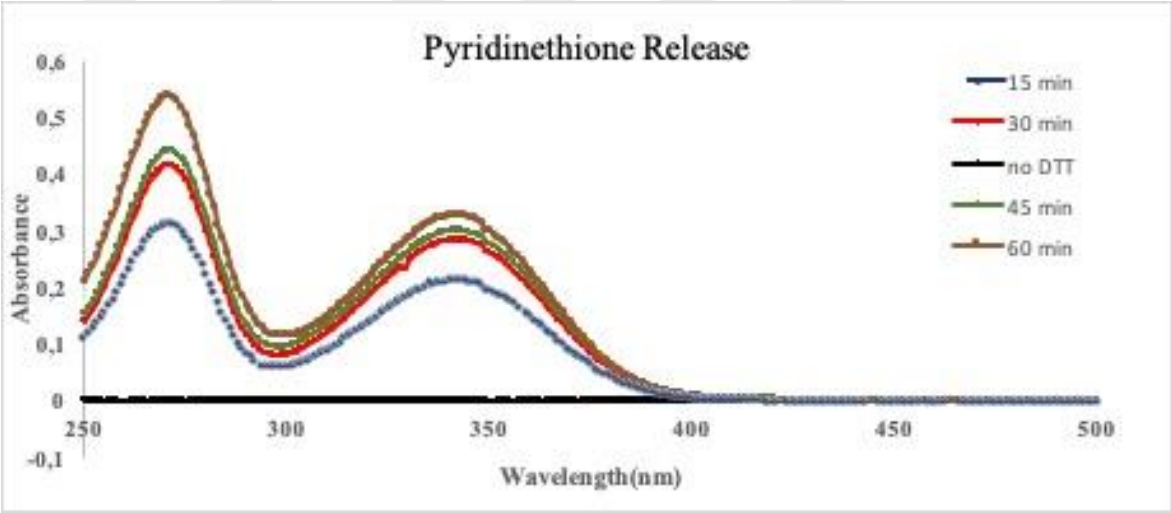

Figure 3.25. Pyridinethione Release from rGO/PPD after DTT treatment.

3.3.9. DTT and GSH Treatment and Characterization of Functionalize rGO/PPD

After functionalization of rGO/PPD, post-modification was carried out using 6-(ferrocenyl)hexanethiol and 1H,1H,2H,2H-perfluorodecanthiol. To characterize functionalization of rGO/PPD with these small molecules, rGO/PPD-FeSH was treated with DTT and rGO/PPD-FSH was treated with DTT and GSH. GSH is a molecule that undergoes thiol-disulfide exchange mechanism whereas DTT cleaves disulfide bonds that are present in the molecular structure.

rGO/PPD-FeSH was expected to release pyridinethione group in the presence of DTT as a result of cleavage of disulfide bond of PDS group (Figure 3.26). As expected, the XPS data indicates the cleavage of disulfide bond since the percentage of sulphur in the rGO surface was decreased compared to XPS of rGO as well as disappearance of iron peaks (Figure 3.27).

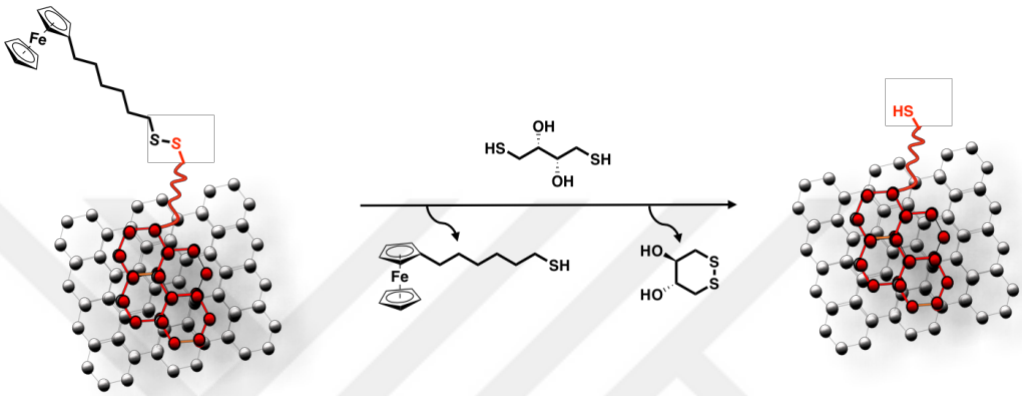

Figure 3.26. Schematic Illustration of DTT Cleavage of rGO/ ppd-FeSH.

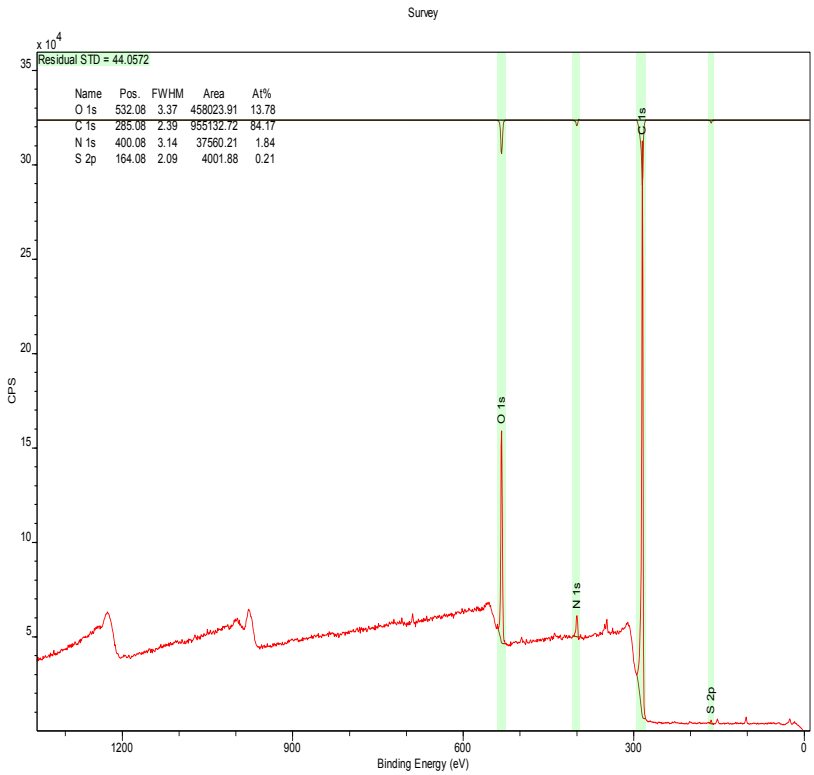

Figure 3.27. XPS data of rGO/PPD-FeSH After DTT Treatment.

On the other hand, rGO/PPD-FSH was treated with GSH and DTT separately (Figure 3.28). In this process, GSH reacts with the disulfide bond of rGO/PPD-FSH via exchange mechanism. The resulting rGO was expected to GSH unit in its structure indicating removal of fluorine. In XPS of GSH treated rGO/PPD-FSH, the intensity of fluorine peak decreases indicating the removal of thiol-fluorine group (Figure 3.29). In addition to that, the DTT treatment was seemed to be more efficient than GSH treatment since all off the fluorine peak was disappeared in the obtained XPS data (Figure 3.30).

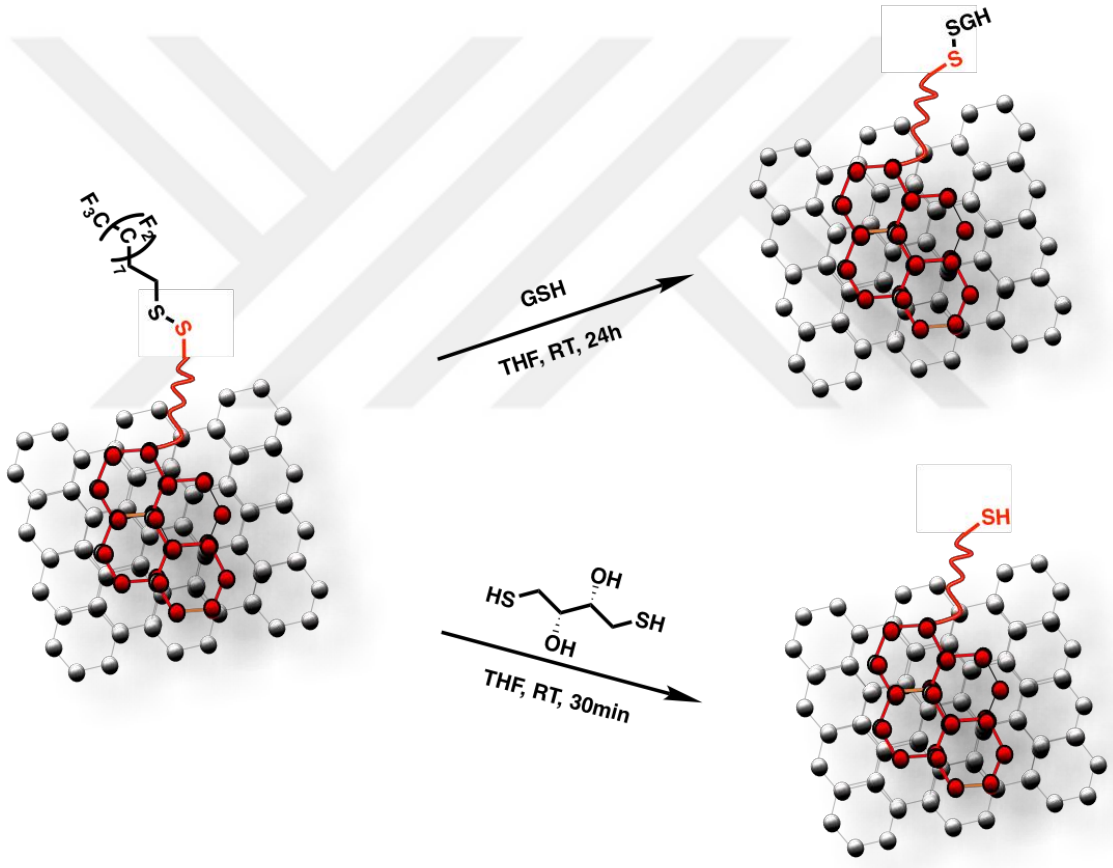

Figure 3.28. Schematic Representation of GSH nad DTT Treatment of rGO/PPD-FSH.

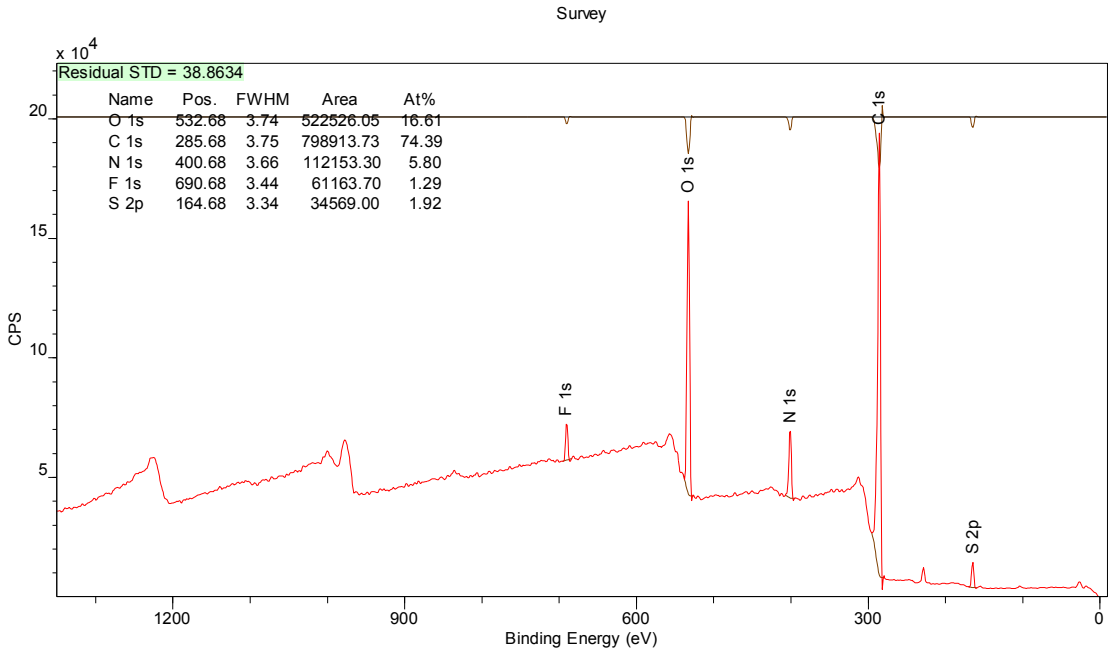

Figure 3.29. XPS Data of rGO/PPD-FSH After GSH Treatment.

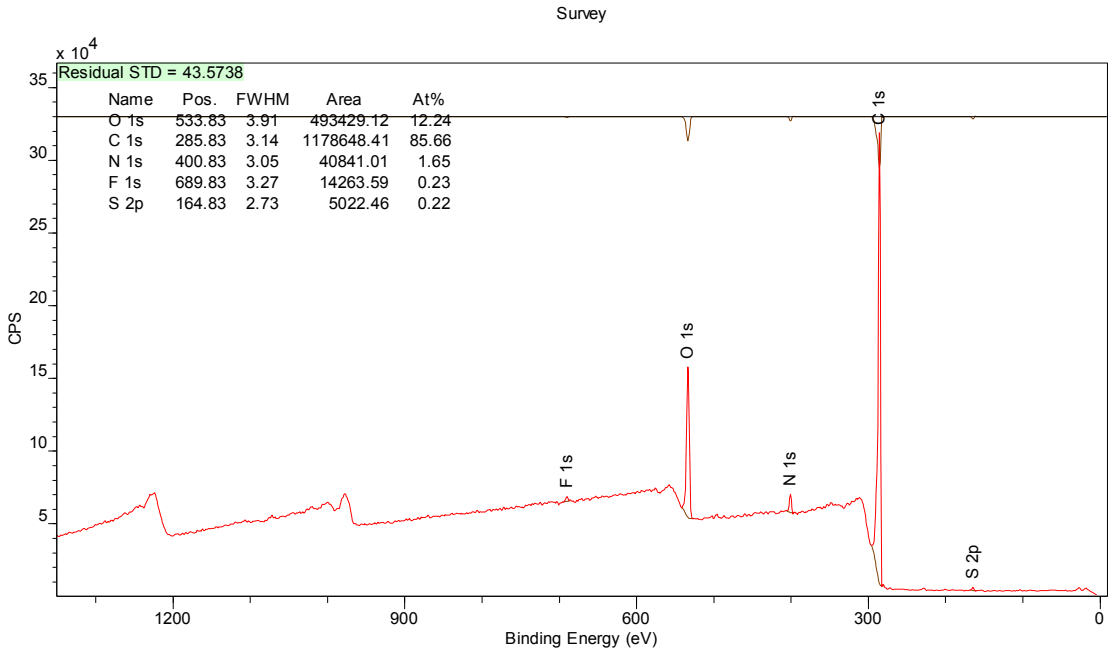

Figure 3.30. XPS data of rGO/PPD-FSH After DTT Treatment.

3.4. Conclusion

In this project, a system in which rGO can be reversibly functionalize via thiol-disulfide exchange reaction was developed. The chemical functionalization of rGO is difficult due to the lack of functional groups on its surface as mentioned before. Thereafter, a system that enables the chemical surface modification of rGO is desirable. For this purpose, we first synthesized a small molecule, PPD, that contains pyrene and pyridyldisulfide functional groups. Here, pyrene can be used to physically functionalize rGO surface while the PDS group can be used to chemically functionalize rGO surface via thiol-disulfide exchange reaction in a reversible way. After the modification of rGO surface with PPD, 6-(ferrocenyl)hexanethiol and 1H,1H,2H,2H-perfluorodecanethiol were used to chemically modify rGO. After the functionalization, DTT and GSH were used to cleave PDS group and to show reversibility of the exchange reaction respectively. The characterizations of the rGO modification with these molecules were done by XPS. Later, a PEG-SH was used to modify rGO/PPD in order to show reversibility of the exchange chemistry as well as to increase dispersibility of rGO in water. Lastly, PDS-PEG-Py was used to functionalize rGO and the solubility experiment of the PEG functionalized rGO was performed. PDS-PEG-Py functionalization of rGO can be promising system for biological applications such as drug or protein delivery due to the reversibility of the thiol-disulfide reaction as well as increased facile dispersibility of rGO in water.

4. CONCLUSION

Throughout the thesis, two projects have been described. Both of the projects were including the concept of rGO in which the great properties of this material enable the utilization of it in different areas. For instance, in the first project, a polymeric network with incorporation of rGO was developed to release proteins in a controlled manner with the help of photothermal effect that comes from rGO incorporation. Here, the release mechanism occurs when the heat supplied by rGO under NIR ruptures the DA cycloadduct that is in the hydrogel network. In this project, characterization of different hydrogels with varying w/v concentrations were carried out by SEM, rheometer as well as swelling experiments. After the characterizations of hydrogels, passive release studies of FITC-Dextran (M_n= 70 kDa) from rGO-containing hydrogels were completed. However, the active release from those hydrogels should be studied. In addition to this project, a pyrene and a PDS group containing small compounds as well as a PEG with the same functional groups were used to functionalize rGO physically via π-π stacking as well as chemically via thiol-disulfide exchange reaction. The PDS group enables the further modification of rGO surface with any thiolated molecule resulting in a reversibly functionalizable rGO that can be used in various application. Also, the PDS-PEG-Py functionalization of rGO surface lead to an increased solubility of rGO. Thereafter, the system can also be used in biological applications.

REFERENCES

1. Smith, A.T., A.M. LaChance, S. Zeng, B. Liu, and L. Sun, “Synthesis, Properties, And Applications Of Graphene Oxide/reduced Graphene Oxide And Their Nanocomposites”, *Nano Materials Science*, Vol. 1, pp. 31–47, 2019.

2. Tarcan, R., O. Todor-Boer, I. Petrovai, C. Leordean, S. Astilean, and I. Botiz, “Reduced Graphene Oxide Today”, *Journal of Materials Chemistry C*, Vol. 8, pp. 1198–1224, 2020.

3. Li, Q., Q. Li, D. Chen, D. Chen, J. Miao, J. Miao, S. Lin, S. Lin, Z. Yu, Z. Yu, Y. Han, Z. Yang, X. Zhi, D. Cui, D. Cui, and Z. An, “Ag-Modified 3D Reduced Graphene Oxide Aerogel-Based Sensor With An Embedded Microheater For A Fast Response And High-Sensitive Detection Of NO2”, *ACS Applied Materials and Interfaces*, Vol. 12, pp. 25243–25252, 2020.

4. Xu, M., J. Qi, F. Li, X. Liao, S. Liu, and Y. Zhang, “Ultra-thin, Transparent And Flexible Tactile Sensors Based On Graphene Films With Excellent Anti-interference”, *RSC Advances*, Vol. 7, pp. 30506–30512, 2017.

5. Choudhary, P., T. Parandhaman, B. Ramalingam, N. Duraipandy, M.S. Kiran, and S.K. Das, “Fabrication Of Nontoxic Reduced Graphene Oxide Protein Nanoframework As Sustained Antimicrobial Coating For Biomedical Application”, *ACS Applied Materials and Interfaces*, Vol. 9, pp. 38255–38269, 2017.

6. Wang, M., L.D. Duong, N.T. Mai, S. Kim, Y. Kim, H. Seo, Y.C. Kim, W. Jang, Y. Lee, J. Suhr, and J. Do Nam, “All-solid-state Reduced Graphene Oxide Supercapacitor With Large Volumetric Capacitance And Ultralong Stability Prepared By Electrophoretic Deposition Method”, *ACS Applied Materials and Interfaces*, Vol. 7, pp. 1348–1354, 2015.

7. Li, T., L. Xia, H. Yang, X. Wang, T. Zhang, X. Huang, L. Xiong, C. Qin, and G. Wen, "Construction Of A Cu-Sn Heterojunction Interface Derived From A Schottky Junction In Cu@Sn/rGO Composites As A Highly Efficient Dielectric Microwave Absorber", *ACS Applied Materials and Interfaces*, Vol. 13, pp. 11911–11919, 2021.

8. Oz, Y., A. Barras, R. Sanyal, R. Boukherroub, S. Szunerits, and A. Sanyal, "Functionalization Of Reduced Graphene Oxide Via Thiol-maleimide 'click' chemistry: Facile Fabrication Of Targeted Drug Delivery Vehicles", *ACS Applied Materials and Interfaces*, Vol. 9, pp. 34194–34203, 2017.

9. Cheng, C., S. Li, A. Thomas, N.A. Kotov, and R. Haag, "Functional Graphene Nanomaterials Based Architectures: Biointeractions, Fabrications, And Emerging Biological Applications", *Chemical Reviews*, Vol. 117, pp. 1826–1914, 2017.

10. Yu, W., L. Sisi, Y. Haiyan, and L. Jie, "Progress In The Functional Modification Of Graphene/graphene Oxide: A Review", *RSC Advances*, Vol. 10, pp. 15328–15345, 2020.

11. Piñeiro-García, A., S.M. Vega-Díaz, F. Tristán, D. Meneses-Rodríguez, G.J. Labrada-Delgado, and V. Semetey, "New Insights In The Chemical Functionalization Of Graphene Oxide By Thiol-ene Michael Addition Reaction", *FlatChem*, Vol. 26, pp. 1–10, 2021.

12. Buwalda, S.J., K.W.M. Boere, P.J. Dijkstra, J. Feijen, T. Vermonden, and W.E. Hennink, "Hydrogels In A Historical Perspective: From Simple Networks To Smart Materials", *Journal of Controlled Release*, Vol. 190, pp. 254–273, 2014.

13. Peppas, N.A., J.Z. Hilt, A. Khademhosseini, and R. Langer, "Hydrogels In Biology And Medicine: From Molecular Principles To Bionanotechnology", *Advanced Materials*, Vol. 18, pp. 1345–1360, 2006.

14. Hoffman, A.S., and B.D. Ratner, “Synthetic Hydrogels For Biomedical Applications - A Review”, *American Chemical Society, Polymer Preprints, Division of Polymer Chemistry*, Vol. 16, pp. 272–275, 1975.

15. Kharkar, P.M., M.S. Rehmann, K.M. Skeens, E. Maverakis, and A.M. Kloxin, “Thiol − Ene Click Hydrogels For Therapeutic Delivery” *ACS Biomater. Sci. Eng.*, Vol. 2, pp. 165-179, 2016.

16. Lin, C., and K.S. Anseth, “Expert Review PEG Hydrogels For The Controlled Release Of Biomolecules In Regenerative Medicine”, Vol. 26 2009.

17. Akhtar, M.F., M. Hanif, and N.M. Ranjha, “Methods Of Synthesis Of Hydrogels … A Review”, *Saudi Pharmaceutical Journal*, Vol. 24, pp. 554–559, 2016.

18. Madduma-Bandarage, U.S.K., and S. V. Madihally, “Synthetic Hydrogels: Synthesis, Novel Trends, And Applications”, *Journal of Applied Polymer Science*, Vol. 138, pp. 1–23, 2021.

19. Ghobril, C., and M.W. Grinstaff, “The Chemistry And Engineering Of Polymeric Hydrogel Adhesives For Wound Closure: A Tutorial”, *Chemical Society Reviews*, Vol. 44, pp. 1820–1835, 2015.

20. Yigit, S., R. Sanyal, and A. Sanyal, “Fabrication And Functionalization Of Hydrogels Through "Click" Chemistry”, *Chemistry: An Asian Journal,* Vol. 6, pp. 2648–2659, 2011.

21. Gregoritza, M., V. Messmann, K. Abstiens, F.P. Brandl, and A.M. Goepferich, “Controlled Antibody Release From Degradable Thermoresponsive Hydrogels Cross-Linked By Diels − Alder Chemistry” *Biomacromolecules,* Vol. 18, pp. 2410-2418, 2017.

22. Matsumura, S., A.R. Hlil, C. Lepiller, J. Gaudet, D. Guay, Z. Shi, S. Holdcroft, and A.S. Hay, "Stability And Utility Of Pyridyl Disulfide Functionality In RAFT And Conventional Radical Polymerizations", *Journal of Polymer Science: Part A: Polymer Chemistry*, Vol. 46, pp. 7207–7224, 2008.

23. Gupta, N., B.F. Lin, L.M. Campos, M.D. Dimitriou, S.T. Hikita, N.D. Treat, M. V. Tirrell, D.O. Clegg, E.J. Kramer, and C.J. Hawker, "A Versatile Approach To High-throughput Microarrays Using Thiol-ene Chemistry", *Nature Chemistry*, Vol. 2, pp. 138–145, 2010.

24. Jansen, L.E., L.J. Negrón-Piñeiro, S. Galarza, and S.R. Peyton, "Control Of Thiol-maleimide Reaction Kinetics In PEG Hydrogel Networks", *Acta Biomaterialia*, Vol. 70, pp. 120–128, 2018.

25. Darling, N.J., Y.S. Hung, S. Sharma, and T. Segura, "Controlling The Kinetics Of Thiol-maleimide Michael-type Addition Gelation Kinetics For The Generation Of Homogenous Poly(ethylene Glycol) Hydrogels", *Biomaterials*, Vol. 101, pp. 199–206, 2016.

26. Hoare, T.R., and D.S. Kohane, "Hydrogels In Drug Delivery: Progress And Challenges", *Polymer*, Vol. 49, pp. 1993–2007, 2008.

27. Narayanaswamy, R., and V.P. Torchilin, "Hydrogels And Their Applications In Targeted Drug Delivery", *Molecules*, Vol. 24 2019.

28. Caló, E., and V. V. Khutoryanskiy, "Biomedical Applications Of Hydrogels: A Review Of Patents And Commercial Products", *European Polymer Journal*, Vol. 65, pp. 252–267, 2015.

29. Li, L., J.M. Scheiger, and P.A. Levkin, "Design And Applications Of Photoresponsive Hydrogels", Vol. 1807333 2019.

30. Wang, D., "Smart Release Of Antibiotics To Combat Bacterial", pp. 432–436, 2017.

31. Ganta, S., H. Devalapally, A. Shahiwala, and M. Amiji, “A Review Of Stimuli-responsive Nanocarriers For Drug And Gene Delivery”, Vol. 126, pp. 187–204, 2008.

32. Fleige, E., M.A. Quadir, and R. Haag, “Stimuli-responsive Polymeric Nanocarriers For The Controlled Transport Of Active Compounds : Concepts And Applications”, *Advanced Drug Delivery Reviews*, Vol. 64, pp. 866–884, 2012.

33. Ahn, S., R.M. Kasi, S. Kim, and Y. Zhou, “Stimuli-responsive Polymer Gels”, *Soft Matter,* Vol. 4, pp. 1151–1157, 2008.

34. Kharkar, P.M., K.L. Kiick, and A.M. Kloxin, “Design Of Thiol- And Light-Sensitive Degradable Hydrogels Using Michael-Type Addition Reactions” *Polymer Chemistry,* Vol. 6, pp. 5565-5574, 2015.

35. Cadamuro, F., L. Russo, and F. Nicotra, “Biomedical Hydrogels Fabricated Using Diels–Alder Crosslinking”, *European Journal of Organic Chemistry*, Vol. 2021, pp. 374–382, 2021.

36. Tasdelen, M.A., “Diels-Alder ‘click’ reactions: Recent Applications In Polymer And Material Science”, *Polymer Chemistry*, Vol. 2, pp. 2133–2145, 2011.

37. Hizal, G., U. Tunca, and A. Sanyal, “Discrete Macromolecular Constructs Via The Diels-Alder ‘click’ reaction”, *Journal of Polymer Science, Part A: Polymer Chemistry*, Vol. 49, pp. 4103–4120, 2011.

38. Wei, H.L., Z. Yang, L.M. Zheng, and Y.M. Shen, “Thermosensitive Hydrogels Synthesized By Fast Diels-Alder Reaction In Water”, *Polymer*, Vol. 50, pp. 2836–2840, 2009.

39. Kirchhof, S., M. Gregoritza, V. Messmann, N. Hammer, A.M. Goepferich, and F.P. Brandl, “Diels-Alder Hydrogels With Enhanced Stability: First Step Toward Controlled Release Of Bevacizumab”, *European Journal of Pharmaceutics and Biopharmaceutics*, Vol. 96, pp. 217–225, 2015.

40. Smith, L.J., S.M. Taimoory, R.Y. Tam, A.E.G. Baker, N. Binth Mohammad, J.F. Trant, and M.S. Shoichet, “Diels-Alder Click-Cross-Linked Hydrogels With Increased Reactivity Enable 3D Cell Encapsulation”, *Biomacromolecules*, Vol. 19, pp. 926–935, 2018.

41. Nimmo, C.M., S.C. Owen, and M.S. Shoichet, “Diels-alder Click Cross-linked Hyaluronic Acid Hydrogels For Tissue Engineering”, *Biomacromolecules*, Vol. 12, pp. 824–830, 2011.

42. Altinbasak, I., R. Sanyal, and A. Sanyal, “Best Of Both Worlds: Diels-Alder Chemistry Towards Fabrication Of Redox-responsive Degradable Hydrogels For Protein Release”, *RSC Advances*, Vol. 6, pp. 74757–74764, 2016.

43. Kirchhof, S., F.P. Brandl, N. Hammer, and A.M. Goepferich, “Investigation Of The Diels-Alder Reaction As A Cross-linking Mechanism For Degradable Poly(ethylene Glycol) Based Hydrogels”, *Journal of Materials Chemistry B*, Vol. 1, pp. 4855–4864, 2013.

44. Northrop, B.H., S.H. Frayne, and U. Choudhary, “Thiol-maleimide ‘click’ chemistry: Evaluating The Influence Of Solvent, Initiator, And Thiol On The Reaction Mechanism, Kinetics, And Selectivity”, *Polymer Chemistry*, Vol. 6, pp. 3415–3430, 2015.

45. Subramani, C., N. Cengiz, K. Saha, T.N. Gevrek, X. Yu, Y. Jeong, A. Bajaj, A. Sanyal, and V.M. Rotello, “Direct Fabrication Of Functional And Biofunctional Nanostructures Through Reactive Imprinting”, *Advanced Materials*, Vol. 23, pp. 3165–3169, 2011.

46. Nair, D.P., M. Podgórski, S. Chatani, T. Gong, W. Xi, C.R. Fenoli, and C.N. Bowman, “The Thiol-Michael Addition Click Reaction: A Powerful And Widely Used Tool In Materials Chemistry”, *Chemistry of Materials*, Vol. 26, pp. 724–744, 2014.

47. Billiet, L., O. Gok, A.P. Dove, A. Sanyal, L.T.T. Nguyen, and F.E. Du Prez, “Metal-free Functionalization Of Linear Polyurethanes By Thiol-maleimide Coupling Reactions”, *Macromolecules*, Vol. 44, pp. 7874–7878, 2011.

48. Long, K.F., H. Wang, T.T. Dimos, and C.N. Bowman, “Effects Of Thiol Substitution On The Kinetics And Efficiency Of Thiol-Michael Reactions And Polymerizations”, *Macromolecules*, Vol. 54, pp. 3093–3100, 2021.

49. Arslan, M., T.N. Gevrek, A. Sanyal, and R. Sanyal, “Cyclodextrin Mediated Polymer Coupling Via Thiol-maleimide Conjugation: Facile Access To Functionalizable Hydrogels”, *RSC Advances*, Vol. 4, pp. 57834–57841, 2014.

50. Fu, Y., and W.J. Kao, “In Situ Forming Poly(ethylene Glycol)-based Hydrogels Via Thiol-maleimide Michael-type Addition”, *Journal of Biomedical Materials Research - Part A*, Vol. 98 A, pp. 201–211, 2011.

51. Kharkar, P.M., R.A. Scott, L.P. Olney, P.J. LeValley, E. Maverakis, K.L. Kiick, and A.M. Kloxin, “Controlling The Release Of Small, Bioactive Proteins Via Dual Mechanisms With Therapeutic Potential”, *Advanced Healthcare Materials*, Vol. 6, pp. 1–12, 2017.

52. Sun, P., T. Huang, X. Wang, G. Wang, Z. Liu, G. Chen, and Q. Fan, “Dynamic-Covalent Hydrogel With NIR-Triggered Drug Delivery For Localized Chemo-Photothermal Combination Therapy”, *Biomacromolecules*, Vol. 21, pp. 556–565, 2020.

53. Wang, X., F. Lv, T. Li, Y. Han, Z. Yi, M. Liu, J. Chang, and C. Wu, “Electrospun Micropatterned Nanocomposites Incorporated With Cu2S Nanoflowers For Skin Tumor Therapy And Wound Healing”, *ACS Nano*, Vol. 11, pp. 11337–11349, 2017.

54. Cheng, M., H. Wang, Z. Zhang, N. Li, X. Fang, and S. Xu, “Gold Nanorod-embedded Electrospun Fibrous Membrane As A Photothermal Therapy Platform”, *ACS Applied Materials and Interfaces*, Vol. 6, pp. 1569–1575, 2014.

55. Maity, S., W.C. Wu, C. Xu, J.B. Tracy, K. Gundogdu, J.R. Bochinski, and L.I. Clarke, “Spatial Temperature Mapping Within Polymer Nanocomposites Undergoing Ultrafast Photothermal Heating Via Gold Nanorods”, *Nanoscale*, Vol. 6, pp. 15236–15247, 2014.

56. Chen, L., L. Si, F. Wu, S.Y. Chan, P. Yu, and B. Fei, "Electrical And Mechanical Self-healing Membrane Using Gold Nanoparticles As Localized 'nano-heaters'", *Journal of Materials Chemistry C*, Vol. 4, pp. 10018–10025, 2016.

57. Li, Y., Y. Fu, Z. Ren, X. Li, C. Mao, and G. Han, "Enhanced Cell Uptake Of Fluorescent Drug-loaded Nanoparticles Via An Implantable Photothermal Fibrous Patch For More Effective Cancer Cell Killing", *Journal of Materials Chemistry B*, Vol. 5, pp. 7504–7511, 2017.

58. Zhang, Z., S. Liu, H. Xiong, X. Jing, Z. Xie, X. Chen, and Y. Huang, "Electrospun PLA/MWCNTs Composite Nanofibers For Combined Chemo- And Photothermal Therapy", *Acta Biomaterialia*, Vol. 26, pp. 115–123, 2015.

59. Zhang, J., T. Zheng, E. Alarçin, B. Byambaa, X. Guan, J. Ding, Y.S. Zhang, and Z. Li, "Porous Electrospun Fibers With Self-Sealing Functionality: An Enabling Strategy For Trapping Biomacromolecules", *Small*, Vol. 13, pp. 1–15, 2017.

60. Abueva, C.D., P.-S. Chung, H.-S. Ryu, S.-Y. Park, and S.H. Woo, "Photoresponsive Hydrogels As Drug Delivery Systems", *Medical Lasers*, Vol. 9, pp. 6–11, 2020.

61. He, J., M. Shi, Y. Liang, and B. Guo, "Conductive Adhesive Self-healing Nanocomposite Hydrogel Wound Dressing For Photothermal Therapy Of Infected Full-thickness Skin Wounds", *Chemical Engineering Journal*, Vol. 394, pp. 124888, 2020.

62. Matai, I., G. Kaur, S. Soni, A. Sachdev, Vikas, and S. Mishra, "Near-infrared Stimulated Hydrogel Patch For Photothermal Therapeutics And Thermoresponsive Drug Delivery", *Journal of Photochemistry and Photobiology B: Biology*, Vol. 210, pp. 111960, 2020.

63. Ruan, C., C. Liu, H. Hu, X.L. Guo, B.P. Jiang, H. Liang, and X.C. Shen, "NIR-II Light-modulated Thermosensitive Hydrogel For Light-triggered Cisplatin Release And Repeatable Chemo-photothermal Therapy", *Chemical Science*, Vol. 10, pp. 4699–4706, 2019.

64. Liu, B., J. Sun, J. Zhu, B. Li, C. Ma, X. Gu, K. Liu, H. Zhang, F. Wang, J. Su, and Y. Yang, "Injectable And NIR-Responsive DNA–Inorganic Hybrid Hydrogels With Outstanding Photothermal Therapy", *Advanced Materials*, Vol. 32, pp. 1–6, 2020.

65. Moorcroft, S.C.T., L. Roach, D.G. Jayne, Z.Y. Ong, Z.Y. Ong, and S.D. Evans, "Nanoparticle-Loaded Hydrogel For The Light-Activated Release And Photothermal Enhancement Of Antimicrobial Peptides", *ACS Applied Materials and Interfaces*, Vol. 12, pp. 24544–24554, 2020.

66. Tang, Y., and G. Wang, "NIR Light-responsive Nanocarriers For Controlled Release", *Journal of Photochemistry and Photobiology C: Photochemistry Reviews*, Vol. 47, pp. 100420, 2021.

67. Hyunwoo, K., L. Duhwan, K. Jinhwan, K. Tae-Il, and K. Won Jong, "Photothermally Triggered Cytosolic Drug Delivery Via Endosome Disruption Using A Functionalized Reduced Graphene Oxide", *ACS Nano*, Vol. 7, pp. 6735–6746, 2013.

68. Wang, C., J. Mallela, U.S. Garapati, S. Ravi, V. Chinnasamy, Y. Girard, M. Howell, and S. Mohapatra, "A Chitosan-modified Graphene Nanogel For Noninvasive Controlled Drug Release", *Nanomedicine: Nanotechnology, Biology, and Medicine*, Vol. 9, pp. 903–911, 2013.

69. Sherlock, S.P., S.M. Tabakman, L. Xie, and H. Dai, "Photothermally Enhanced Drug Delivery By Ultrasmall Multifunctional FeCo/graphitic Shell Nanocrystals", *ACS Nano*, Vol. 5, pp. 1505–1512, 2011.

70. Matteini, P., F. Tatini, L. Cavigli, S. Ottaviano, G. Ghini, and R. Pini, "Graphene As A Photothermal Switch For Controlled Drug Release", *Nanoscale*, Vol. 6, pp. 7947–7953, 2014.

71. Pan, Y., H. Bao, N.G. Sahoo, T. Wu, and L. Li, "Water-soluble Poly(N-isopropylacrylamide)-graphene Sheets Synthesized Via Click Chemistry For Drug Delivery", *Advanced Functional Materials*, Vol. 21, pp. 2754–2763, 2011.

72. Teodorescu, F., Y. Oz, G. Quéniat, A. Abderrahmani, C. Foulon, M. Lecoeur, R. Sanyal, A. Sanyal, R. Boukherroub, and S. Szunerits, "Photothermally Triggered On-demand Insulin Release From Reduced Graphene Oxide Modified Hydrogels", *Journal of Controlled Release*, Vol. 246, pp. 164–173, 2017.

73. Wang, X., W. Guo, L. Li, F. Yu, J. Li, L. Liu, B. Fang, and L. Xia, "Photothermally Triggered Biomimetic Drug Delivery Of Teriparatide Via Reduced Graphene Oxide Loaded Chitosan Hydrogel For Osteoporotic Bone Regeneration", *Chemical Engineering Journal*, Vol. 413, pp. 127413, 2021.

74. Sun, H., C.P. Kabb, Y. Dai, M.R. Hill, I. Ghiviriga, A.P. Bapat, and B.S. Sumerlin, "Macromolecular Metamorphosis Via Stimulusinduced Transformations Of Polymer Architecture", *Nature Chemistry*, Vol. 9, pp. 817–823, 2017.

75. Johra, F.T., and W.G. Jung, "Hydrothermally Reduced Graphene Oxide As A Supercapacitor", *Applied Surface Science*, Vol. 357, pp. 1911–1914, 2015.

76. Al Nafiey, A., A. Addad, B. Sieber, G. Chastanet, A. Barras, S. Szunerits, and R. Boukherroub, "Reduced Graphene Oxide Decorated With Co3O4 Nanoparticles (RGO-Co3O4) Nanocomposite: A Reusable Catalyst For Highly Efficient Reduction Of 4-nitrophenol, And Cr(VI) And Dye Removal From Aqueous Solutions", *Chemical Engineering Journal*, Vol. 322, pp. 375–384, 2017.

77. Ghann, W.E., H. Kang, J. Uddin, F.A. Chowdhury, S.I. Khondaker, M. Moniruzzaman, M.H. Kabir, and M.M. Rahman, "Synthesis And Characterization Of Reduced Graphene Oxide And Their Application In Dye-sensitized Solar Cells", *ChemEngineering*, Vol. 3, pp. 1–13, 2019.

78. Zhu, X., X. Xu, F. Liu, J. Jin, L. Liu, Y. Zhi, Z.W. Chen, Z.S. Zhou, and J. Yu, "Green Synthesis Of Graphene Nanosheets And Their In Vitro Cytotoxicity Against Human Prostate Cancer (DU 145) Cell Lines", *Nanomaterials and Nanotechnology*, Vol. 7, pp. 1–7, 2017.

79. Bej, R., J. Sarkar, and S. Ghosh, "Structural Diversity In Poly(disulfide)s", *Journal of Polymer Science, Part A: Polymer Chemistry*, Vol. 56, pp. 194–202, 2018.

80. Ryu, H., J.H. Baek, M.G. Choi, J.C. Lee, and S. Chang, "Cu 2 + -selective Turn-on Fluorescence Signaling Based On Metal-induced Hydrolysis Of Pyrenecarbohydrazide", *Tetrahedron Letters*, Vol. 58, pp. 2927–2930, 2017.

APPENDIX A: ADDITIONAL DATA

IR spectra of four-armed PEG polymers and linear PEG polymers are represented as additional data.

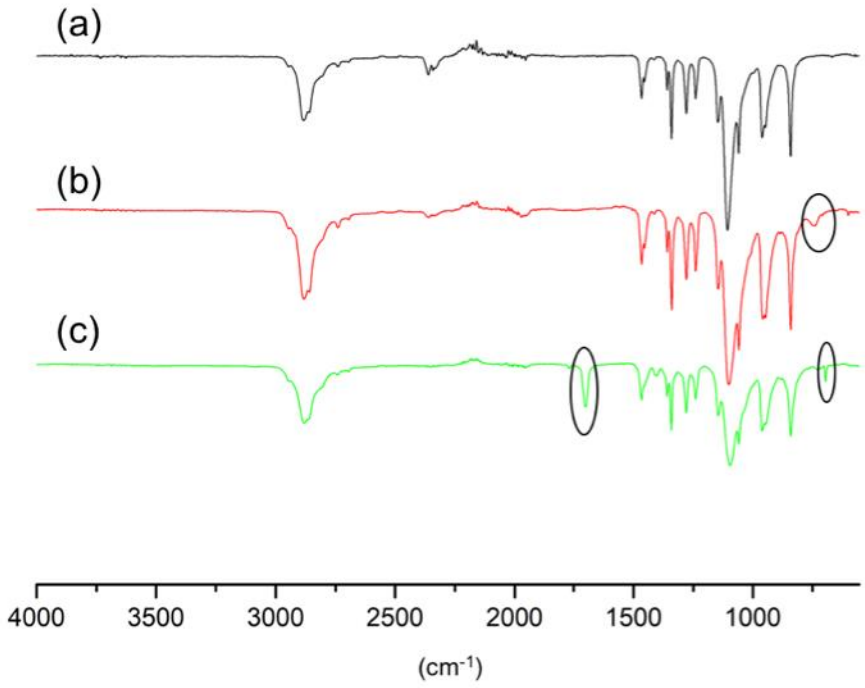

Figure A. 1. ATR-FT-IR data of (a) PEG-Bis-A, (b) PEG-Bis-F and (c) PEG-Bis-M.

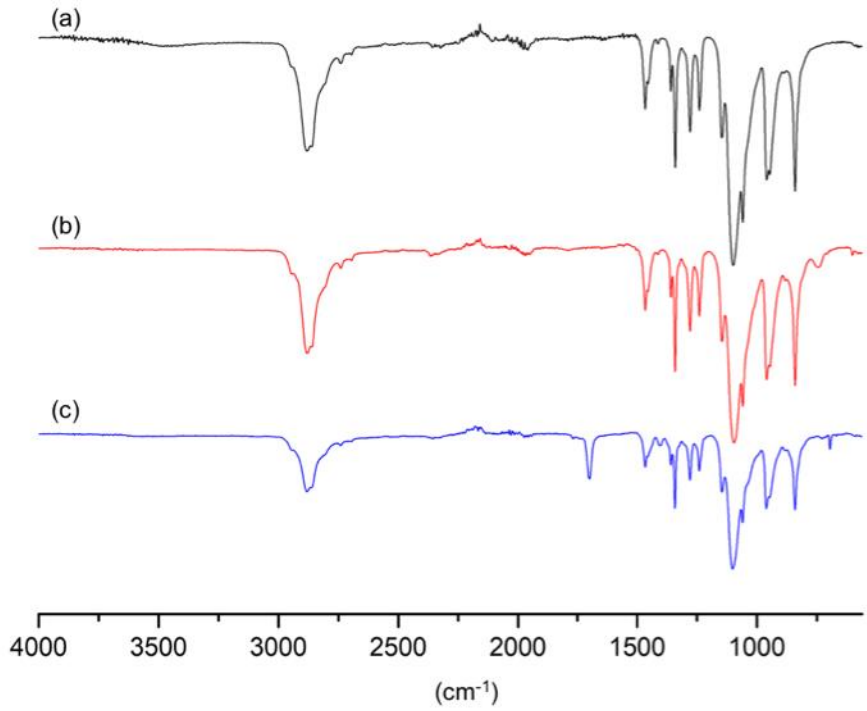

Figure A. 2. ATR-FT-IR data of (a) PEG-Tetra-A, (b) PEG-Tetra-F and (c) PEG-Tetra-M.

APPENDIX B: COPYRIGHT NOTICES

Copyrights notices for the figures used are represented in this section.

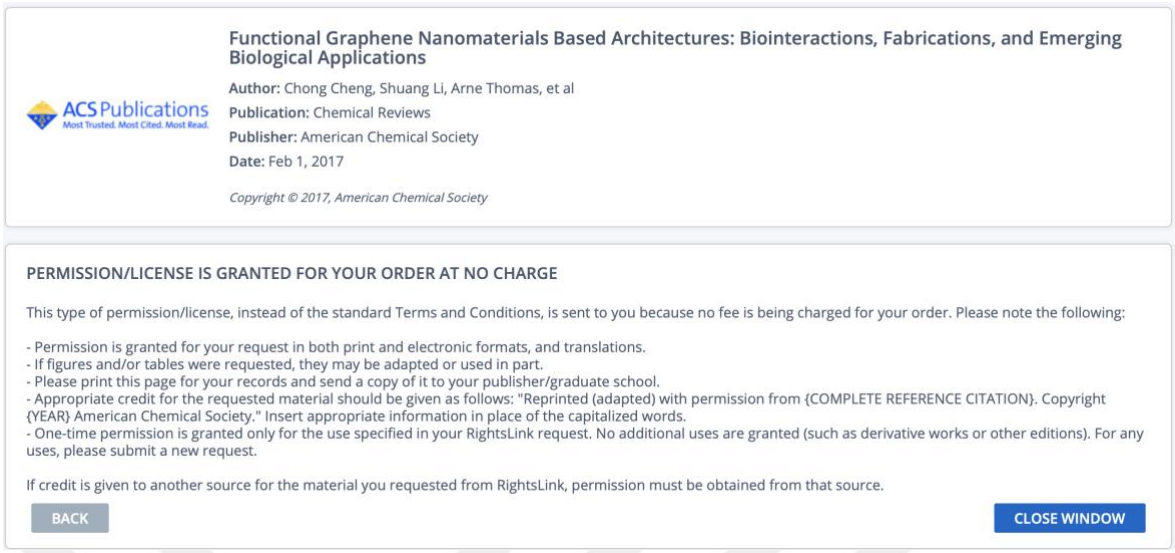

Functional Graphene Nanomaterials Based Architectures: Biointeractions, Fabrications, and Emerging Biological Applications

Author: Chong Cheng, Shuang Li, Arne Thomas, et al
Publication: Chemical Reviews
Publisher: American Chemical Society
Date: Feb 1, 2017

Copyright © 2017, American Chemical Society

PERMISSION/LICENSE IS GRANTED FOR YOUR ORDER AT NO CHARGE

This type of permission/license, instead of the standard Terms and Conditions, is sent to you because no fee is being charged for your order. Please note the following:

- Permission is granted for your request in both print and electronic formats, and translations.
- If figures and/or tables were requested, they may be adapted or used in part.
- Please print this page for your records and send a copy of it to your publisher/graduate school.
- Appropriate credit for the requested material should be given as follows: "Reprinted (adapted) with permission from {COMPLETE REFERENCE CITATION}. Copyright {YEAR} American Chemical Society." Insert appropriate information in place of the capitalized words.
- One-time permission is granted only for the use specified in your RightsLink request. No additional uses are granted (such as derivative works or other editions). For any uses, please submit a new request.

If credit is given to another source for the material you requested from RightsLink, permission must be obtained from that source.

BACK CLOSE WINDOW

Figure B. 1. Copyright notice for Figure 1.1.

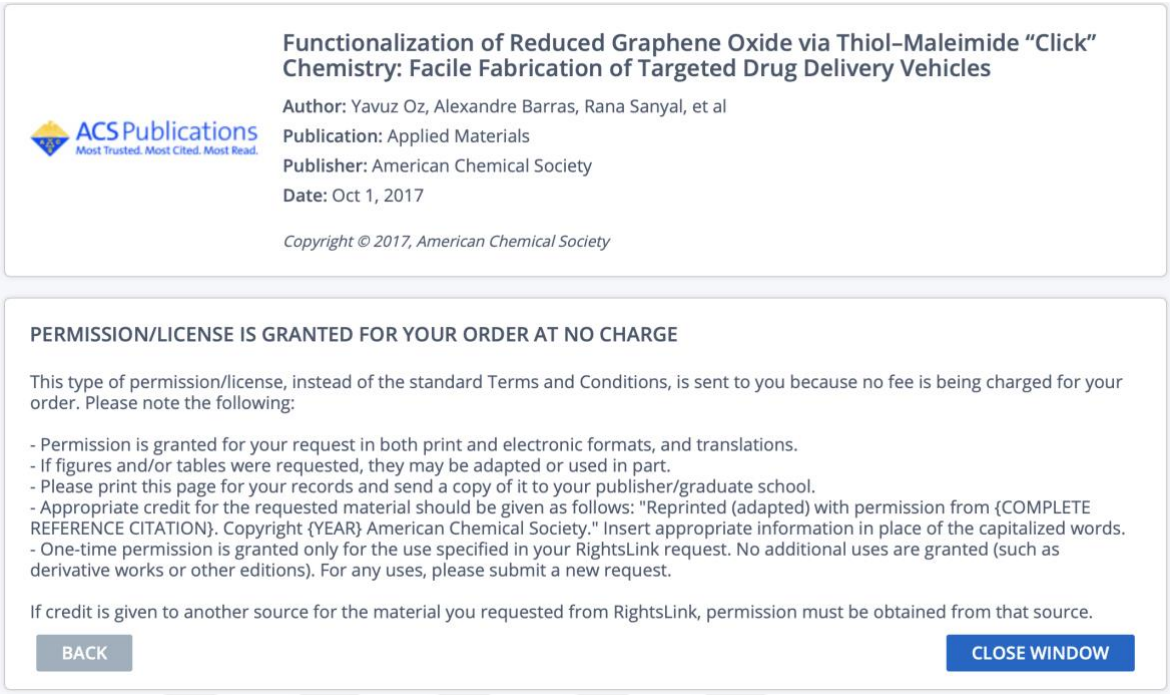

Figure B. 2. Copyright notice for Figure 1.2.

License Details

This Agreement between Bogazici University -- Merve Aslan ("You") and John Wiley and Sons ("John Wiley and Sons") consists of your license details and the terms and conditions provided by John Wiley and Sons and Copyright Clearance Center.

Print Copy

License Number	5126620933010
License date	Aug 12, 2021
Licensed Content Publisher	John Wiley and Sons
Licensed Content Publication	Advanced Healthcare Materials
Licensed Content Title	Controlling the Release of Small, Bioactive Proteins via Dual Mechanisms with Therapeutic Potential
Licensed Content Author	April M. Kloxin, Kristi L. Kiick, Emanual Maverakis, et al
Licensed Content Date	Oct 12, 2017
Licensed Content Volume	6
Licensed Content Issue	24
Licensed Content Pages	12
Type of Use	Dissertation/Thesis
Requestor type	University/Academic
Format	Print and electronic
Portion	Figure/table
Number of figures/tables	1
Will you be translating?	No
Title	Thesis
Institution name	Boğaziçi University
Expected presentation date	Sep 2021
Portions	Figure 1 in page 3
Requestor Location	Bogazici University Bebek Istanbul, 34343 Turkey Attn: Bogazici University
Publisher Tax ID	EU826007151
Total	**0.00 USD**

BACK

Figure B. 3. Copyright notice for Figure 1.3.

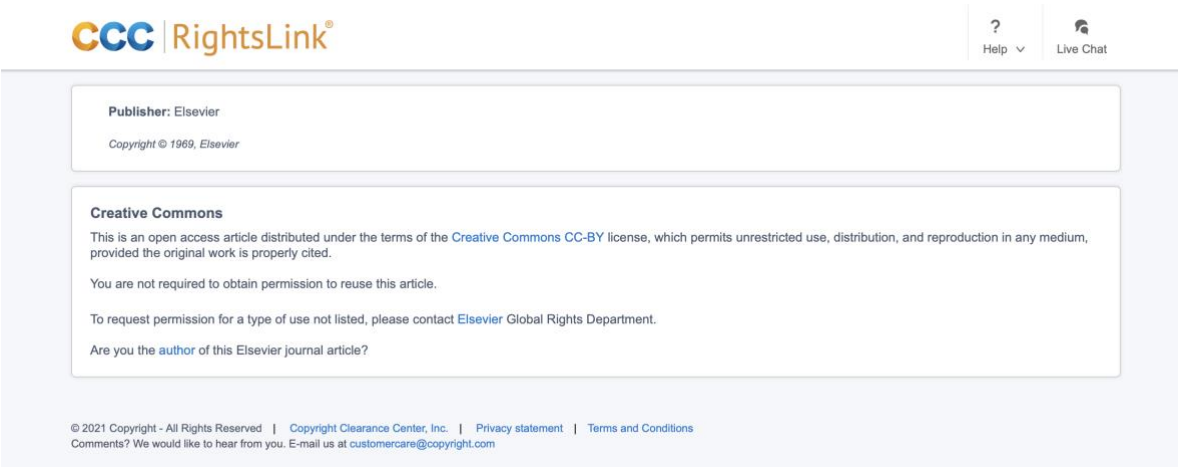

Figure B. 4. Copyright notice for Figure 1.4 and Figure 1.5.

Manage Account 6.08.2021 00:15

CCC Marketplace™

Order Number: 1138727
Order Date: 06 Aug 2021

Payment Information

Merve Aslan
merve.aslan1@boun.edu.tr
Payment method: Invoice

Billing Address:
Ms. Merve Aslan
Bogazici University
Bebek
Istanbul, 34343
Turkey

+90 (546)2438545
merve.aslan1@boun.edu.tr

Customer Location:
Ms. Merve Aslan
Bogazici University
Bebek
Istanbul, 34343
Turkey

Order Details

1. Polymer chemistry

Billing Status: Open

Article: Design of Thiol- and Light-sensitive Degradable Hydrogels using Michael-type Addition Reactions.

Order License ID	1138727-1	**Type of use**	Republish in a thesis/dissertation
Order detail status	Completed	**Publisher**	Royal Society of Chemistry
ISSN	1759-9962	**Portion**	Image/photo/illustration
			0.00 US Republication Permissic

LICENSED CONTENT

Publication Title	Polymer chemistry	**Publication Type**	e-Journal
Article Title	Design of Thiol- and Light-sensitive Degradable Hydrogels using Michael-type Addition Reactions.	**Start Page**	5565
		End Page	5574
		Issue	31
Author/Editor	Royal Society of Chemistry (Great Britain)	**Volume**	6
Date	01/01/2010	**URL**	http://www.rsc.org/Publishing/Journals PY/Index.asp
Language	English		
Country	United Kingdom of Great Britain and Northern Ireland		
Rightsholder	Royal Society of Chemistry		

REQUEST DETAILS

Portion Type	Image/photo/illustration	**Distribution**	Worldwide
Number of images / photos / illustrations	1	**Translation**	Original language of publication
		Copies for the disabled?	No
Format (select all that apply)	Print	**Minor editing privileges?**	No
Who will republish the content?	Academic institution	**Incidental promotional use?**	No
Duration of Use	Life of current edition	**Currency**	USD
Lifetime Unit Quantity	Up to 499		
Rights Requested	Main product		

NEW WORK DETAILS

Title	Thesis	**Institution name**	Boğaziçi University
Instructor name	Amitav Sanyal	**Expected presentation date**	2021-08-31

ADDITIONAL DETAILS

The requesting person / organization to appear on the license	Merve Aslan

REUSE CONTENT DETAILS

Title, description or numeric reference of the portion(s)	1 Figure	**Title of the article/chapter the portion is from**	Design of Thiol- and Light-sensitive Degradable Hydrogels using Michael-type Addition Reactions.
Editor of portion(s)	Kharkar, Prathamesh M; Kiick, Kristi L; Kloxin, April M	**Author of portion(s)**	Kharkar, Prathamesh M; Kiick, Kristi L; Kloxin, April M
Volume of serial or monograph	6		
Page or page range of portion	5565-5574	**Issue, if republishing an article from a serial**	31
		Publication date of portion	2015-08-21

Figure B. 5. Copyright notice for Figure 1.6.

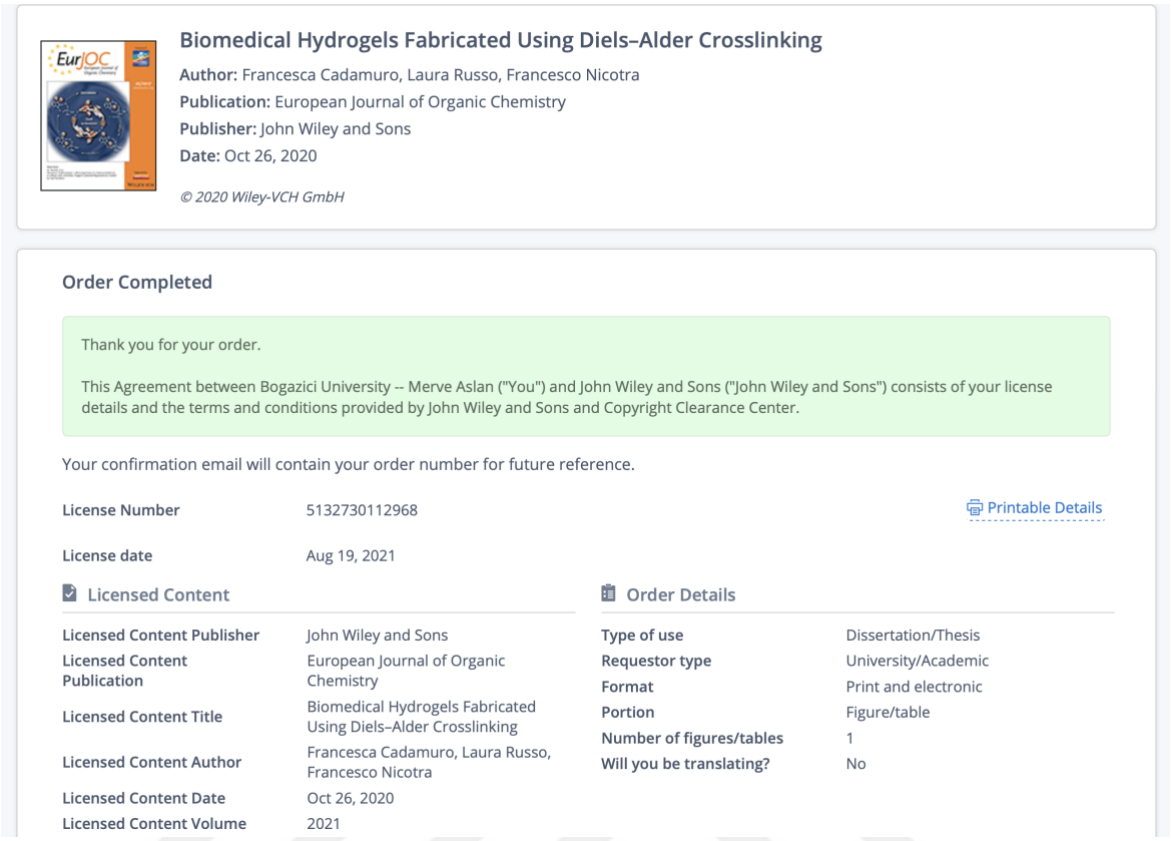

Biomedical Hydrogels Fabricated Using Diels–Alder Crosslinking

Author: Francesca Cadamuro, Laura Russo, Francesco Nicotra
Publication: European Journal of Organic Chemistry
Publisher: John Wiley and Sons
Date: Oct 26, 2020

© 2020 Wiley-VCH GmbH

Order Completed

Thank you for your order.

This Agreement between Bogazici University -- Merve Aslan ("You") and John Wiley and Sons ("John Wiley and Sons") consists of your license details and the terms and conditions provided by John Wiley and Sons and Copyright Clearance Center.

Your confirmation email will contain your order number for future reference.

License Number	5132730112968
License date	Aug 19, 2021

Printable Details

Licensed Content

Licensed Content Publisher	John Wiley and Sons
Licensed Content Publication	European Journal of Organic Chemistry
Licensed Content Title	Biomedical Hydrogels Fabricated Using Diels–Alder Crosslinking
Licensed Content Author	Francesca Cadamuro, Laura Russo, Francesco Nicotra
Licensed Content Date	Oct 26, 2020
Licensed Content Volume	2021

Order Details

Type of use	Dissertation/Thesis
Requestor type	University/Academic
Format	Print and electronic
Portion	Figure/table
Number of figures/tables	1
Will you be translating?	No

Figure B. 6. Copyright notice for Figure 1.7.

Order Details

1. RSC advances

Billing Status: Open

Article: Best of both worlds: Diels–Alder chemistry towards fabrication of redox-responsive degradable hydroge...

Print License

Order License ID	1140185-1	**Type of use**	Republish in a thesis/dissert...
Order detail status	Completed	**Publisher**	RSC Publishing
ISSN	2046-2069	**Portion**	Image/photo/illustration

0.00 USD
Republication Permission

Hide Details

LICENSED CONTENT

Publication Title	RSC advances	**Publication Type**	e-Journal
Article Title	Best of both worlds: Diels–Al...	**Start Page**	74757
Date	01/01/2011	**End Page**	74764
Language	English	**Issue**	78
Country	United Kingdom of Great Bri...	**Volume**	6
Rightsholder	Royal Society of Chemistry	**URL**	http://pubs.rsc.org/en/Journ...

REQUEST DETAILS

Portion Type	Image/photo/illustration	**Distribution**	Worldwide
Number of images / photos / illustrations	1	**Translation**	Original language of publica...
		Copies for the disabled?	No
Format (select all that apply)	Print,Electronic	**Minor editing privileges?**	No
Who will republish the content?	Academic institution	**Incidental promotional use?**	No
		Currency	USD
Duration of Use	Life of current edition		
Lifetime Unit Quantity	Up to 499		
Rights Requested	Main product, any product r...		

NEW WORK DETAILS

Title	Scheme 1	**Institution name**	Boğaziçi University
Instructor name	Amitav Sanyal	**Expected presentation date**	2021-08-31

ADDITIONAL DETAILS

The requesting person / organization to appear on the license	Merve Aslan

Figure B. 7. Copyright notice for Figure 1.8.

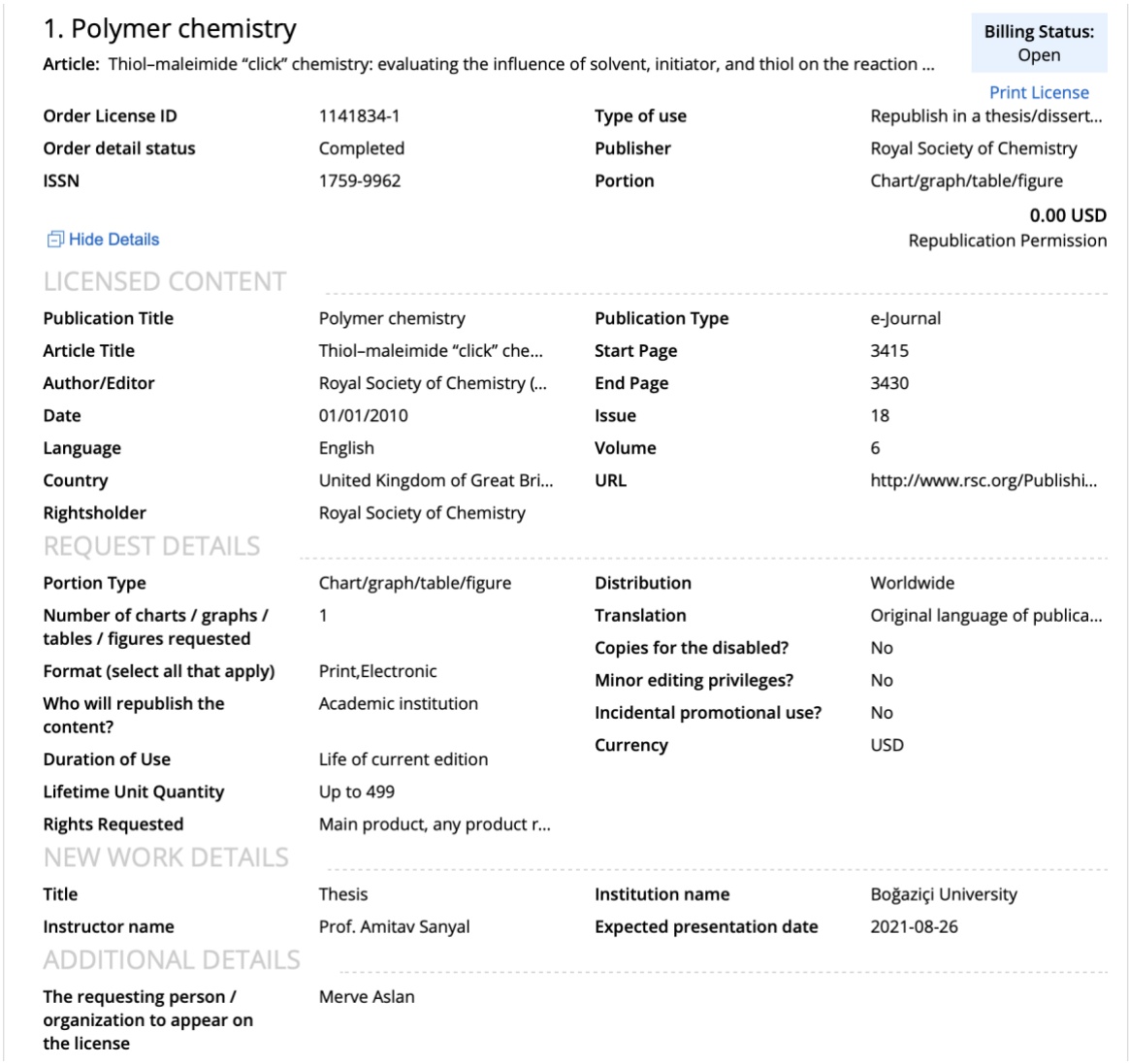

1. Polymer chemistry

Article: Thiol–maleimide “click” chemistry: evaluating the influence of solvent, initiator, and thiol on the reaction ...

Billing Status: Open

Print License

Order License ID	1141834-1	**Type of use**	Republish in a thesis/dissert...
Order detail status	Completed	**Publisher**	Royal Society of Chemistry
ISSN	1759-9962	**Portion**	Chart/graph/table/figure

0.00 USD

Hide Details

Republication Permission

LICENSED CONTENT

Publication Title	Polymer chemistry	**Publication Type**	e-Journal
Article Title	Thiol–maleimide “click” che...	**Start Page**	3415
Author/Editor	Royal Society of Chemistry (...	**End Page**	3430
Date	01/01/2010	**Issue**	18
Language	English	**Volume**	6
Country	United Kingdom of Great Bri...	**URL**	http://www.rsc.org/Publishi...
Rightsholder	Royal Society of Chemistry		

REQUEST DETAILS

Portion Type	Chart/graph/table/figure	**Distribution**	Worldwide
Number of charts / graphs / tables / figures requested	1	**Translation**	Original language of publica...
		Copies for the disabled?	No
Format (select all that apply)	Print,Electronic	**Minor editing privileges?**	No
Who will republish the content?	Academic institution	**Incidental promotional use?**	No
		Currency	USD
Duration of Use	Life of current edition		
Lifetime Unit Quantity	Up to 499		
Rights Requested	Main product, any product r...		

NEW WORK DETAILS

Title	Thesis	**Institution name**	Boğaziçi University
Instructor name	Prof. Amitav Sanyal	**Expected presentation date**	2021-08-26

ADDITIONAL DETAILS

The requesting person / organization to appear on the license	Merve Aslan

Figure B. 8. Copyright for Figure 1.9.

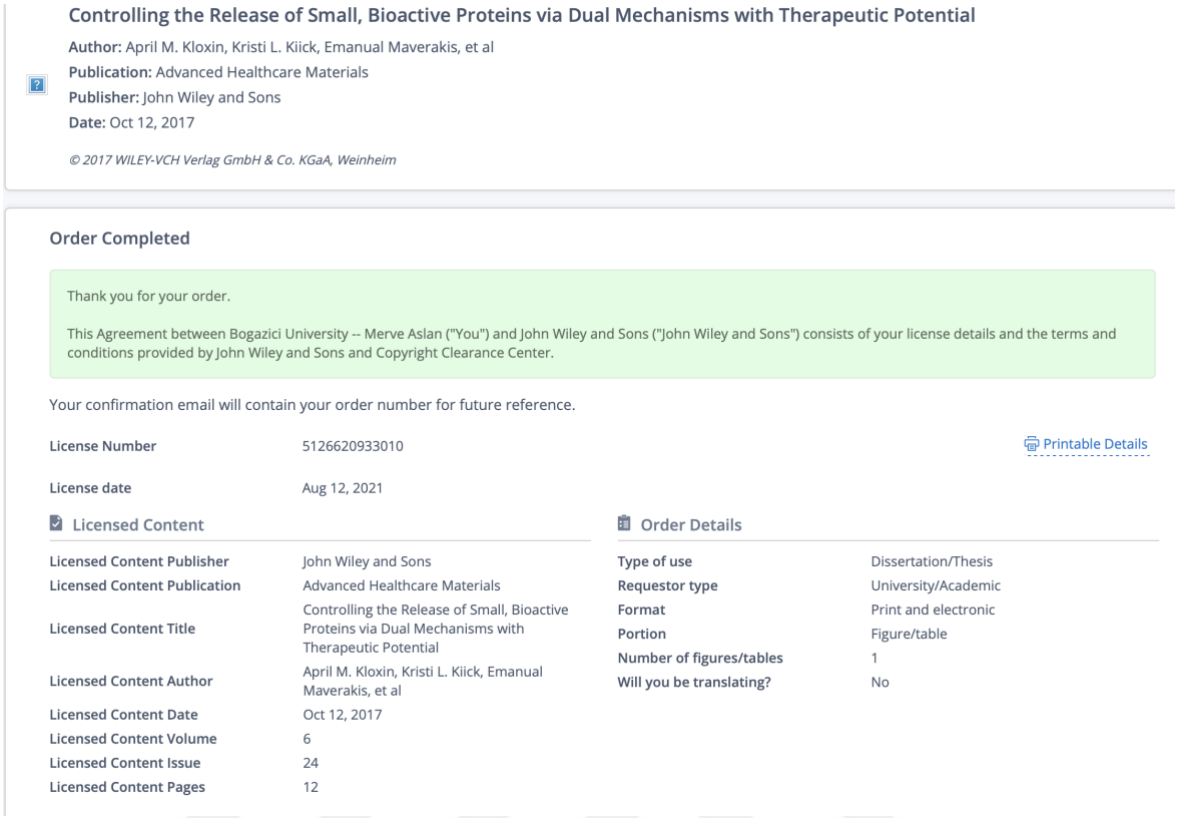

Controlling the Release of Small, Bioactive Proteins via Dual Mechanisms with Therapeutic Potential

Author: April M. Kloxin, Kristi L. Kiick, Emanual Maverakis, et al
Publication: Advanced Healthcare Materials
Publisher: John Wiley and Sons
Date: Oct 12, 2017

© 2017 WILEY-VCH Verlag GmbH & Co. KGaA, Weinheim

Order Completed

Thank you for your order.

This Agreement between Bogazici University -- Merve Aslan ("You") and John Wiley and Sons ("John Wiley and Sons") consists of your license details and the terms and conditions provided by John Wiley and Sons and Copyright Clearance Center.

Your confirmation email will contain your order number for future reference.

License Number	5126620933010
License date	Aug 12, 2021

Printable Details

Licensed Content

Licensed Content Publisher	John Wiley and Sons
Licensed Content Publication	Advanced Healthcare Materials
Licensed Content Title	Controlling the Release of Small, Bioactive Proteins via Dual Mechanisms with Therapeutic Potential
Licensed Content Author	April M. Kloxin, Kristi L. Kiick, Emanual Maverakis, et al
Licensed Content Date	Oct 12, 2017
Licensed Content Volume	6
Licensed Content Issue	24
Licensed Content Pages	12

Order Details

Type of use	Dissertation/Thesis
Requestor type	University/Academic
Format	Print and electronic
Portion	Figure/table
Number of figures/tables	1
Will you be translating?	No

Figure B. 9. Copyright for Figure 1.10.

License Details

This Agreement between Bogazici University -- Merve Aslan ("You") and Elsevier ("Elsevier") consists of your license details and the terms and conditions provided by Elsevier and Copyright Clearance Center.

Print Copy

License Number	5123200884006
License date	Aug 06, 2021
Licensed Content Publisher	Elsevier
Licensed Content Publication	Journal of Controlled Release
Licensed Content Title	Photothermally triggered on-demand insulin release from reduced graphene oxide modified hydrogels
Licensed Content Author	Florina Teodorescu,Yavuz Oz,Gurvan Quéniat,Amar Abderrahmani,Catherine Foulon,Marie Lecoeur,Rana Sanyal,Amitav Sanyal,Rabah Boukherroub,Sabine Szunerits
Licensed Content Date	Jan 28, 2017
Licensed Content Volume	246
Licensed Content Issue	n/a
Licensed Content Pages	10
Type of Use	reuse in a thesis/dissertation
Portion	figures/tables/illustrations
Number of figures/tables/illustrations	1
Format	both print and electronic
Are you the author of this Elsevier article?	No
Will you be translating?	No
Title	Thesis
Institution name	Boğaziçi University
Expected presentation date	Sep 2021
Portions	1 Figure
Requestor Location	Bogazici University Bebek Istanbul, 34343 Turkey Attn: Bogazici University
Publisher Tax ID	GB 494 6272 12
Total	**0.00 USD**

Figure B. 10. Copyright notice for Figure 1.12.